AN ABSTRACT OF THE THESIS OF

Michael J. Iademarco for the degree of Master of Science in Geology presented on August 5, 2009
Title: Volcanism and Faulting along the Northern Margin of Oregon's High Lava Plains: Hampton Butte to Dry Mountain

Abstract approved:

_____

Anita L. Grunder

Oregon's High Lava Plains Province (HLP) has strongly bimodal basalt and rhyolitic volcanism. The Province caps the northern margin of the Basin and Range Province and serves as a transitional region between westward extension of the Basin and Range Province and unextended crust to the north . The High Lava Plains overlap an area dominated by abundant minor northwest-striking faults of the Brothers Fault Zone. About 10 million years ago, silicic volcanism began at the eastern end of the HLP and spread west, younging towards the Cascade arc. Basalts erupted along the HLP are not age progressive. Most work in the High Lava Plains and Blue Mountains has left the interface between the two provinces as a nondescript region with few data capable to provide insight into processes active within this transitional region. This thesis focuses on the transition near Hampton Butte. New ^{40}Ar-^{30}Ar ages for Hampton Butte and adjacent Cougar Butte definitively assign both to volcanism during the emplacement of the John Day Formation and indicates a common origin. These units underlie basalts and an andesite that have ages consistent with a pulse of basaltic volcanism along the High Lava Plains around 8 Ma. An ignimbrite with

composition and age (3.8 ± 0.6 Ma) consistent with outcrops at Espeland Draw, near the town of Hampton, has a probable origin at Frederick Butte and is grouped here as the Hampton Tuff. Further east, along the northern margin of the HLP, an age of 4.18 (± 0.14 Ma) was obtained for the basaltic andesite scoria cone of Grassy Butte. At Dry Mountain a summit sample produced an age of 7.91 ± 0.12 Ma and is basaltic, a contradiction with previous reports. A sample of rhyolite from Potato Hills, adjacent to Hat Butte, yielded an age of 6.52 ±.07 Ma.

Basaltic melts of this study appear to be near direct partial melts of the mantle and are part of the volcanism of the High Lava Plains related to fault propagation and extension. More evolved magmas of the High Lava Plains originate from isobaric fractionation in isolated small magma chambers with little if any assimilation. The eruption of these lavas may be a result of the timing between northeast to southwest extension and Basin and Range east to west extension. The older (> 20 Ma) high silica rocks of Hampton Buttes are the result of diverse fractional crystallization paths from a common basaltic source with little or no assimilation.

Volcanism and Faulting along the Northern Margin of Oregon's High Lava Plains: Hampton Butte to Dry Mountain.

by

Michael J. Iademarco

A THESIS

submitted to

Oregon State University

in partial fulfillment of
the requirements for the
degree of

Master of Science

Presented August 5, 2009

Commencement June 2010

Master of Science thesis of Michael J. Iademarco presented on August 5, 2009.

APPROVED:

Major Professor, representing Geology

Chair of the Department of Geosciences

Dean of the Graduate School

I understand that my thesis will become part of the permanent collection of Oregon State University libraries. My signature below authorizes release of my thesis to any reader upon request.

Michael J. Iademarco, Author

ACKNOWLEDGEMENTS

I express sincere appreciation to Anita Grunder for her guidance and support during my time as an undergraduate and graduate student. I also wish to extend my appreciation to Adam Kent who, during the course several conversations expressed confidence in my ability to pursue an advanced degree which lead to my applying for graduate school. I also wish to thank the National Science Foundation for their support. I also wish to thank the owner of Desert Springs Ranch for permission to conduct much of the mapping done for this thesis on their property in Hampton Buttes.

CONTRIBUTION OF AUTHORS

During the course of my work I have had the privilege to discuss and work with numerous people whose ideas helped shape my ideas about the High Lava Plains. Anita Grunder, Andrew Meigs, Adam Kent, Kaleb Scarberry, Mark Ford, Manggon Abot, and others have helped me, through discussion and/or field assistance, to form ideas and interpretations presented in this thesis which are entirely my own.

TABLE OF CONTENTS

TABLE OF CONTENTS (Continued)

Page

LIST OF FIGURES

LIST OF FIGURES (Continued)

LIST OF FIGURES (Continued)

LIST OF FIGURES (Continued)

LIST OF TABLES

LIST OF TABLES

LIST OF PLATES

Plates are located in a pocket at the back of the book.

Volcanism and Faulting along the Northern Margin of Oregon's High Lava Plains: Hampton Butte to Dry Mountain

Chapter One: Introduction

Oregon's High Lava Plains Province has had strongly bimodal basalt and rhyolitic volcanism and caps the northwestern margin of the Basin and Range Province of western North America where it serves as a transitional region between west-northwest extension of the Basin and Range Province and unextended crust to the north (Figure 1.1). The High Lava Plains (HLP) overlap an area dominated by abundant minor northwest-striking faults of the Brothers Fault Zone. Silicic volcanism within the province began 10 Ma at the eastern end and spread west, younging towards the Cascade Arc (Figure 1.2). Basalt erupted along the High Lava Plains is not age progressive (Jordan, 2002a). To gain a better understanding of the High Lava Plains it is essential to gain a better understanding of the margin between it and the Blue Mountains Province to the north.

Most work undertaken in the High Lava Plains and Blue Mountains has left the interface between the two provinces as a nondescript region with little specific petrochemical and chronological data capable of providing insight into processes active within this transitional region. Recent research efforts in the High Lava Plains have been directed at determining the geochronology and composition of basalt and silicic volcanic centers within the boundaries of the province (Grunder, 1995; Johnson, 2000; Jordan, 2002b; Jordan, 2004; Jordan, 2005). Prior to this, Walker and coworkers compiled most of the available data on silicic and basaltic rocks and volcan-

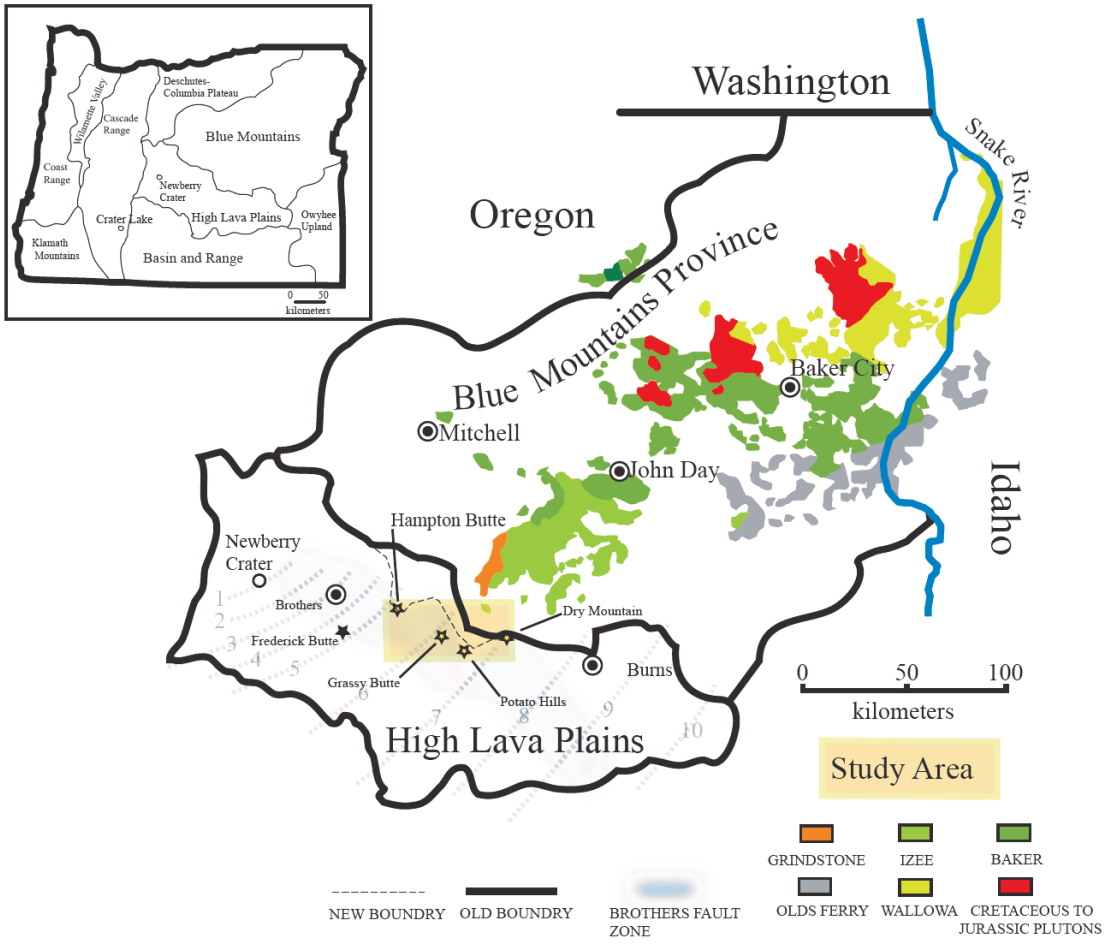

Figure 1.1: Generalized map of the High Lava Plains and Blue Mountains Province showing the relationship between the accreted terrains of the Blue Mountains Province and features of the High Lava Plains that are discussed in this thesis. Inset- Geomorphic provinces of Oregon. Maps after U.S. Forest Service.

ism of the HLP while reconnaissance-mapping the area (MacLeod, 1975; Walker, 1974; Walker and Nolf, 1981).

This thesis focuses on the western half of Hampton Buttes, unique for its record of volcanism, faulting, and petrology that spans the time between the early Oligocene to early Pliocene with magmatic roots that likely draw some material from the underlying older John Day and Clarno Formations. Geochronology and petrologic research was also done on Grassy Butte, Potato Hills, and Dry Mountain, all

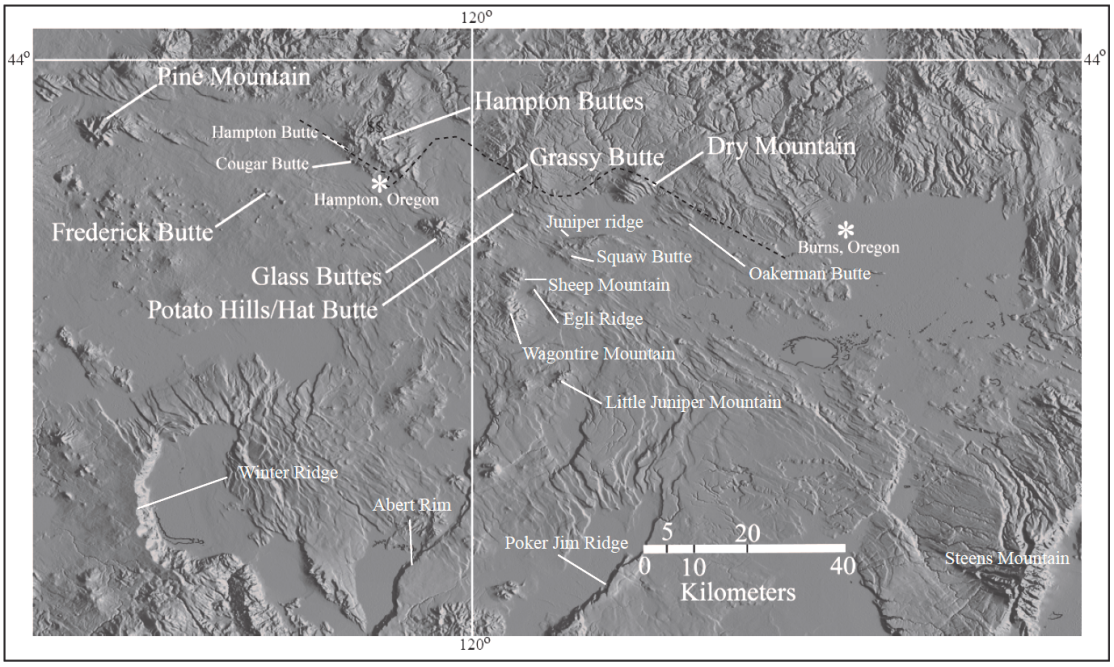

Figure 1.2: Shuttle Radar Topography Mission (SRTM) based map revealing regional fault patterns. Basin and Range northeast to southwest oriented normal faulting transforms to northwest to southeast normal faulting of the High Lava Plains (USGS, 2004). The Image has been highlighted by light at a 30-degree angle from north, south, east and west. The location of the Brothers Fault Zone relative to the labeled locations is highlighted in Figure 1. Appendix 2 is a larger version of the region.

east of and within 30 kilometers of Hampton Buttes. As part of a larger project funded by the National Science Foundation (US NSF Continental Dynamics), this thesis adds to our understanding of (1) types of volcanism and ages; (2) timing of faulting; (3) the relationship between volcanism and faulting; and (4) geochemical data for sample collected along the northern margin of this region of bimodal volcanism and extension.

Geologic mapping of the western half of Hampton Buttes was supplemented by ^{40}Ar-^{39}Ar dating on samples representative of rock units in the area (Plate 1). Chapter 2 contains a summary of stratigraphic relationships and petrologic character-

istics as well as a summary of data obtained for Grassy Butte, Potato Hills and Dry Mountain. The results from geochemical analysis completed by the Washington State University GeoAnalytical Laboratory, Pullman, Washington are in Chapter 3 followed by a discussion of the petrogenesis of selected samples for each of the sites in Chapter 4. Chapter 5 is dedicated to discussion and conclusions.

1.1 Tectonic setting: High Lava Plains and Blue Mountains

1.1.1 High Lava Plains: The High Lava Plains are an enigmatic geologic province with abundant Late Cenozoic volcanic rocks in geomorphic continuity with the Snake River Plain. In contrast to the decreasing ages for volcanism to the northeast along the Snake River Plain, the High Lava Plains exhibit westward younging silicic volcanism opposite to the "Yellowstone hotspot track" and overlie an anomalously hot region of the mantle (Nathenson and Guffanti, 1988; Roth et al., 2008). The High Lava Plains are the northwestern boundary of the Basin and Range province, and are cut by a series of northwest-striking sub-parallel faults called the Brothers Fault Zone, which contrasts in fault orientation and strike with regularly spaced, northwest-striking normal faults that yield the distinctive horst and graben structure of the Basin and Range. The Blue Mountains terrain to the north of the High Lava Plains are largely unextended (Lawrence, 1976) (Figure 1.1 and 1.3).

The Olympic-Wallowa lineament, Eugene-Denio, Vale and McLaughlin zones, have also been cited as features separating the extended and unextended regions and are part of the northwest trending fabric (Walker and Robinson, 1990a).

Atwater (1970), Livaccari (1979) and Lawrence (1976) infer that Oregon is the limit of dextral shear related to the transform San Andreas fault system, but evidence of significant strike-slip movement has yet to be found on faults within the Brothers fault zone (MacLean, 1994). Some lateral displacement may be evidenced by the relationship of small monoclinal folds or ramp structures to normal faults and indicate probable right lateral displacement (Lawrence, 1976).

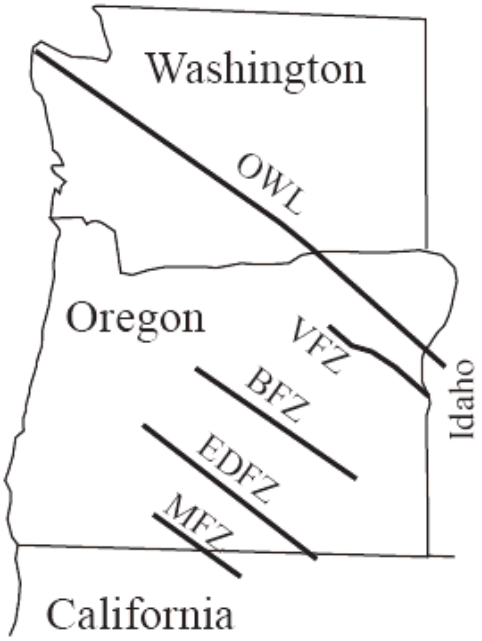

Figure 1.3 Features cited as separating extended and unextended regions of the Pacific Northwest.

Widely spaced Basin and Range normal faults dominate a regional structure that declines in relief and structural separation northward, where they intersect abundant smaller northwest striking faults of the Brothers Fault Zone (BFZ). The northwest trending faults of the BFZ and the north to northeast striking faults of the Basin and Range Province are contemporaneous (Hemphill-Haley et al., 2000; Scarberry et al., in Press; Trench, 2008). Both sets cut all Miocene rocks, possibly a result of reactivation in the late Miocene (Camp et al., 2003).

Seismic studies of the High Lava Plains have revealed an the upper mantle and crustal structure consisting of up to 5 kilometers of sedimentary and volcanic debris overlying deep basins and brittlely extended horst and graben structures

(Catchings and Mooney, 1988). The lower crust is thinnest beneath Newberry Volcano (≈3 km), and thickens to the east, under the High Lava Plains, and to the west beneath the Cascade Range (Figure 1.4).

Recent tomographic modeling of the Pacific Northwest region of the United States has revealed an unexpectedly pronounced reduced velocity anomaly below Newberry volcano and northward (Figure 1.5). The geochemical signature of Newberry volcano, and the Cascade Range, retains a strong slab-derived fluid component and the reduced velocity zone may be a result of slab released fluids inducing partial melting in the hot asthenospheric mantle below the High Lava Plains above the down going slab (Carlson et al., 2008; Roth et al., 2008)

There are abundant late Miocene to Quaternary rhyolitic and basaltic vents throughout and adjacent to the Brothers Fault Zone. These vents are thought to be the surface expression of, and caused by magmatism associated with transtensional deformation of Paleozoic and Mesozoic terranes underlain by oceanic or rifted type crust (Hamilton and Myers, 1966). Normal faults at the surface may represent the brittle rocks response to movement on the buried structure. Pre-Tertiary basement rocks represent both allochthonous terranes and autochthonous terranes and could indicate a wide (500 km) transitional zone between young oceanic crust on the west and older continental crust to the east (Catchings and Mooney, 1988).

1.1.2 The Blue Mountains: One of the few areas in eastern Oregon not extensively covered by Cenozoic volcanism is the Blue Mountains Province. To the north, south, and west the Blue Mountains are ringed by Miocene and younger continental

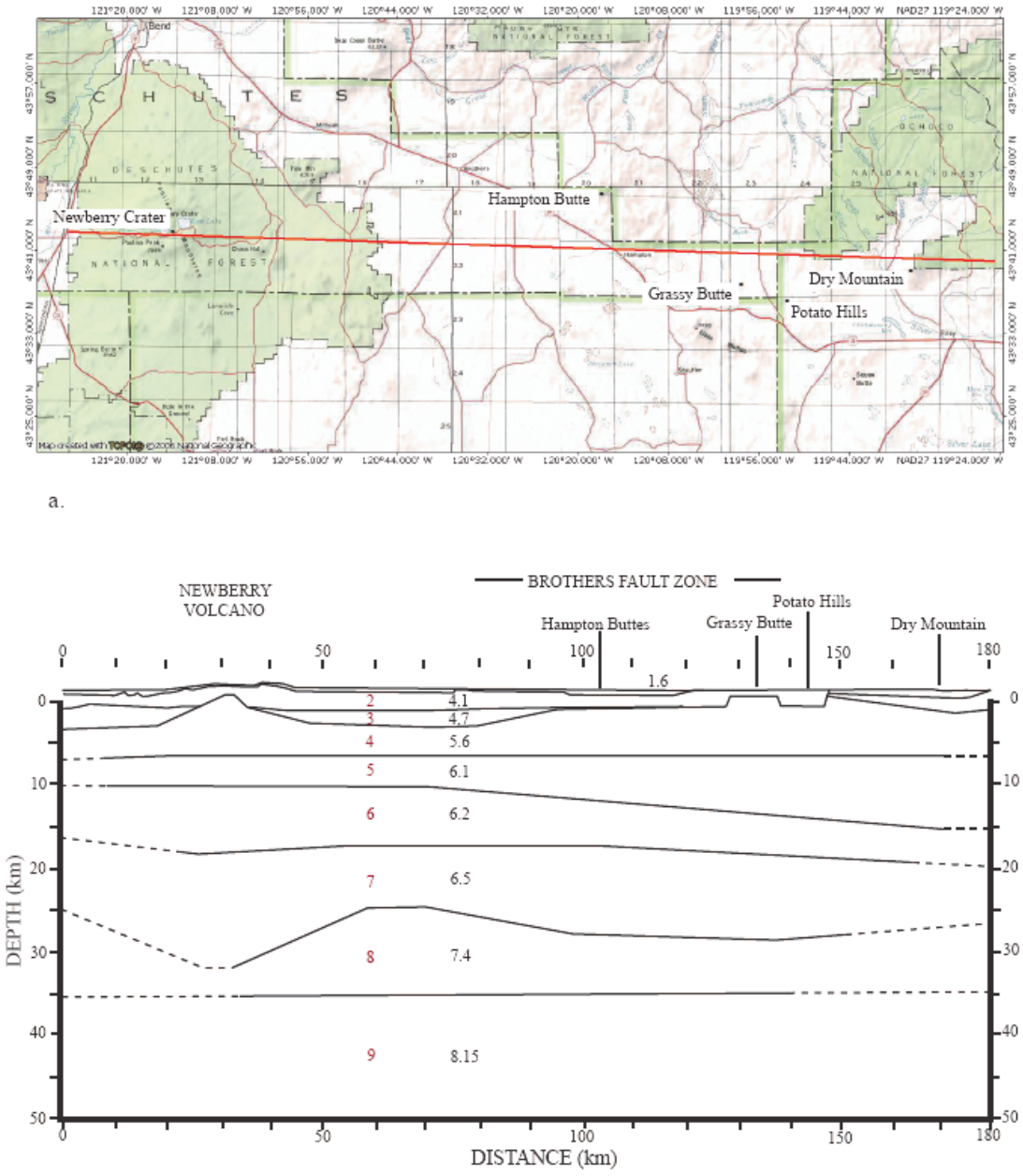

Figure 1.4: a. Location map for the seismic transect of Catchings and Mooney (1988) and the location of principal vents discussed in this thesis. b. Velocity (km/s) structure beneath the High Lava Plains from 30 kilometers west of Newberry Volcano to the east side of Dry Mountain. (After Catchings and Mooney, 1988)

sediments and volcanic rocks surrounding five separate accreted terranes. The northern most terrane is the Wallowa Terrain, the Baker Terrane occupies the central and southwestern part of the province and from southeast to south central are the Olds Ferry, Izee, and Grindstone terranes (Figure 1.2). As a result, this region exposes early Tertiary volcanic rocks and Mesozoic and Paleozoic metamorphic rocks.

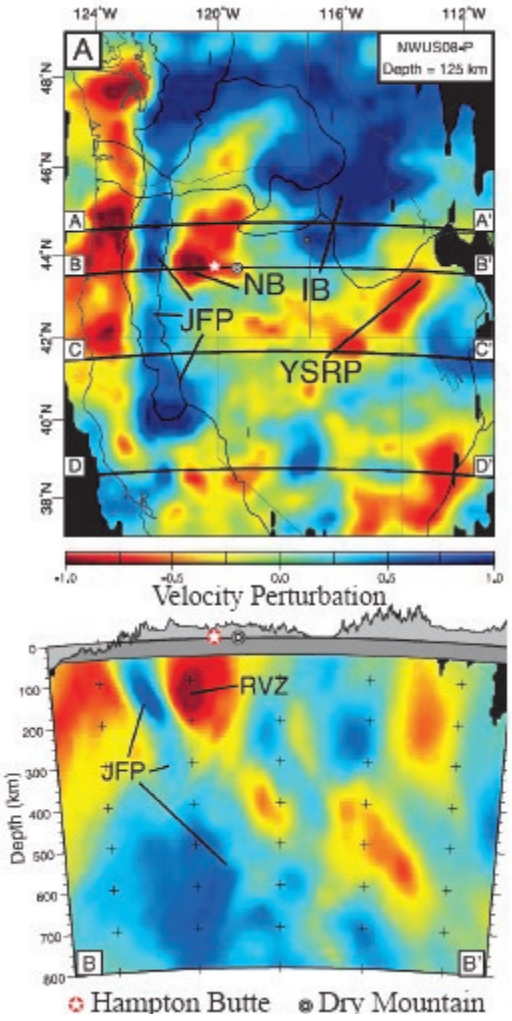

Figure 1.5: High resolution 3-D p-wave tomographic image of the Pacific Northwest and cross section through the High Lava Plains. (After Roth, 2008)

Inliers of Mesozoic and Paleozoic rock, that are surrounded by continentally derived sedimentary rock, imply that a large part of the Blue Mountains are a complex uplifted crustal block made up of Cenozoic and older rocks (Brooks, 1978; Dickinson, 1978; Walker and Robinson, 1990b). Fault relationships and stratigraphy have helped identify a complex tectonic history. In east-central Oregon, volcanic rocks of the Clarno Formation are a result of a northeast to southwest-trending andesite belt undergoing northwest to southeast compression (Taylor, 1977). Taylor's model is consistent with east-west convergence directions put forth by Dickinson

(1979) and requires a trench to be located about 100 kilometers northwest of the andesite belt as well as that both the belt and trench be parallel with the present continental margin (Walker and Robinson, 1990a).

Late Eocene uplift, concentrated along pre-existing structures, created an erosional surface used to mark the transition between the Clarno and John Day Formations (Waters, 1954).The overlying John Day Formation is initiated by an ash-flow tuff dated by the $^{40}Ar/^{39}Ar$ method at 39.22 ± 0.03 Ma. Northeast trending folds (the result of northwest-southeast compression) dominate a subordinate set of folds trending northwest that were developed during the late Eocene and early Oligocene. In one area of the Blue Mountains, the folding postdates the basal ash flow sheet of the 37 Ma John Day Formation (Swanson, 1968). Weaker Oligocene and early Miocene folding also trended northeast, parallel to the structures developed in the Eocene to early Oligocene (Walker and Robinson, 1990a). Middle Miocene time saw the compressional regime greatly diminish and replaced by extension related to presumed transform faulting in the Brothers Fault Zone and other parts of western North America related to major crustal extension principally in the Basin and Range from 17 to 16 Ma (Couch and Lowell, 1971; Walker and Robinson, 1990a). Deformation between 4 Ma and the present has been mild (Barrash et al., 1983).

Three types and ages of deformational structures have been identified in the Blue Mountains resulting from northwest moving Basin and Range lithosphere interacting with a seemingly stationary block of the Blue Mountains. From 36 to17 Ma northeast and east-striking fold axes and reverse faults developed. Strike-slip faults

striking north, with northwest-trending fissures developed between 17 and 10 Ma. Conjugate faults trending northwest and northeast have formed between 10 Ma and the present. According to Walker (1990a), many Miocene and younger folds and faults are explained by adjustment to transform movement on bounding faults.

1.2 Volcanism: High Lava Plains and Blue Mountains

1.2.1 High Lava Plains: The late Cenozoic brought bimodal volcanism to the area of the High Lava Plains, which extend from the Owyhee Plateau westward to the present day Cascade Range. Isochrons, first defined by MacLeod et al. (1975) showed that silicic volcanism originated in the SE corner of the state near McDermott about 16 Ma and progressed west along the High Lava Plains starting about 10 Ma. Initial propagation rates were about 33 km/million years from 10 to 5 Ma slowing to roughly 13 km/million years since that time for silicic volcanism with no discernable progression for basalts (Jordan et al., 2004). Hart et al. report that three major pulses of high alumina low potassium olivine tholeiite (HAOT) magmatism are suggested by data collected for their study: 0 to 2.5 Ma, 3.5 to 6 Ma, 7 to 10 Ma (Hart, 1984). These dates were refined by Jordan et al. (2004) to distinct and dominant pulses at ~ 8 Ma, 6 Ma, and another at 3 Ma. High alumina tholeiitic basalts dominate the HLP, but close to 25% of the mafic samples analyzed are basaltic andesites and some are calc-alkaline. Basalt, unusually enriched in incompatible elements, is aphanitic to sparsely porphyritic with common plagioclase, clinopyroxene, and olivine phenocrysts. Diktytaxitic textures are also common, as are glomerocrysts of two or three phenocryst phases (Figure 1.6).

Figure 1.6: Glomerocryst of plagioclase and olivine, typical of High Lava Plains basalts. This sample is from Hampton Buttes. Sample number HTB-0501.

Metaluminous to peralkaline high silica rhyolites originated from three major (and several minor) ash-flow tuffs and over 60 domes and dome complexes. The aphanitic to moderately porphyritic rhyolitic lavas and tuffs hold differing combinations of anorthoclase, biotite, hornblende, and clinopyroxene or plagioclase, quartz, and sanidine phenocrysts (e.g., Johnson and Grunder, 2000; MacLean, 1994; Streck and Grunder, 1995). Intermediate composition rocks less than 11 Ma are uncommon and are mainly the result of mixing of mafic and silicic compositions (Linneman and Myers, 1990; MacLean, 1994; Streck et al., 1999).

1.2.2 Blue Mountains Province: The Blue Mountains are a complex uplifted crustal block made up of Cenozoic and older rocks preserving an extensive record of Cenozoic volcanism. Rocks in the Blue Mountains region are a record of extensional tectonism and subsequent isolated bimodal volcanism within the province and also along its southern boundary with the High Lava Plains. Younger volcanic activity both in the Blue Mountains and adjacent to them may be related to younger arc volcanism, bimodal volcanism generated by extensional tectonics, or isolated eruptive centers within both provinces related to extension (Walker and Robinson, 1990a).

The earliest know volcanism in the Blue Mountains produced a 53.7 ±1.0 Ma plagioclase-phyric andesite near the axis of the Blue Mountains uplift in the Eocene Clarno Formation (see compilation by Fiebelkorn et al, 1983). The distribution of the Clarno Formation suggests existence of a north to south trending volcanic arc whose axis is east of the present day Cascades (Walker and Robinson, 1990a). Until the late Eocene, volcanism produced calc-alkaline, dacitic, and andesitic rock near the axis of the uplift and further to the southeast (Robinson and Walker, 1990). Clarno volcanic rocks are thought to be represented in east-central Oregon by a northeast to southwest trending andesite belt during a period when the Clarno formation was undergoing northwest-southeast compression (Taylor, 1977). Walker and Robinson (1995) propose that the volcanism in the Blue Mountains during the Eocene is a result of eruptions along a north to northeast oriented arc over a subduction zone parallel to today's continental margin. According to Walker and Robinson (1990) the andesites of the Lakeview and Cedarville areas, if some left lateral offset is allowed along the Brothers Fault Zone and in other features, are representative of the southward extension of the belt towards the Oregon-California State line (Walker and Robinson, 1990a).

From 37 to 23 Ma, more or less continuous and dominantly rhyolitic and dacitic volcanism took place in the Blue Mountains province and is preserved as the John Day Formation. Vents were located in and slightly west of, the present Cascade Range as indicated by prevalence of silicic lavas and domes and thick ash flow tuff deposits. To the east, the volcanic deposits are dominated by pyroclastic fall facies.

Local eruptions within the province produced silicic lava flows and domes. Intermediate composition volcanic centers of this age are now recognized well south of the John Day Formation, at Hampton Butte (this study), and in southeastern Oregon at Coleman Hills, Rabbit Hills, Coyote Hills, Hart Mountain and Steens scarps (Scarberry, 2007). Between 25 and 20 Ma eruptions of trachyandesite, rhyolite and basalt in the Blue Mountains ceased while eruptions in the Cascade Range continued to form the upper part of the John Day Formation. By 18 million years ago the John Day Formation had been deposited (McBirney et al., 1974).

Large volumes of tholeiitic flood basalt characterize volcanism in the Blue Mountains since the cessation of John Day age volcanism. Thick extensive mafic lavas of the Columbia River Basalt Group are primarily found north of the Blue Mountains uplift and range from 17 to 6 Ma in age. The Columbia River Basalt Group erupted most of it between 17 and 14 Ma. (Baksi et al., 1989; Watkins and Baksi, 1974) with peak volume between ~ 15-16 Ma (Hooper et al., 2002). Small amounts of silicic volcanism took place in the province about 12 Ma. At the eastern end of the High Lava Plains at Steens Mountain, a subalkalic, high Al_2O_3 , basalt containing large plagioclase phenocrysts known as the Steens Basalt erupted ~16 Ma (e.g. Hart and Mertzman, 1982; Rytuba and McKee, 1984; Watkins and Baksi, 1974) and is correlated with the CRB flood basalt event (Hooper et al., 2002). 12 m.y. ago saw the eruption of relatively minor amounts of silicic rock. Volcanism younger than Pliocene age is confined to small eruptions of basalt along the western and southern margins of the Blue Mountains.

In the Blue Mountains, Robyn and Hoover (1982) have identified three types and ages of structures related to deformation. From 36 to 17 Ma, reverse faults and northeast- and east-striking fold axes formed followed by north-striking transform faults and fissures striking north-west between 17 and 10 Ma. Between 10 Ma and the present, northeast-and northwest-trending conjugate faults have formed. According to Robyn and Hoover (1982), major east-west extension along the Brothers Fault Zone and other bounding faults interacting with a relatively immobile lithosphere beneath the Blue Mountains explains the adjustment of brittle layers of volcanic and tuffaceous sediments to the transform movement.

2. STRUCTURE AND STRATIGRAPHY ALONG THE NORTHERN MARGIN OF THE HIGH LAVA PLAINS

2.1: Introduction

Hampton Buttes are located 60 kilometers east of Bend, Oregon at the transition between the High Lava Plains and the Blue Mountains province and preserve a record of volcanism and faulting starting 30 Ma during John Day time. Hampton Butte, a rhyodacitic lava dome complex and the genetically related, dacitic Cougar Butte predate a much younger Lower Miocene vent that produced minor amounts of andesite during a time when tholeiitic basalt, massive and blocky with flow layers separated by a sparse rubbly zones, lapped onto the southern side of Hampton Butte. What appear to be fault scarps on the east and west sides of the outcrop are only remnants of erosion now lapped on by the Hampton Tuff. To the south the basalt is covered by Tertiary silicic tuffaceous sediments , the Hampton Tuff, younger basalt and aeolian, fluviatile and lacustrine tuffaceous sedimentary rocks (Plate 1).

Cougar Butte is a haystack shaped extrusive dome on the down dropped south side of the normal fault that forms the southern boundary of Hampton Buttes. The 28 ± 0.12 Ma dacite must have erupted before the main fault developed since the 3.8 ± 0.6 Ma Hampton Tuff is cut by the fault. Remnants of the tuff and the basal vitrophyre that were banked on Cougar Butte before faulting can be found near the base of the butte. The butte later acquired a facet on its southern flank as another normal fault (now hidden) developed along that face and destabilized the hillside. A rhyodacite dike of probable Hampton Butte age extends west from the west side of Cou-

gar Butte, and is cut by a normal fault, down to the east, isolating the butte from the surrounding area (Plate 1 and Figure 2.1).

The southern flank of Hampton Butte and Cougar Butte are faulted and dropped with Cougar Butte showing a faceted southern slope. Faults in the area are mainly northwest-striking and have cut all volcanic units. The Hampton Tuff, cut by ongoing faulting, and lapped onto Cougar Butte constrains the timing of the most recent faulting in the buttes to less than 3.8 ± 0.6 Ma. A series of northwest striking faults break the low shield-like silhouette of Dry Mountain and cause the mountain to present a stepped graben structure when viewed from the southeast.

The 7.81 (± 0.12) Ma andesite in the buttes erupted on the east side of the rhyodacite ridge that nearly connects Hampton Butte with Cougar Butte. The vent forms a small promontory overlying an older, north to south striking fault that separates it from part of the flow on the opposite side of the stream that now follows the fault trace. This fault intersects another older fault that strikes northeast and accounts for the abrupt turn of the drainage on the east side of Cougar Butte (Plate 1 and Figure 2.1). Conclusive evidence for the direction of lateral fault movement for either fault was not found.

Forty kilometers east of the buttes, and at the about the same time that basalt and andesite were being erupted at the flanks of the buttes, tholeiitic basalt was building Dry Mountain, a shield volcano. Dry Mountain is a shield volcano nine kilome-

Figure 2.1: Geologic map of the southeast corner of Hampton Buttes, Deschutes and Crook Counties, Oregon. The oldest units, Hampton Butte and Cougar Butte are lapped on by the younger basalt and rhyolitic Hampton Tuff. Plate1 is a larger version of the map with unit descriptions and cross sections. Units are also described in

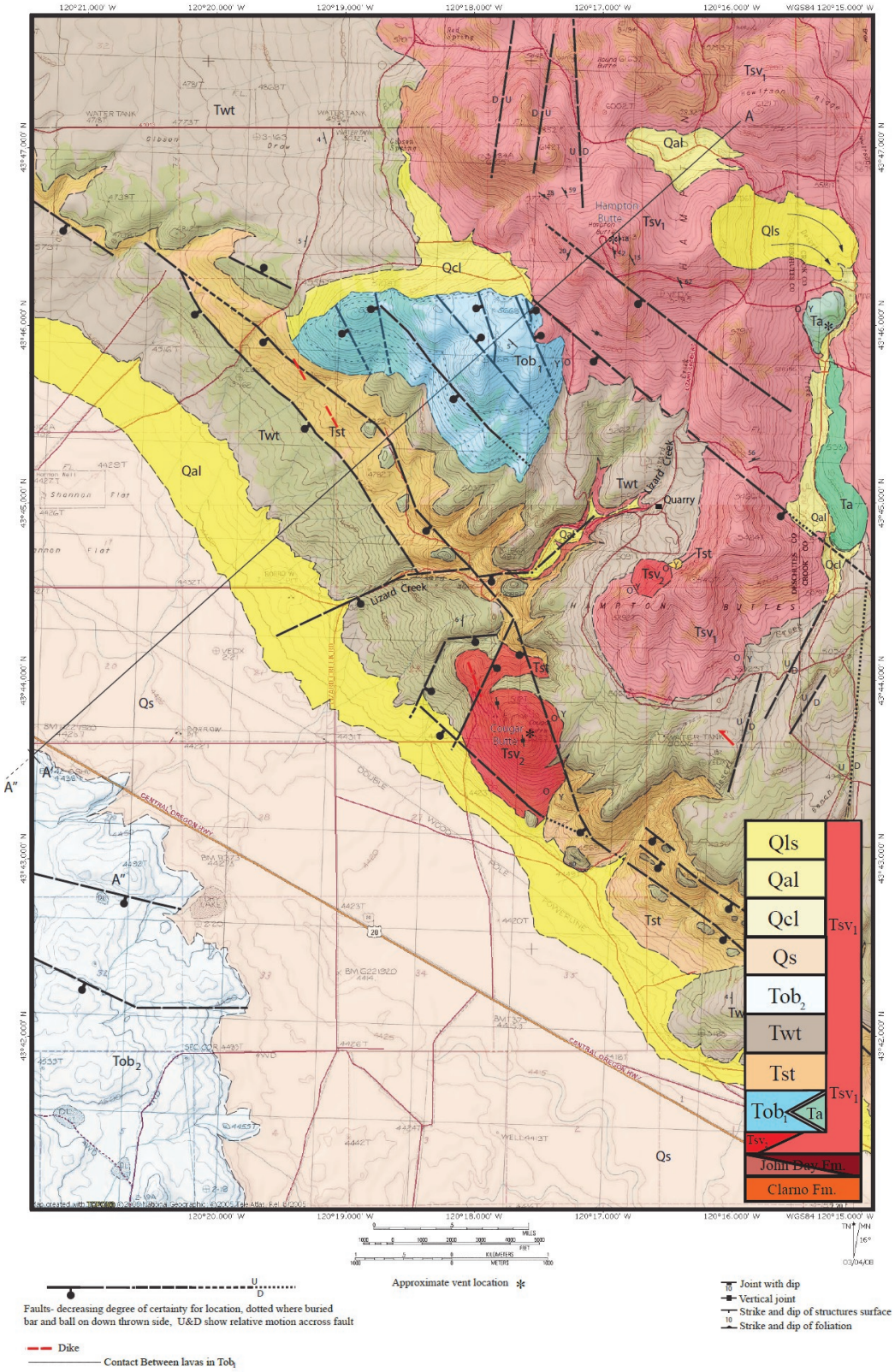

Figure 2.1: Continued

ters in diameter and rises nearly six hundred meters above the adjacent High Lava Plains 59 km east- southeast of Hampton Butte (Figure 1, Plate II). Northwest striking synthetic and antithetic faulting has resulted in northeast to southeast extension of 1.9 kilometers over a distance of 14.6 kilometers (13%) since it last erupted 7.91 Ma, about 24 cm of extension every million years (Figure 2.2). Dry Mountain is bounded and partially covered on the north, east, and west sides by the 7.05 ± 0.01 Ma Rattlesnake Tuff, erupted from a source located a few tens of kilometers to the south (Streck, 1995).

Between Hampton Butte and Dry Mountain (Figure 1.2) Grassy Butte, a low grass-covered cone composed of basaltic andesite scoria separates alkali rhyolite of Potato Hills from Hampton Buttes' Oligocene and younger rock (Figure 1.2). Fault scarps south of Grassy Butte, that offset the scoria, constrain fault timing in the area. East of Hampton Butte, Potato Hills and Hat Butte rise above younger surrounding rock marking a geomorphic and geochronologic boundary to the northern margin of the High Lava Plains (Figure 1.1).

2.2 Hampton Buttes

The following rock unit descriptions correspond to the Geologic Map of Western Hampton Buttes, Plate 1 and Figure 2.1

2.2.1 Rhyodacite (Tsv_1)

:The rhyodacite of Hampton Butte is the oldest rock in the area known as Hampton Buttes. The 30.39 (± 0.25) Ma gray to pinkish gray flow layered rock makes up Hampton Butte, Round Butte and Hewitson ridge (Plate 1 and Figure 2.1). North of Round Butte and Hewitson ridge, the rhyodacite abuts volcanic and sedimentary rock of the John Day Formation, which along

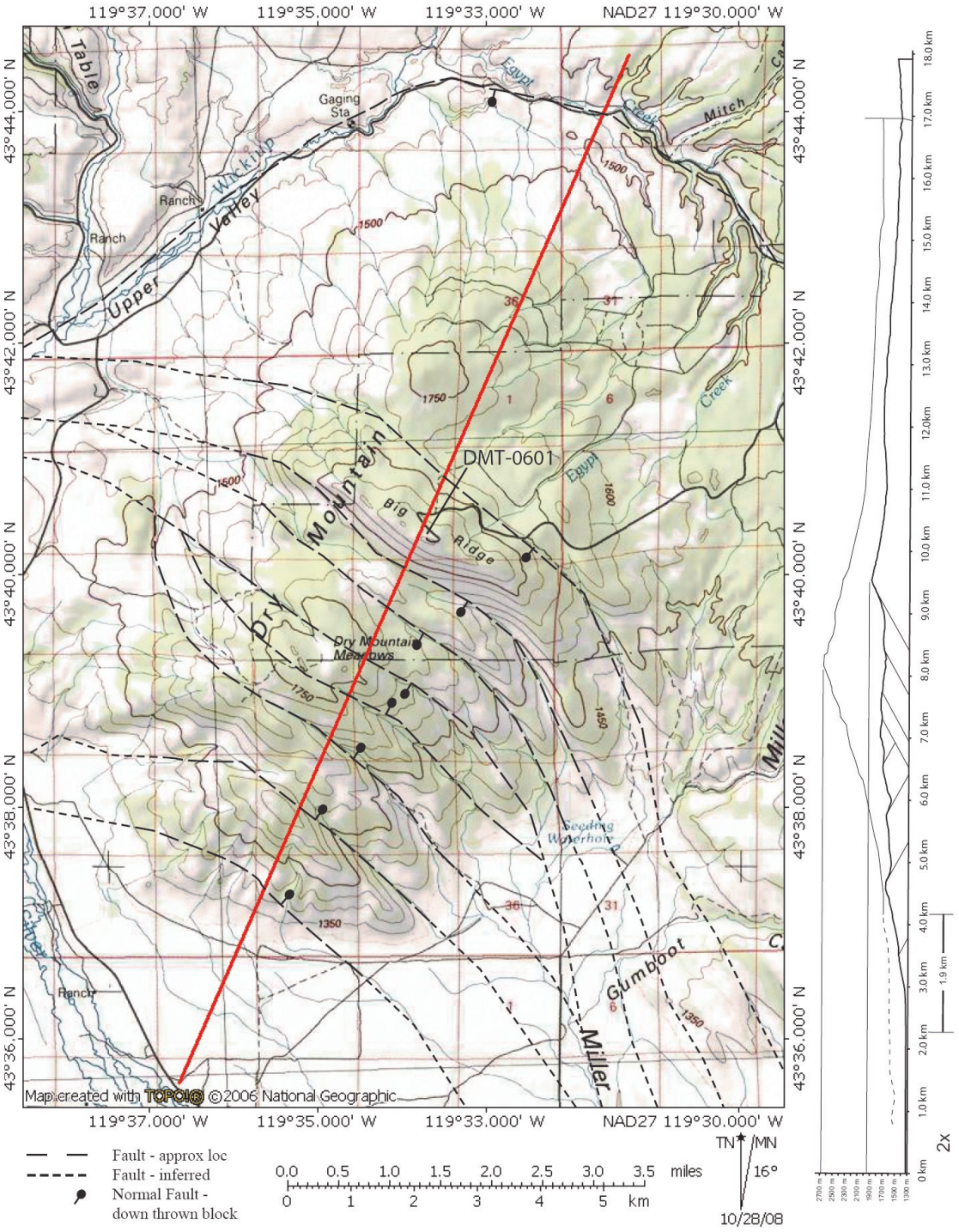

Figure 2.2: Line of the cross section through Dry Mountain. Sample DMT-0601 is from the summit of Big Ridge. The generalized cross section on the right is an illustration of the faulting that divides the mountain and when restored provides an estimate of its original elevation and the amount of extension since the last eruption. Vertical exaggeration of the cross section is 2 x.

with the older Clarno Formation crops out on the periphery of Hampton Buttes and presumably underlies it. On the east side of Hampton Butte, the rhyodacite forms a ridge that turns south and ends short of Cougar butte (Plate 1 and Figure 2.1). Individual flows cannot be mapped and the unit may be the result of an ongoing dome building eruption with individual lobes now covered by a thin veneer of alluvium, colluvium, and aeolian deposits. Breccia from the carapace that formed over the emerging lava remains on the top and much of the sides of the extreme southern lobe and in places has sloughed off of the top and sides of the northern half of the lobe and can be found exposed in several places along Lizard Creek Road (Plate 1 and Figure 2.1). Two large outcrops of rhyodacite on the southern face of Hampton Butte are a result of two northwest striking normal faults that have lowered both outcrops and isolated a small outcrop of rhyodacite adjacent to the basalt (Tob_1, section 2.2.4).

In hand sample the rhyodacite is porphyritic with a finely phaneritic groundmass, reddish brown when weathered, pinkish gray if fresh. Inclusions of subrounded pumice up to 3 cm are present; crystals are aligned sub parallel, the dominant crystals being plagioclase (3-5 mm, 50%), quartz (20%) and sparse pyroxene (2%). Oikocrysts of augite surrounding plagioclase are present but are not common.

Thin section examination revealed acicular crystallites (20µm) in a felty (0.5µm) glassy groundmass that makes up 50% of the thin section . Thirty five percent of the thin section is plagioclase, which can be divided into two nearly equal populations, 0.1- 0.2 mm, and 0.2 - 0.4 mm. The smaller plagioclase is subhedral to

euhedral, zoned, and fractured. Resorbtion is evident and sieve textures are present in the largest laths of this population. New plagioclase has rimmed the sieved crystals. The larger population is euhedral to subhedral with zoning not as evident. Fully one-half of the crystals in this size range are fractured and have a resorbed and sieved texture. Clinopyroxene (5%) is present in the section up to 0.8mm in length, euhedral to subhedral, granular, and fractured, with reaction rims of leucoxene. Clinopyroxene rimmed with uralite appears as anhedral grains that were once part of a larger crystal. Sparse hornblende (<1%) is rimmed by plagioclase, pyroxene, and ilmenite. Magnetite (2%) is present in the embayed and sieved plagioclase as well as in the groundmass, reaching lengths up to 0.4 mm. Anhedral quartz is 7% of the thin section (Figure 2.3).

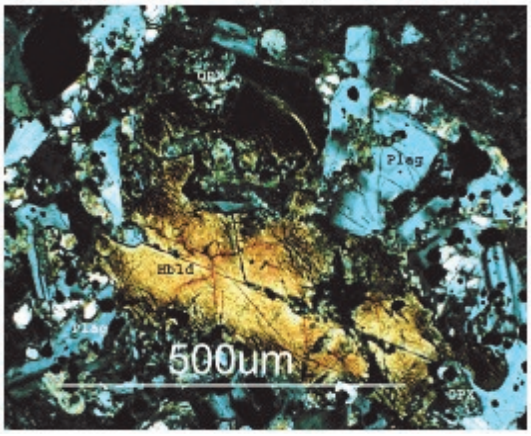

Figure 2.3: Photomicrograph of Hampton Butte hornblende surrounded by plagioclase, ilmenite, and clinopyroxene (HTB-0501).

2.2.2 Dacite (Tsv_2): Dacite can be found in two places at Hampton Buttes, at Cougar Butte and at a small remnant dome north of Cougar Butte on the west side of the ridge of rhyodacite that extends south from Hampton Butte. When viewed from above, the small remnant dome is in the center of a hollow, which defines the ground level extent of the eroded glassy carapace that once shrouded the core of the dome.

Weathered samples of the dacite of Hampton Buttes are sandy, light yellowish tan to pink in color; fresh samples are light greenish gray. Hand samples are fine-

grained holocrystalline, porphyritic with crystals to 0.4mm for hornblende or biotite and to 0.2 mm for quartz and plagioclase. Plagioclase makes up about 90% of the rock followed by 2% biotite, 6% hornblende and 2% or less accessory dark minerals. Samples examined from the small dome north of Cougar Butte are more altered than those at Cougar Butte, but retain enough of the texture and fabric to determine that they are the same unit.

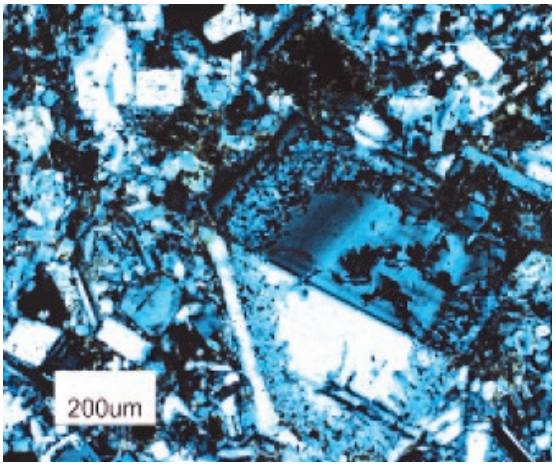

Figure 2.4 : Overgrowth of new plagioclase on older crystal from Cougar butte Sample number HTB-0511.

Plagioclase, as fractured and altered phenocrysts up to 1mm, makes up 8% of the thin section. As part of the groundmass, plagioclase averages 0.1mm, is anhedral, and for the most part untwinned. Sparse magnetite is present and sericite, a result of plagioclase alteration separates and rims the laths. Larger phenocrysts of plagioclase display an overgrowth of new plagioclase on a crystal that had already undergone some alteration. Hornblende is present to 4 mm when lath-like and 2mm when lens shaped, both have reaction rims (Figure 2.4).

2.2.3Andesite (Ta): Hand samples of the andesite are dark gray when fresh and medium gray when weathered. A fine-grained groundmass of plagioclase is punctuated by glomerocrysts of enstatite and augite with laths of plagioclase.

A thin section reveals a felty groundmass of subhedral plagioclase laths averaging between 0.4 and 0.6mm with anhedral grains of pyroxene and olivine scattered

among them. Glomerocrysts are 2% of the thin section with total olivine, augite and enstatite content estimated as 4% each. Magnetite and ilmenite are 2% of the section with plagioclase as the remaining 86% (Figure 2.5).

Figure 2.5: Glomerocryst of clinopyroxene, orthopyroxene, and plagioclase surrounding a small olivine crystal in andesite (HTB-0623).

2.2.4 Basalt (Tob_1): A fresh, light to medium gray, basalt consisting of 4 flows forms a small plateau at the southern base of Hampton Butte that dips five degrees to the south (Figure 2.1 and Plate 1) . These fine grained, ophitic, and glomerophyric basalts are essentially chemically, macroscopically, and microscopically the same. In hand sample, the basalt contains about 10% plagioclase from 3 to 4 mm, honey colored olivine up to 2 mm, and 5 mm diameter glomerocrysts of plagioclase, clinopyroxene, and olivine. Microscopic examination of a thin section shows that the basalt is about 50% plagioclase of which

Figure 2.6: Flow layered basalt at the base of Hampton Butte, view is looking southwest from southeast base of Hampton Butte.

80 % is 0.2 to 0.4mm long, euhedral to anhedral, zoned and in laths. Augite is 20% of the thin section and both poikilitically encloses laths of plagioclase and is part of the glomerocrysts. Seventy five percent of the augite that encloses plagioclase is 0.4 mm - 1.5mm, anhedral, and the remaining 25% that exist are part of the glomerocrysts with plagioclase. Olivine that makes up 15% of the hand sample is partially altered to iddingsite and appears in both the groundmass and as altered anhedral crystals (Figure 2.7).

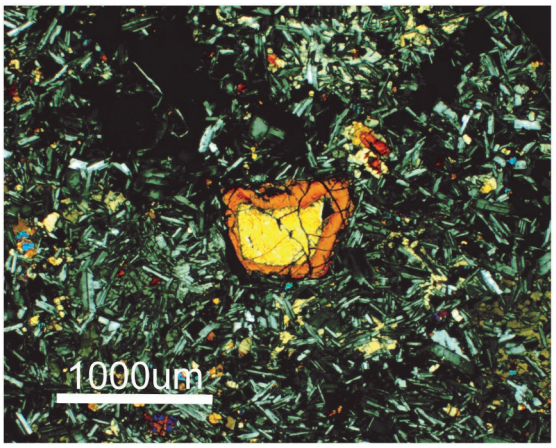

Figure 2.7: Photomicrograph from a thin section of the Basalt at the base of Hampton Butte (Sample HTB-0523). Iddingsite rim on olivine with augite surrounding plagioclase microlites.

2.2.5 Hampton Tuff (Twt): Much of the area mapped is blanketed by a variably welded ash-flow tuff, the full extent of which has not been determined. The tuff banks on some older units and covers others. Measured thickness for the tuff ranges from 4 meters, at a quarry on Lizard Creek road, to less than 30 cm for a partial section 300 meters east of a pumice quarry also located just off Lizard Creek road. The welded tuff is cut by faults that define the southern limit of the area known as Hampton Buttes, dropping it to the level of the small basin adjacent to it. The tuff also extends to the east, west, and south beyond the mapped area for an undetermined distance.

At the quarry on Lizard Creek Road, the tuff can be divided into seven facies. First, a dark gray to black non-welded basal vitrophyre containing sparse fractured

plagioclase and quartz (to 1 mm), fine grained light colored angular lithic fragments (to 3 mm) and flattened as well as angular pumice (to 10 mm). Total lithic, plagioclase, quartz and pumice fragments are estimated to be 5 % of the rock. Topping the basal vitrophyre is a partially welded second layer not visible in the photograph but exposed in other locations within the quarry (Figure 2.8 and 2.9). This second facies is partially welded and medium gray colored (weathered and fresh). Flattened pumice up to 2 cm is present. The larger pumice is sub rounded and many have a sub angular cross section. Smaller flattened pumice in cross section appears needle-like. Small, dark and light, fine-grained lithic fragments are sparse; pyroxene (1% to 2mm), quartz (2% to 1mm), and plagioclase (3% to 3 mm) total about 6% of the rock.

The third facies is a densely welded, 0.8-meter-thick section with blocky jointing and fiamme. Fiamme coarsen up section and terminate in a 12-cm-thick platy layer containing flattened pumice and compacted ash with fewer lithic and crystal fragments than layer two. This facies weathers to a brownish pink color and is dark gray-green when fresh. Plagioclase laths (to 3 mm) and flattened pumice (to 4 mm) share a noticeable sub parallel arrangement that contains sparse euhedral sanidine (to 1 mm), fractured quartz (<1 mm) and blocky orthopyroxene (to 1 mm). Some of the small microscopic dark minerals in the groundmass (< 0.5 mm) produce a bronze-like luster and are most likely enstatite. Some voids are partially filled with yellowish and reddish brown secondary minerals. Lithic fragments are rare in this

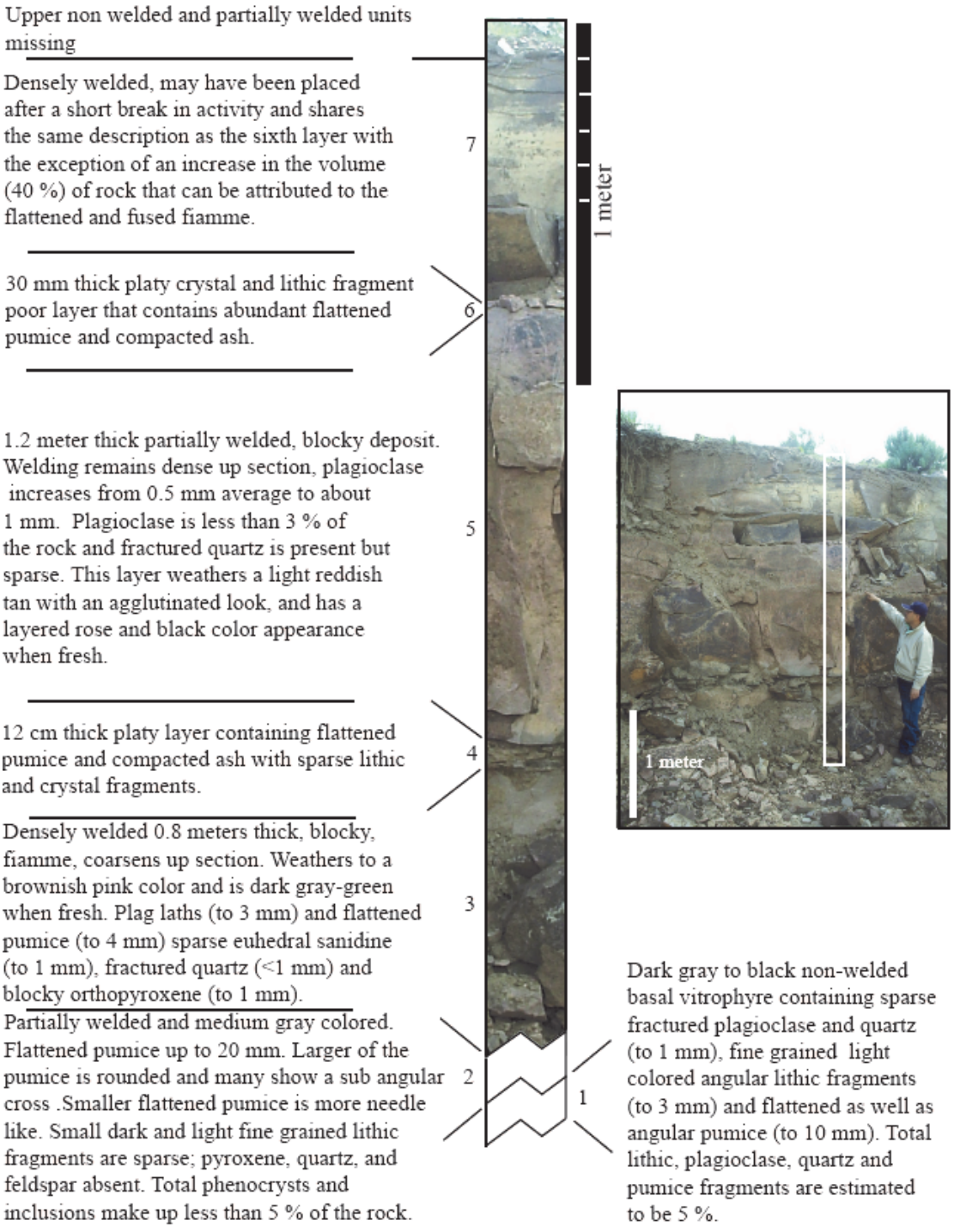

Figure 2.8: Section of the Hampton tuff at a quarry on lizard Creek road. Sample HTB -0701 from layer 7 returned a date of 3.7 (± 0.5) Ma. Layers 1 and 2 are not exposed where the photograph was taken but are found in other parts of the quarry. The Biological unit is Manggon Abot.

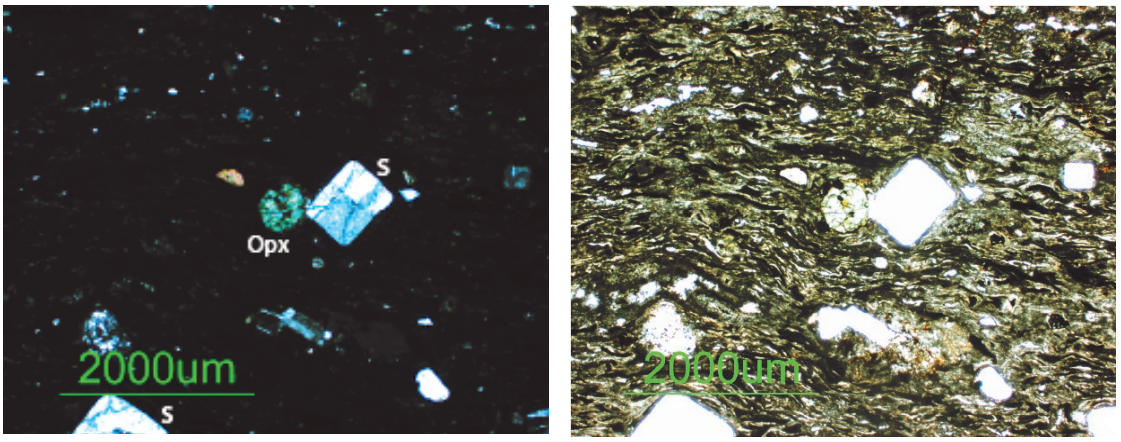

Figure 2.9: Photomicrograph of densely welded Hampton Tuff (HTB-0701) at the quarry on Lizard Creek road. Left, crossed polars reveal low sanidine (s) and opx phenocrysts in an opaque background with fragments of sanidine. Right, uncrossed polars expose the details of the densely welded groundmass.

layer. Coarse, red, vesicular, weathered pumice is small and round yielding the appearance of scoria.

The fifth facies is 1.2 meter thick, partially welded and massive with blocky joints. It includes a cap of made of a thin (3 cm) platy crystal and lithic fragment poor layer that contains abundant flattened pumice (facies 6). Welding remains dense up section in the layer and plagioclase increases from 0.5 mm average to about 1 mm. Plagioclase is less than 3 % of the rock and fractured quartz is present but sparse. Flattened and fused fiamme are 25 % of the rock. This facies weathers a light reddish tan with an agglutinated look, and has a layered rose and black color appearance when fresh. Densely welded facies seven may have been placed after a short break in activity and shares the same description as the sixth facies with the exception of an increase in the volume (40 %) of rock that can be attributed to the flattened and fused fiamme.

Capping layers of less densely and non welded rock are missing at the quarry site. The multiple layers of dense welding indicate that this ignimbrite was emplaced fitfully. There is no evidence for weathering or erosion between welding units and I interpret this ignimbrite to be from a single eruption with 2 cooling units. The lower cooling unit (Facies 1-5) includes a 12 cm thick, flattened pumice and ash section that responded differently to welding and compaction than the compacted pumice and ash zone at the base of the upper cooling unit. I interpret facies 6 as being deposited during or immediately following a short break in the robust phase of the eruption , followed by deposition of a new cooling unit.

Neither the age of the Tuff of Espeland Draw (3.7 ± 0.6 Ma, K/Ar) or the Hampton Tuff (3.8 ± 0.6 Ma, $^{40}Ar/^{39}Ar$) correlates with the much older ~6.85 Ma (Streck and Grunder, 2007) Buckaroo Tuff. The age of the Hampton Tuff overlaps that of Frederick Butte, the likely source region, as proposed by Johnson, (1998) The distribution of this tuff, its age and its mineralogical characteristics, correlate with the tuff of Espeland Draw (Johnson, 1998). I also correlate the tuff in the Hampton area described by Walker (1981) , the Hampton Tuff, and Tuff of Espeland Draw to be the same unit.

The much larger 7.05 Ma Rattlesnake Tuff of eastern Oregon has been well documented (cf. Streck and Grunder, 1995, Streck and Grunder, 2007) and a schematic vertical distribution of welding facies resulted from these efforts. The single cooling unit section of Streck and Grunder (1995) compares favorably to the 2 cooling units of the Hampton Tuff found at the quarry on Lizard Creek Road (Figure

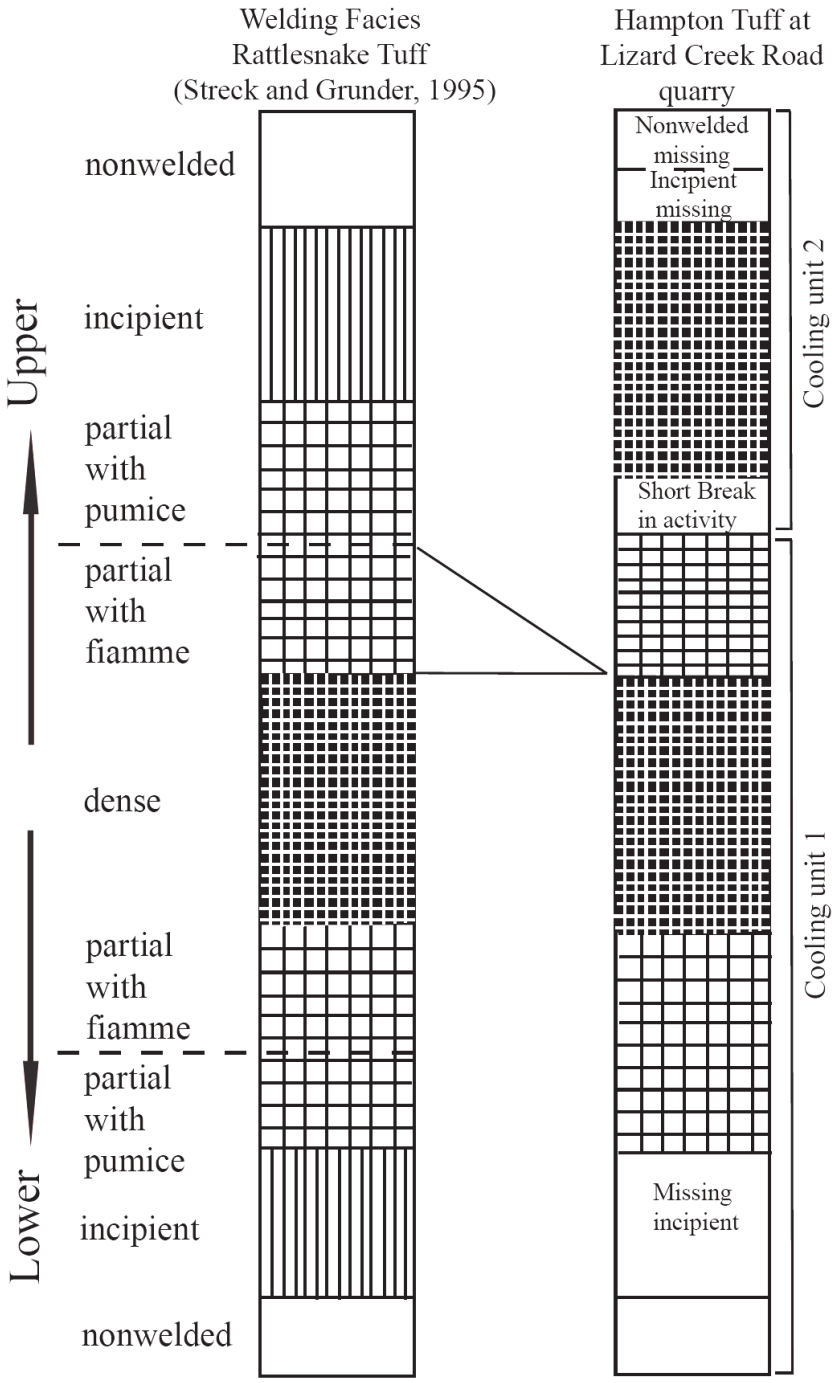

Figure 2.10: Single cooling unit section of Streck and Grunder (1995) compared to the 2 cooling units of the Hampton Tuff found at the quarry on Lizard Creek Road. The missing incipient layer in the lower cooling unit may exist at the quarry but not be exposed. The cooling unit 2 nonwelded and incipiently welded facies have most likely been eroded at this location. A general congruity between the section exists until an apparent change in volcanic activity after emplacement of the densely welded facies in cooling unit 2.

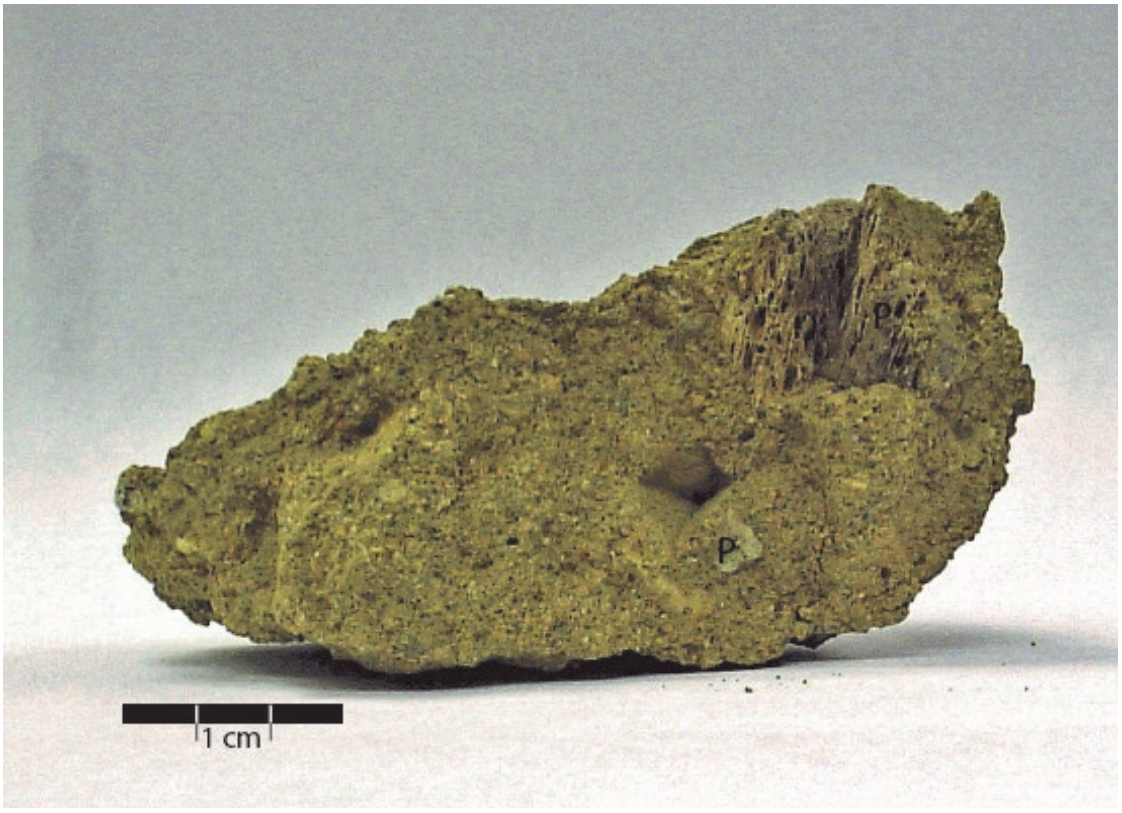

Figure 2.11: Tertiary Silicic tuffaceous sediment is found along Lizard Creek Road and to the east and west of the road where faulting has exposed the deposit and weathering has reduced most outcrops to the consistency of a loose soil. P=pumice

2.10). Missing facies at the quarry can be attributed to erosion at the surface or, in the case of the lower cooling units' incipiently welded facies, it may not be exposed. A general congruity between the section exists until an apparent change in volcanic activity after emplacement of the densely welded facies in cooling unit 1, causing a partially welded facies to be placed before a short break in activity. After which a sudden resumption of more robust activity resumed deposition consistent with that presented by Streck and Grunder (1995) (Figure 2.10).

2.2.6 Tertiary siliceous tuffaceous sediments (Tst): A pale yellow to tan semi- to poorly consolidated tuffaceous sandstone lies stratigraphically below the Hampton

Tuff. Included in the sediments are dark angular to sub-rounded lithic fragments less than one centimeter long, but rare fragments as long as 4 cm can be found. Angular to sub rounded pumice fragments up to 1.5 cm are present (Figure 2.11). Sand-sized lithic fragments, quartz, and obsidian can also be seen with a hand lens. This unit appears to be a well indurated mixture of pyroclastic fall deposits re-worked by lacustrine or fluvial activity. Outcrops of the tuffaceous sediment are found along Lizard Creek Road and to the east and west of the road where faulting has exposed the deposit and weathering has reduced it to the consistency of a loose soil.

2.2.7 Quaternary alluvium, colluvium, and sediments (Qs, Qcl, Qal, Qls): Quaternary deposits at Hampton Butte consist of small alluvial deposits in drainages where natural and man made barriers cause a change in stream velocity, resulting in the deposit of material carried by the stream or periodic floodwaters through normally dry gullies. Steep slopes and scarps are covered with a veneer of colluvium and aeolian deposits that markedly thin towards higher elevations, forming a thick gusset of colluvium at their base. Deposits are mapped only when they are significant enough to hide underlying structure or petrology, prohibiting accurate interpretation.

The following rock descriptions refer to locations outside the mapped area at Hampton Buttes, their locations are shown on Plate II and Figure 1.1 .

2.3 Basalt of Dry Mountain: The analyzed sample, collected from Big Ridge summit, is platy in outcrop, fine-grained light to medium gray (when fresh) rock that weathers to dark gray. Oval shaped vesicles up to 1 centimeter, sparsely distributed through the rock, are oriented long axis vertical in outcrop. Plagioclase, when

euhedral and visible with a hand lens, is less than 0.5 millimeters. Honey colored olivine are to 0.5 mm, and in glomerocrysts to 3 millimeters comprising less than 2% of the rock. Subhedral fractured microlitic laths of plagioclase averaging 400 to 500 µm with no evidence of resorption or zoning are 55 % of the rock in thin section (Figure 2.15). Twenty percent of the thin section is subhedral to anhedral orthopyroxene up to 800 µm with a birefringence of .007 (enstatite). Iddingsite and chlorophaeite alteration is present along cracks in olivine that is mantled by enstatite; the latter is a result of reaction between olivine and melt (Figure 2.16). Olivine is 15% of the thin section as phenocrysts to 180 µm and anhedral grains in the groundmass. Groundmass is determined to be 8% of the slide. Opaque minerals, approximately 2% of the slide are Fe-Ti oxides.

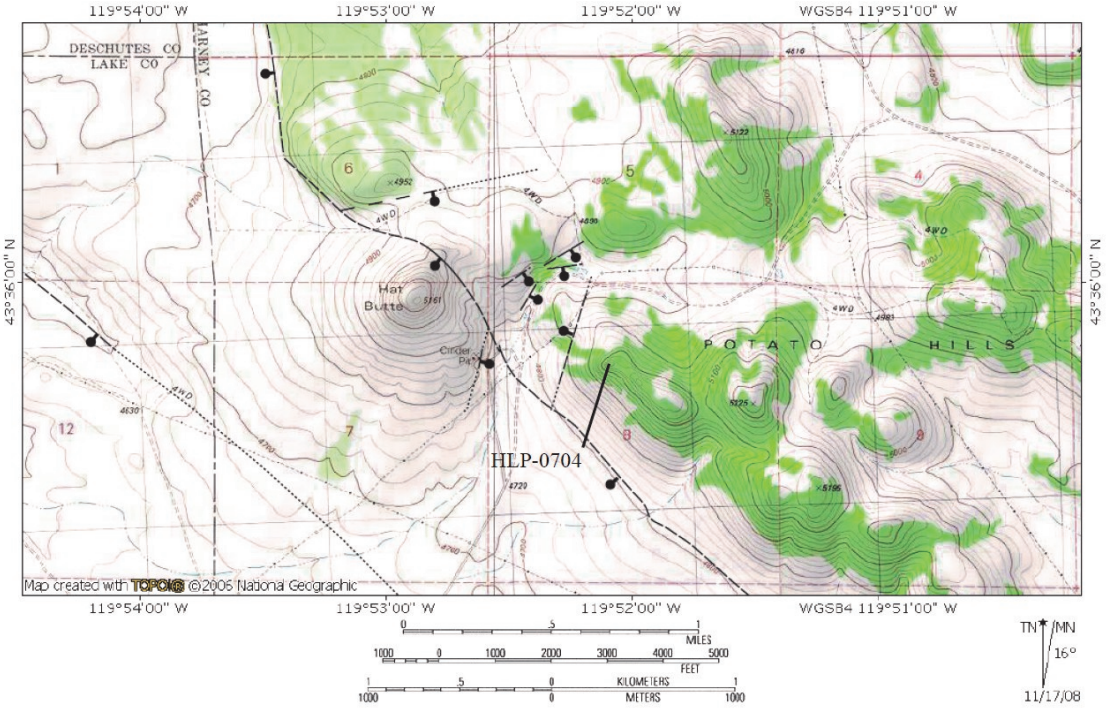

Figure 2.12: Map of the area surrounding Hat Butte showing faults and sample location.

2.4 Potato Hills and Hat Butte: Adjacent to and east of Hat Butte are Potato Hills which are bounded on their south side by a rhyolite-capped ridge formed by a normal fault that also cuts the north side of Hat Butte (Figure 2.12). Normal faults bounding Hat Butte on the east and northwest have lowered the rhyolite outcrops (forming a ring-like structure 150 meters in diameter on the top of the butte) twenty meters below the same rhyolite to the east.

In hand sample the Potato Hills ridge rock is highly weathered, reddish brown, to gray and black in outcrop, gray to pink when fresh, hypocrystalline, commonly spherulitic, and abundantly flow layered. Phenocryst phases are subhedral quartz (to 3 mm) and plagioclase (to 2 mm). Each phenocryst phase makes up less than 3% of the rock (Figure 2.13). Age relationships are discussed in chapter 4. In

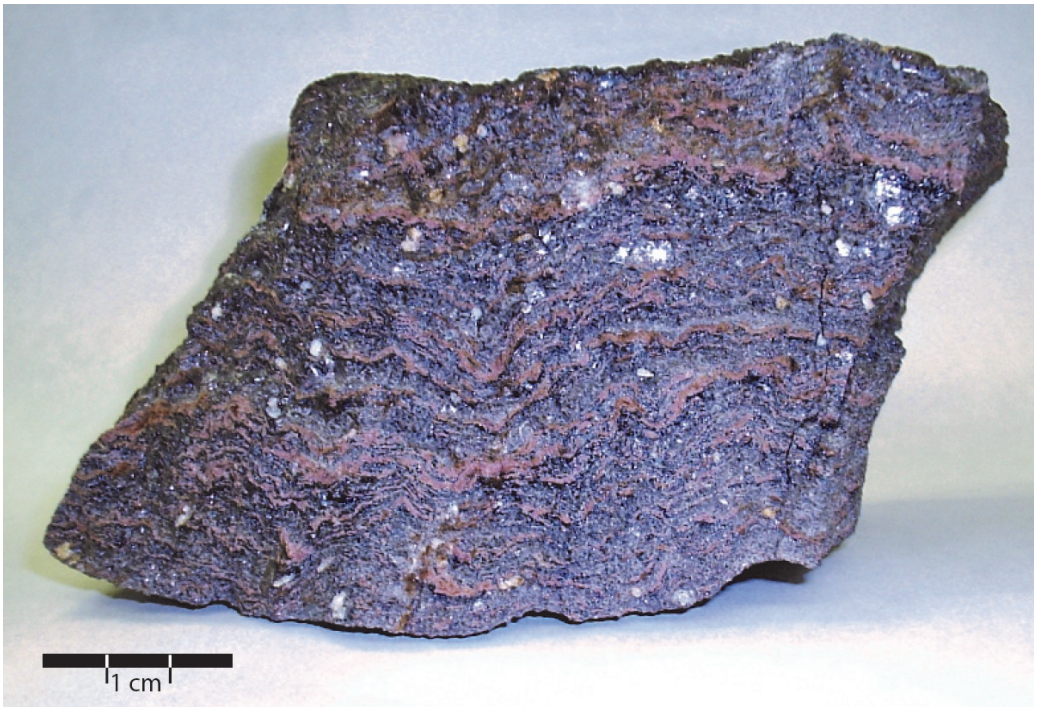

Figure 2.13: Flow layering and clay alteration of Potato Hills rhyolite (HLP-0704). Visible phenocryst phases are quartz and plagioclase. Upper 25% of the rock is the weathered surface.

thin section flow-aligned microlitic plagioclase averages 100 mm in a glassy groundmass with pink to red clay alteration products encircling or separating areas of unaltered glass. I interpret the rhyolite of Potato Hills to be a flow and dome complex of related to High Lava Plains volcanism.

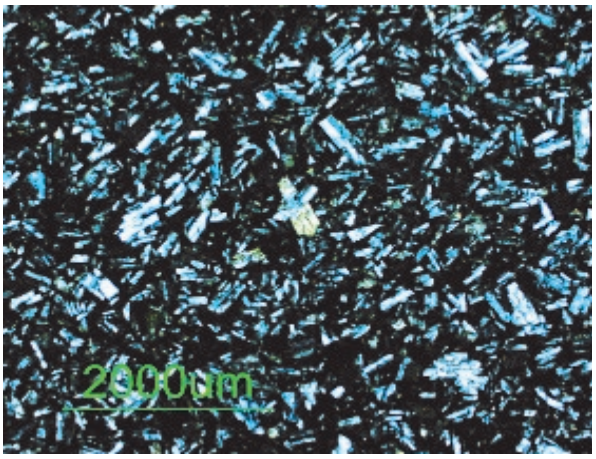

Figure 2.14: Photomicrograph of the felty plagioclase and an enstatite phenocryst (center) from sample DMT-0603

Normal faults exposed in a cinder pit on the west side of Hat Butte strike north eighteen degrees east, dipping 80 degrees to the east. The angle of repose for the cinder layers in the pit is 40 degrees. The rhyolite capping Hat Butte constrains the age of the underlying basaltic structure to > 6.54 Ma.

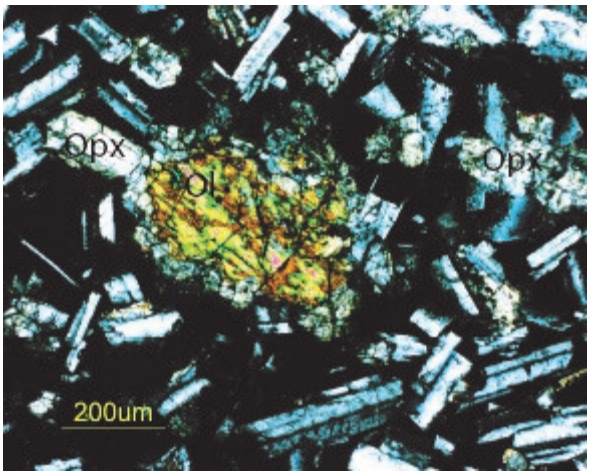

Figure 2.15: Photomicrograph of olivine with iddingsite (yellow-orange) and chlorophaeite (green) alteration along cracks. Orthopyroxene mantles the olivine as well as appearing as sub to anhedral crystals in the plagioclase dominated sample DMT-0601.

2.5 Basaltic andesite of Grassy Butte: Grassy Butte is a low, broad basaltic andesite scoria cone having a profile more like a shield volcano than the cone shaped edifice of scoria usually associated with this type of eruption. Located thirty kilometers east southeast of Hampton Butte and directly north of Glass Buttes, Grassy Butte sits in the midst of normal faults that

are deviating from the northwest to south-east trend of the Brothers Fault Zone to a more north northwest trend, consistent with Basin and Range normal faulting. Grassy Butte is the only vent between Hampton Buttes and Hat Butte (Plate II). Mingled with the oxidized (red) scoria that comprises 99 % of the butte are blocks of un-oxidized (black) scoria.

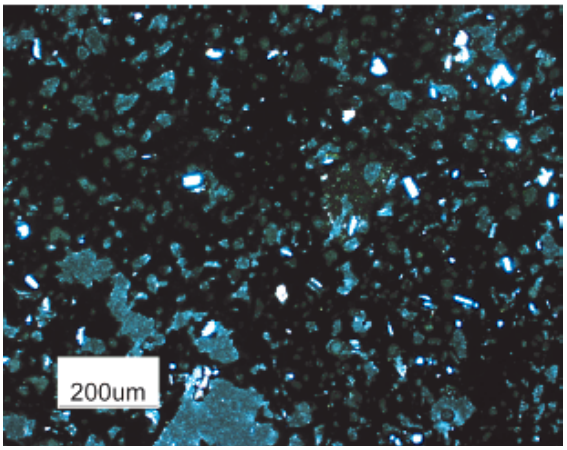

Figure 2.16: Sparse plagioclase and augite in the glassy groundmass of Grassy Butte sample GB-0601. Vesicles are lighter gray areas.

Hand samples collected are black with spherical vesicles to 2 mm and elongated pipe like vugs to 3 cm. Plagioclase to 3 mm is easily seen against the dark background of the sample and is 15 % of the rock. A sparse dark mineral can be seen but is not identifiable in the hand sample.

In thin section, this basaltic andesite rock (Table 3.2) plagioclase is 2% of the slide with augite being less than 1%. of the phenocrysts. The remaining rock consists of a glassy groundmass with 30% vesicles (Figure 2.16).

CHAPTER THREE: GEOCHEMISTRY AND GEOCHRONOLOGY

3.1: Introduction

Eighty samples were collected from Hampton Butte and east to Dry Mountain for the purposes of geochemistry, geochronology, petrographic examination, and stratigraphic correlation. Whole rock chemical analyses, obtained for sixteen key samples are used for regional comparisons and geochemical modeling. Nine of the samples chosen for chemical analysis were dated using the $^{40}Ar/^{30}Ar$ method.

3.2 Geochronology

3.2.1 Methods: Nine samples, selected on a basis that would allow the determined ages to help constrain episodes of volcanism and faulting, were dated by the $^{40}Ar/^{39}Ar$ method at the Oregon State University Noble Gas Mass Spectrometry Lab using a Mass Analyzer Products MAP 215-50 rare-gas mass spectrometer (Table 3.1). Both single crystal laser fusion, using a Merchantek carbon-dioxide continuous-fire laser, and incremental heating using a double-vacuum Heine low-blank resistance furnace were used to obtain gas from whole rock or plagioclase samples. The Noble Gas Mass Spectrometry Laboratory employs the ^{40}Ar-^{39}Ar dating method to determining the crystallization age of geologic material using methods described by Duncan and Hogan (1993). Data is calculated using ArArCalc, an Excel® spread sheet developed by Koppers (2002) (Appendix 1). In all cases the plateau age, 3 or more consecutive steps with over 50 % of the total ^{39} Ar released, is chosen as the preferred age and is reported in the text to 2 sigma.

3.2.2 Results

The first run of the Potato Hills sample produced an age of 78.44 ± 8.43 Ma, the large error is attributable to low a percentage of radiogenic ^{40}Ar (Duncan and Hogan, 1994) released during incremental heating of plagioclase (Appendix 1). A rerun of the sample yielded an age of 6.52 ± 0.07 Ma, which I take to be the correct age.

Samples from Hampton Buttes yielded ages of 30.39 ± 0.25 Ma for the rhyodacite dome named Hampton Butte, and the 1 - 1.5 million year younger 28.63 ± 0.34 Ma for Cougar Butte, both with good concordance between plateau and isochron ages (Table 3.1) The ages and composition of these units are consistent with

Table 3.1: Results of geochronology done at the Oregon State University Noble Gas Mass Spectrometry Lab. Locations are given in Table 3.2 and 3.3. Detailed results are in Appendix 1.

					Plateau			Normal Isochron		
Sample	Location	Rock Type [b]	Material Dated [c]	Heating Device [d]	Age, Ma	±2σ	Steps	Age, Ma	±2σ	$^{40}Ar/^{36}Ar$. Intercept
HLP-0704*	Potato Hills	Ar	P	F	79.44	8.43	14	96.63	24.16	293
HTB-0501	Hampton Butte	Rhyodacite	P	F	***30.39***	0.25	8	30.26	0.3	312
HTB-0613	Cougar Butte	Dacite	P	F	***28.63***	0.34	5	28.58	0.55	297
HTB-0523*	South side base Hamptom Butte layer 3	Basalt	WR	F	12.82	1.25	10	11.84	2.21	297
DMT-0601	Dry Mountain	B	WR	F	***7.91***	0.12	5	8	0.42	291
HTB-0623	Hampton Buttes andesite	Andesite	WR	F	***7.81***	0.12	9	7.79	0.17	297
HTB-0631	South-side base of Hamptom Butte layer 1	Basalt	P	L	***7.75***	0.12	6	7.74	0.14	299
HTB-0523	South side base Hamptom Butte layer 3	Basalt	P	F	***7.67***	1.31	7	7.35	1.77	299
HLP-0704a	Potato Hills	Ar	P	L	***6.52***	0.07	9	6.54	0.14	295
GB-0701	Grassy Butte	Ba	WR	F	***4.18***	0.14	8	4.1	0.29	298
HTB-0701	Hampton Butte Tuff from quarry, Lizard Creek Rd.	Rt	P	L	***3.8***	0.16	8	3.7	0.16	310

[a] Bold italic typeface, preferred age.
[b] Ar, Alkali rhyolite; B, basalt; Ba, Basaltic andesite; A, andesite; D, dacite; R, rhyodacite; Rt, rhyolite tuff.
[c] P, plagioclase; WR, whole rock
[d] F, furnace; L, laser *First analysis

correlation to the John Day Formation to which I assign them. Previous work without the benefit of geochronology or geochemistry had assigned Hampton Butte to the Clarno Formation (Bowman, F.J., 1940).

Sample DMT-0601, from the summit of Dry Mountain, returned an age of 7.91 ± 0.12 Ma with plateau age concordant with the isochron age. Basalts that lap onto the southern side of Hampton Butte have ages of 7.75 ± 0.12 Ma (HTB-0631) and 7.67 ± 1.31 Ma (HTB-0523). HTB-0523 returned an age of 12.82 ± 1.25 Ma on its first run, unusually high for basalt of that region (cf. Jordan et al., 2004). The unusually old age compared to other basalts in the area and the large error brought suspicion about the validity of the data and prompted a re-analysis. Both analyses of the HTB-0523 rock have large errors (Table 3.1), also attributable to a low percentage of radiogenic ^{40}Ar (Duncan and Hogan, 1994) released during incremental heating of whole rock (HTB-0523) and plagioclase (HTB-0523) (Appendix 1). The amount of radiogenic ^{40}Ar produced during the second run is significantly greater than the first run and ^{39}Ar produced shows better consistency across the steps compared to the first run (Appendix 1), therefore the second run is the preferred, though not ideal, result. The basalts in this study have ages clustered close to a 7.7 Ma maximum in the mode of age probability for ^{40}Ar - ^{39}Ar ages determined by Jordan (2004) for the High Lava Plains. These data reinforce the existence of a ~ 8 Ma pulse of regional basaltic volcanism. (Jordan and Grunder, 2004). Although not basalt, a sample from a small vent that produced andesite 2 km east of Hampton Butte (Plate 1), yielded an age of 7.81 ± 0.12 Ma that coincides with the pulse of basalt.

There appears to have been a hiatus in volcanic activity on the High Lava Plains near Hampton Buttes between 8 and ~ 4 Ma. Volcanism recommenced with the eruption of Grassy Butte 4.18 ± 0.14 Ma. This is only slightly older than the 3.8 ± 0.16 Ma age of the Hampton Tuff (Table 3.1) and consistent with the on-lapping relationship with the 7.8 Ma basalts (Tob_1)at the base of Hampton Butte. 23 km SSE of Hampton Butte is Frederick Butte, a dacite and andesite dome complex, the presumed source of the Hampton Tuff. At 3.9 ± 0.4 Ma Frederick Butte (walker, 1981), as well as Grassy Butte and the Hampton Tuff, have ages consistent with the passage of silicic volcanism after a break in volcanism between ~8 and ~4 Ma (Jordan, 2004). The youngest activity on the High Lava Plains close to Hampton Buttes is the 2.3 ± 0.15 Ma (Jordan 2004) basalt at Espeland Draw, 11 km southwest of Hampton Butte just out of the mapped area.

3.3 Geochemistry

3.3.1 Introduction: The analyzed samples have a compositional range that spans from basalt to high-silica rhyolite. With the exception of the basalts of Long Barn all samples are metaluminous to mildly peralkaline, silica saturated and subalkaline (Shand, 1927) (Figure 3.1). Of the two groups that the samples can be divided into, the oldest group consists of a cluster of rhyodacite and dacite from Hampton Butte and Cougar Butte, respectively, and the rhyolite of Potato Hills, all older than 30 Ma. Younger volcanic rocks include a cluster of basalts, scattered rhyolites, a basaltic andesite from Grassy Butte, and an andesite from within Hampton Buttes. Overall this suite conforms to the regional pattern of intermediate compositions prior

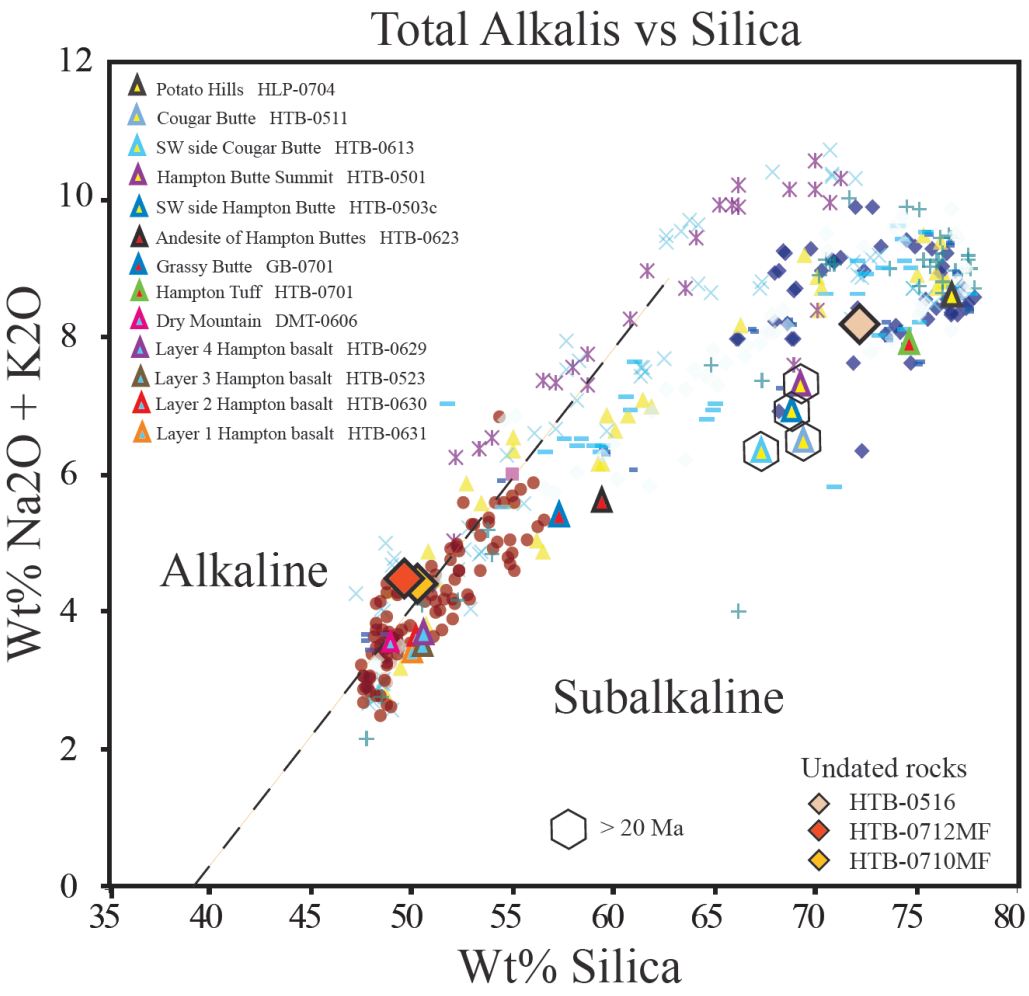

Figure 3.1: TAS plot of samples from the study area compared to samples of the High Lava Plains. See Table 3.2 for data and approximate ages. Other data (differing symbols) from: Walker, 1981, Johnson, 1998, Johnson and Grunder, 2000, Jordan and Grunder,2004, Hart and Carlson, 1987, Hart, 1984, Jordan, et al., 2002, Berri, 1982, Johnson,1984, Langer, 1991, Mathis, 1993, MacLean, 1994, Johnson, 1995, Jordan, 2001, Scarberry, 2007, Ford, unpub., Streck & Grunder , unpub., Iademarco, unpub.

to ~ 12 Ma and strongly bimodal basalt - rhyolite thereafter followed by sparse intermediate activity.

The remainder of the chapter presents methods then focuses on attributes of individual units, presented in stratigraphic order from oldest to youngest.

3.3.2 Methods: Major and trace element compositions were obtained for whole rock compositions by analysis at the Washington State University GeoAnalyti-

cal Laboratory, Pullman Washington. X-Ray florescence (XRF) results were obtained using a ThermoARL Advant'XP+ sequential X-ray fluorescence spectrometer, and ICP-MS results are a result of analysis using a Hewlett-Packard 4500+ ICP-MS, a quadrupole mass spectrometer. A continuing instrument check on internal precision is done by using two standard beads (GSP-1 and BCR-P) run between every 28 unknown samples also providing a check on instrument precision over long periods and within single runs. Accuracy of analyses is estimated in two ways by the lab. One compares values obtained for the same sample with results from another lab using different techniques, and by the scatter around the calibration curve of each element of the standard samples (Johnson et al., 1999) (Appendix 2).

3.3.3 Results

3.3.3.1 Rhyodacite of Hampton Butte (HTB-0501, HTB-0503c) and dacite of Cougar Butte (HTB-0511, HTB-0613): The 30.39 ± 0.25 Ma rhyodacite (Shand, 1927; Macdonald, 1968) of Hampton Butte is represented by two virtually identical samples of subalkaline rock (Figure 3.1). Both samples are enriched in the light rare earth elements (LREE) with only a slight difference in cerium, with a small separation in the heavy rare earth elements (HREE) (Figure 3.2). Of the samples collected and analyzed the Hampton Butte summit sample (HTB-0501) has the lowest sodium and high potassium relative to the sample from the south side. Major elements plotted against silica show a similarity with the trend of samples collected and analyzed, with the exception of lower sodium in the sample from the summit of Hampton Butte (HTB-0501).

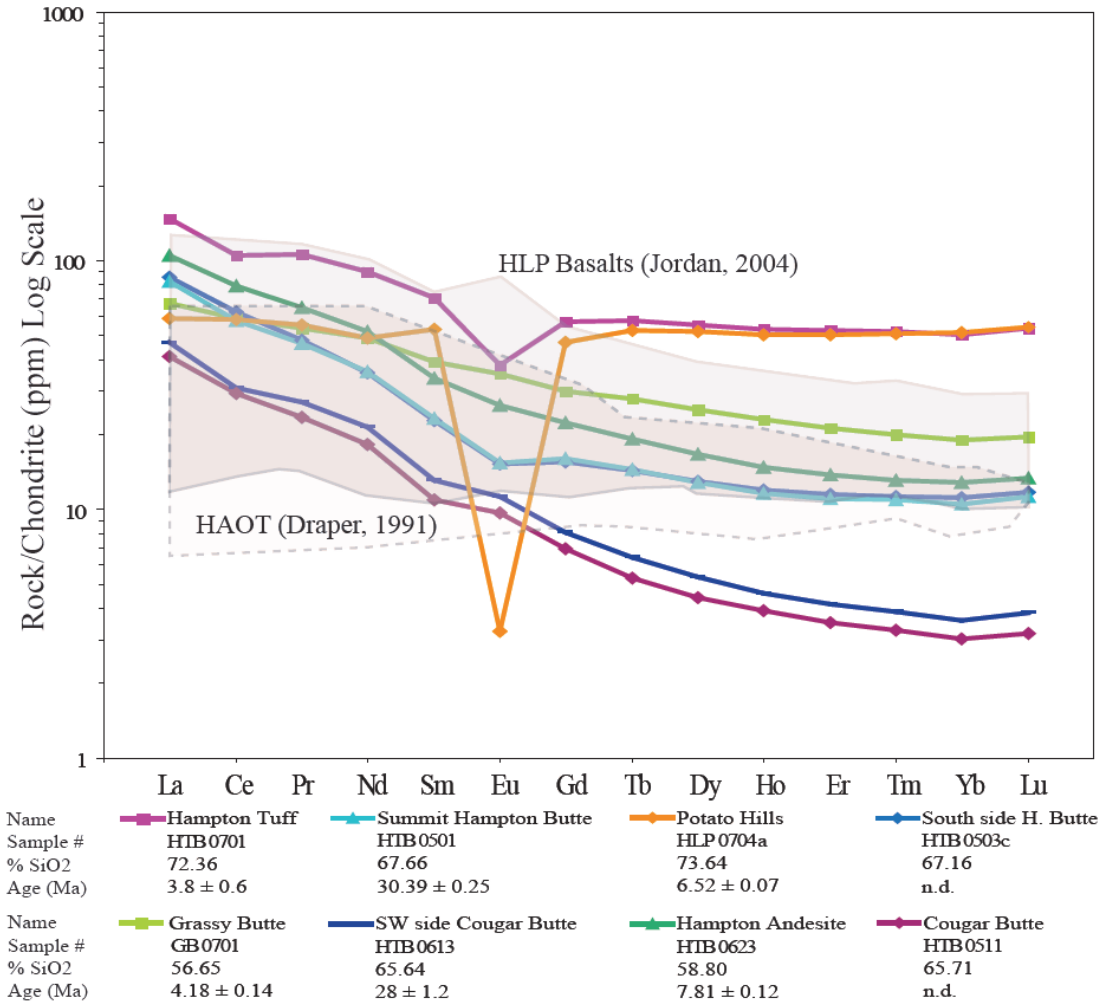

Figure 3.2: Rare earth element plot comparing basaltic andesite and higher silica rocks collected along the northern margin of the High Lava Plains. The two Cougar Butte samples show slight positive europium anomalies. The remaining samples show varying degrees of plagioclase involvement in the removal of europium. Darkest gray region is the overlapping regions of Jordan and Draper.

The less silicic summit sample from Cougar Butte (HTB-0511) contains less of the incompatible elements barium and rubidium and compatible strontium compared to HTB-0613, a sample from the south side of Cougar Butte (Table 2 and 2a). Hampton and Cougar Butte samples form a cluster with respect to most element plots and are depleted in potassium and barium compared to the trend of younger High Lava Plains rocks. The Cougar Butte samples are nearly identical in major element

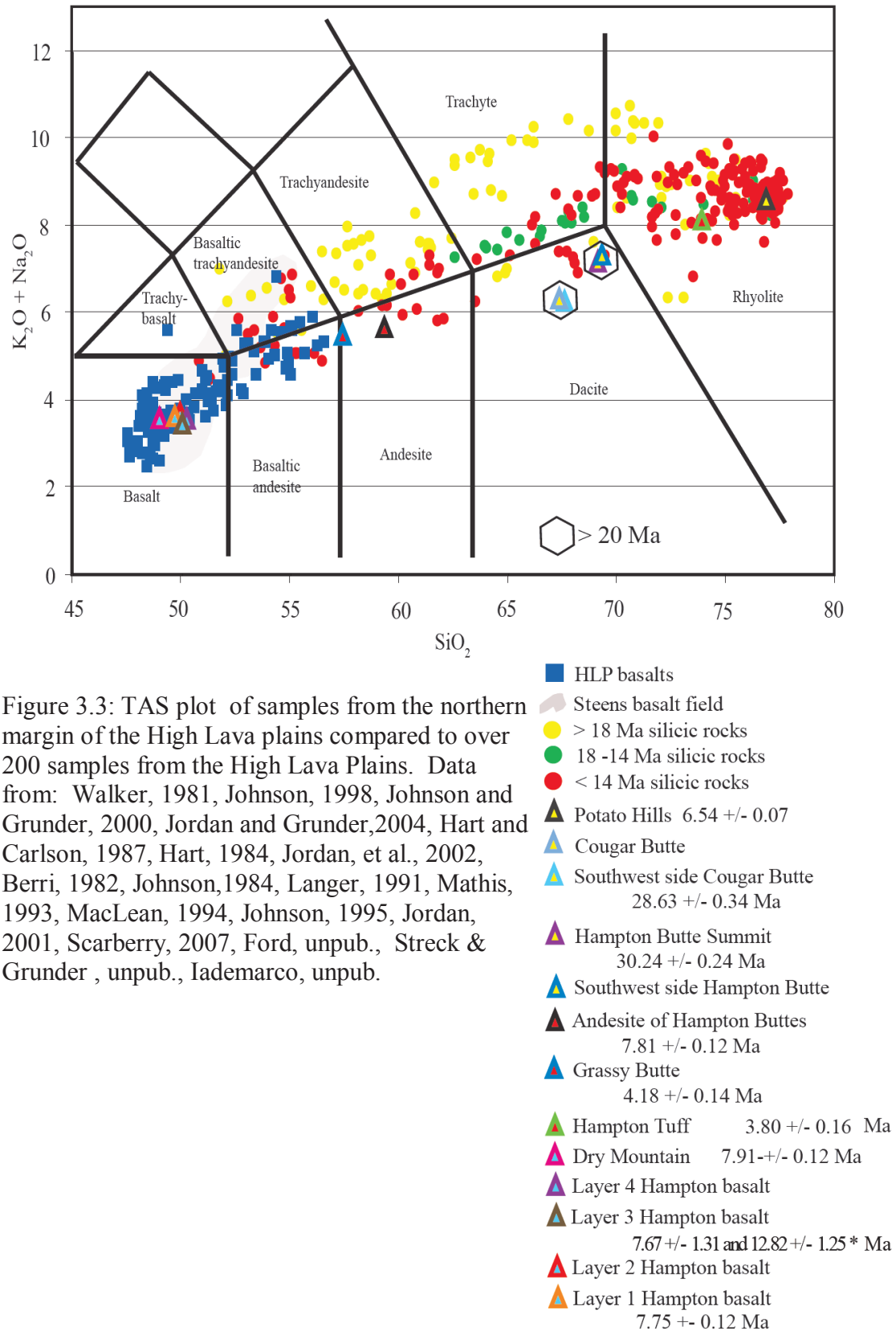

Figure 3.3: TAS plot of samples from the northern margin of the High Lava plains compared to over 200 samples from the High Lava Plains. Data from: Walker, 1981, Johnson, 1998, Johnson and Grunder, 2000, Jordan and Grunder,2004, Hart and Carlson, 1987, Hart, 1984, Jordan, et al., 2002, Berri, 1982, Johnson,1984, Langer, 1991, Mathis, 1993, MacLean, 1994, Johnson, 1995, Jordan, 2001, Scarberry, 2007, Ford, unpub., Streck & Grunder , unpub., Iademarco, unpub.

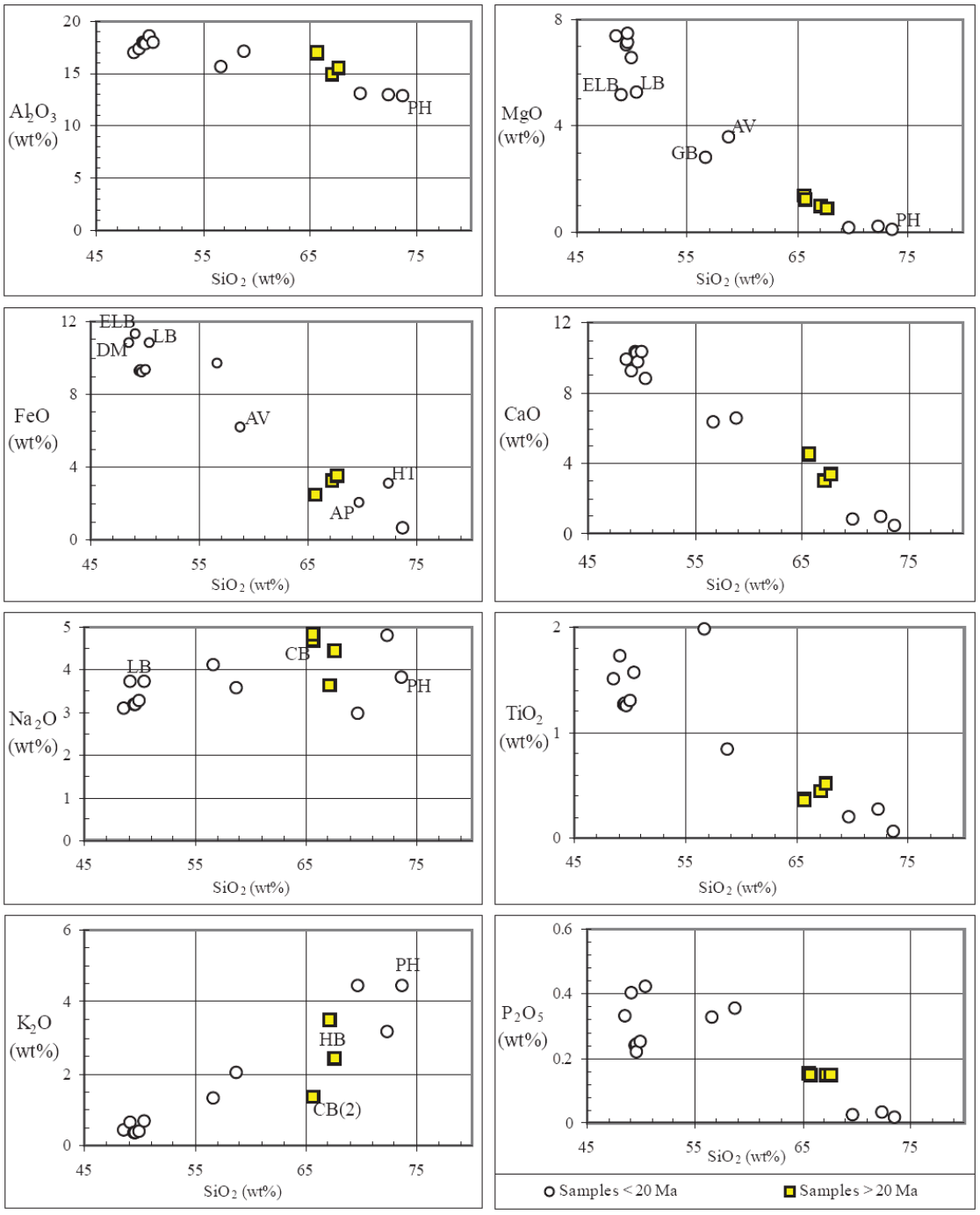

Figure 3.4: Harker diagrams of major elements verses silica discussed in text. HB = Hampton Butte (HTB-0501), CB = Cougar Butte (HTB-0613), DM = Dry Mountain (DMT-0601), LB = Long Barn (HTB-0712MF), ELB = East of Long Barn (HTB-0710MF), AV = Andesite Vent (HTB-0623), PH = Potato Hills (HLP-0701), AP = Ash (HTB-0516). Appendix 4 is a comparison to over 200 rocks of the High Lava Plains.

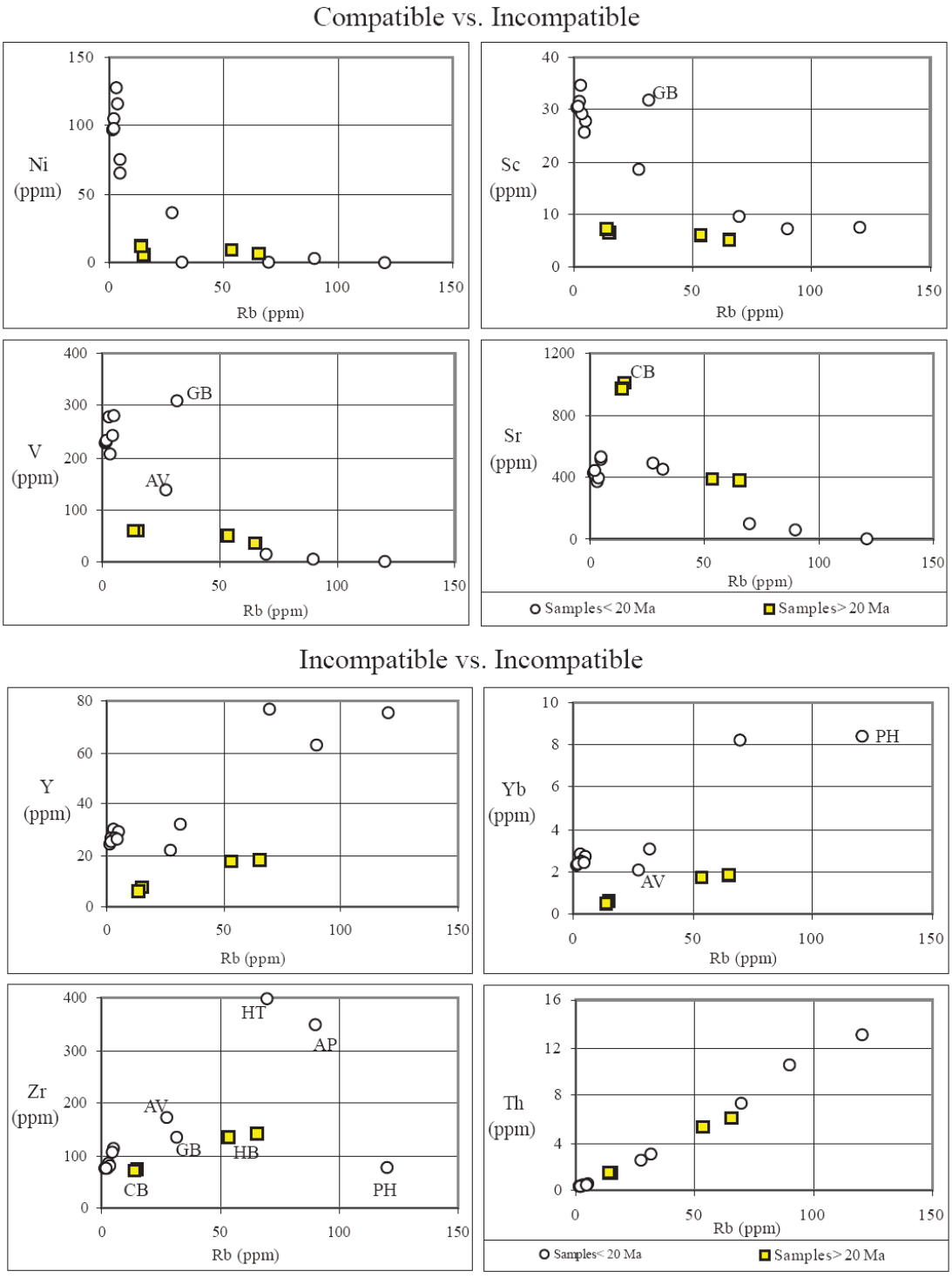

Figure 3.5: Harker diagrams of compatible (top) and incompatible (bottom) elements verses incompatible rubidium discussed in text. HB = Hampton Butte (HTB-0501), CB = Cougar Butte (HTB-0613), AV = Andesite Vent (HTB-0623), PH = Potato Hills (HLP-0701), AP = Ash (HTB-0516). Appendix 4 is a comparison to over 200 rocks of the High Lava Plains.

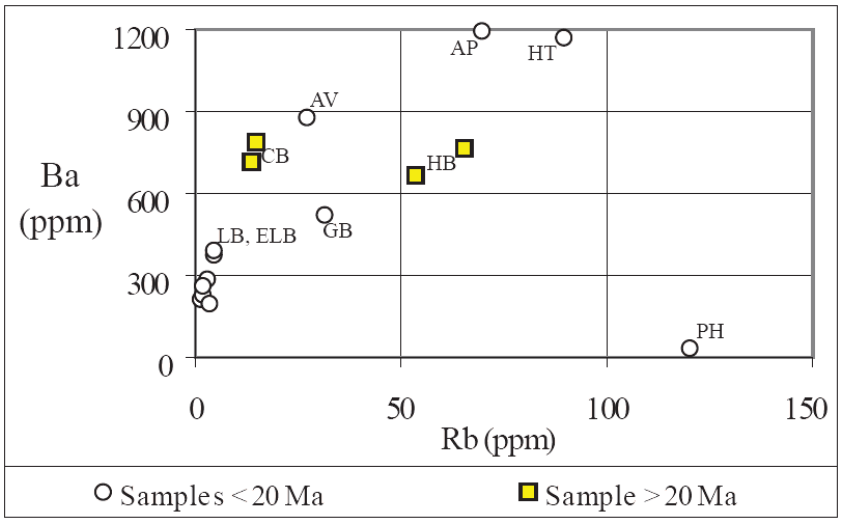

Figure 3.6: Harker diagram of barium verses rubidium discussed in text. HB = Hampton Butte (HTB-0501), CB = Cougar Butte (HTB-0613), LB = Long Barn (HTB-0712MF), ELB = East of Long Barn (HTB-0710MF), AV = Andesite Vent (HTB-0623), PH = Potato Hills (HLP-0701), GB = Grassy Butte (GB-0701, HT = Hampton Tuff (HTB-0701AP = Ash (HTB-0516)).

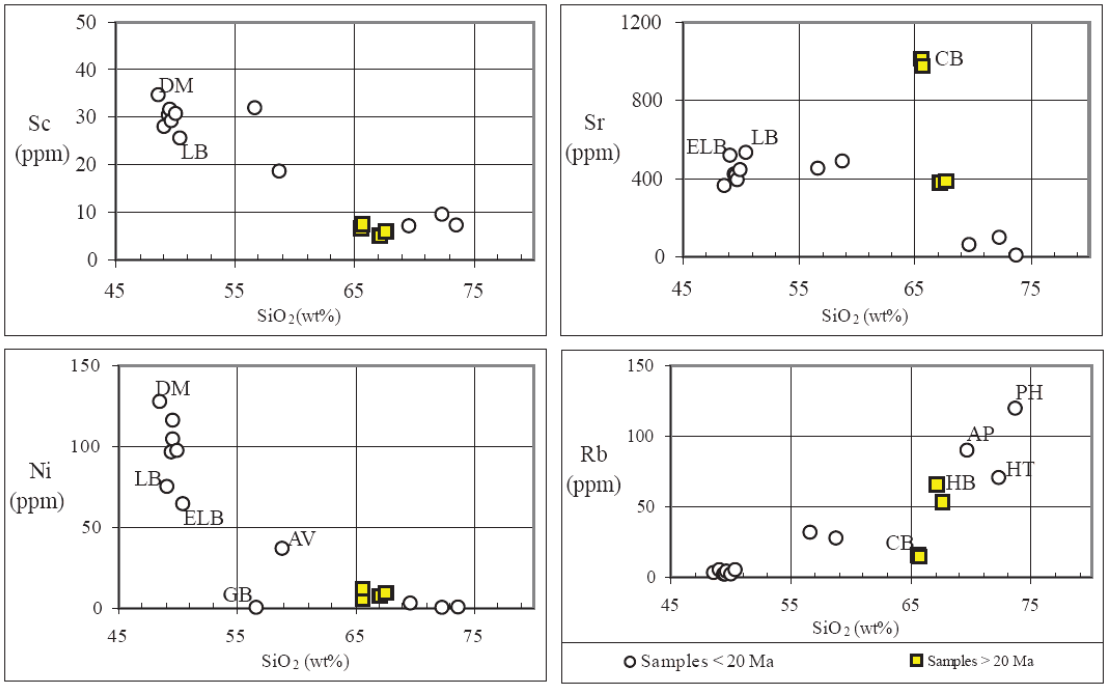

Figure 3.7: Selected REE vs. SiO_2 HB = Hampton Butte (HTB-0501), CB = Cougar Butte (HTB-0613), DM = Dry Mountain (DMT-0601), LB = Long Barn (HTB-0712MF), ELB = East of Long Barn (HTB-0710MF), AV = Andesite Vent (HTB-0623), PH = Potato Hills (HLP-0701)AP = Ash (HTB-0516). Appendix 4 is a comparison to over 200 rocks of the High Lava Plains.

composition. Magnesium, calcium, titanium, iron and phosphorus all form a single point for both samples; only alkalis differ and likely reflect hydration of HTB-0513 (Figure 3.4, Table 2 and 2a).

In the plot of incompatible and compatible trace elements against rubidium the Cougar Butte samples (HTB-0613, HTB-0511) are richer in strontium and contain less vanadium and scandium than other samples and, when plotted against SiO_2, rubidium is low (Figure 3.7).The dacite of Cougar Butte shares many characteristics with Hampton Butte, although it has less silica. I consider them closely related geochemically and temporally.

3.3.3.2 Potato Hills (HLP-0704): The subalkaline peraluminous silica oversaturated rhyolite of Potato Hills is the most evolved of the silicic rocks greater than 16 million years old when compared to samples from the High Lava Plains (Figure 3.1, and 3.3). A comparison of major elements to other samples collected for this study shows that Potato Hills conforms to the overall trend established by plotting all rocks collected for this thesis and occupies a position at the end of the calc-alkaline trend on a ternary plot (Figure 3.8).

A plot of chondrite normalized rare earth elements from basaltic andesite and higher silica rock samples reveals that the Potato Hills rhyolite sample is depleted in the LREE elements compared to the Hampton Tuff rhyolite (HTB-0701) while HREE elements for the samples are nearly equal (Figure 3.2). There is a depletion of strontium, scandium, vanadium and nickel relative to the other samples and a general trend for the more evolved older and higher silica rocks to have a lower ratios of

Table 3.2: Un-normalized major and trace element compositions of volcanic rocks from the northern margin of The High Lava Plains

Sample	DMT	HTB	HTB	HTB	HTB	HTB	HTB	GB
Number	0601	0710MF	0630	0631	0629	0523	0712MF	0701
Location	Dry Mountain	Long Barn east	Layer 2	Layer 1	Layer 4	Layer 3	Long Barn	Grassy Butte
Longitude (NAD 27)	119°33.85'	120°12.06'	120°17.55'	120°17.44'	120°19.27'	120°17.29'	120°13.29'	119°58.07'
Latitude	43°40.33'	43°42.85'	43°45.73'	43°45.80'	43°46.05'	43°45.96'	43°45.16'	43°37.45'
			Hampton Butte Basalts					
Age Ma (approx)	7.91	< 8	< 8	7.75	< 8.	7.67	< 8	4.18
Classification	Basalt lava	Basalt lava	Basalt lava	Basalt lava	Basalt lava	Basalt lava	Basalt lava	Basaltic andesite scoria
SiO2 (Wt%)	48.56	49.11	49.47	49.59	49.66	50.01	50.41	56.65
TiO2	1.50	1.72	1.26	1.28	1.25	1.30	1.56	1.97
Al2O3	16.97	17.37	17.87	17.88	17.86	18.55	17.90	15.56
FeO*	10.84	11.33	9.25	9.32	9.21	9.37	10.82	9.71
MnO'	0.18	0.20	0.16	0.16	0.16	0.16	0.18	0.19
MgO	7.39	5.17	7.04	7.15	7.47	6.57	5.26	2.78
CaO	9.88	9.23	10.36	10.27	9.78	10.36	8.81	6.30
Na2O	3.09	3.70	3.19	3.18	3.16	3.26	3.70	4.09
K2O	0.43	0.65	0.34	0.37	0.35	0.38	0.68	1.31
P2O5	0.33	0.40	0.24	0.24	0.22	0.25	0.42	0.32
Total %	99.17	98.87	99.18	99.45	99.11	100.21	99.75	98.88
Trace elements by XRF								
Ni	***128***	***75***	***96***	***105***	***116***	***98***	***65***	***0***
Cr	173.7	29.7	145.8	147.8	136.6	142.2	40.4	2.0
V	***277***	***280***	***227***	***230***	***206***	***232***	***241***	***307***
Ba	293	388	217	230	201	273	407	516
Th	0.8	0.3	0.3	0.2	0.9	0.0	0.0	2.1
Nb	4	6	3	3	2	3	7	8
Y	30	28	24	27	26	25	24	31
Pb	2	3	2	0	2	3	3	6
Rb	3.5	5.5	2.7	2.0	4.2	0.5	5.4	32.0
Sr	364	508	422	415	386	436	530	444
Sc	***34.6***	***27.8***	***30.2***	***31.4***	***29.0***	***30.5***	***25.6***	***31.7***
Zr	90	118	80	81	84	81	113	140
Ga	17	19	17	16	15	16	18	20
Cu	104	81	86	86	80	92	93	5
Zn	90	105	72	72	72	75	99	117
La	11.8	16.7	9.0	8.6	8.9	8.8	17.2	17.9
Ce	19	30	12	14	17	18	30	30
Nd	15.7	20.1	11.2	12.1	13.6	12.7	19.4	20.7
Trace elements by ICP-MS (ppm)								
La	9.8	12.5	6.6	7.5	7.0	8.0	12.8	16.1
Ce	22	29	16	16	16	17	30	36
Pr	3.5	4.3	2.6	2.8	2.7	2.8	4.3	5.0
Nd	16.9	19.9	12.8	13.8	13.4	13.8	19.6	22.3
Sm	4.58	5.24	3.70	3.97	3.86	3.82	4.96	5.80
Eu	1.69	1.83	1.40	1.47	1.47	1.48	1.80	1.98
Gd	5.35	5.43	4.24	4.50	4.54	4.44	5.12	5.96
Tb	0.91	0.92	0.73	0.78	0.77	0.74	0.84	1.01
Dy	5.63	5.61	4.55	4.84	4.93	4.65	5.06	6.23
Ho	1.17	1.13	0.93	1.02	1.03	0.96	1.02	1.26
Er	3.19	3.07	2.56	2.73	2.81	2.64	2.74	3.40
Tm	0.46	0.43	0.37	0.39	0.40	0.38	0.39	0.49
Yb	2.78	2.71	2.28	2.39	2.44	2.32	2.42	3.06
Lu	0.45	0.42	0.36	0.38	0.39	0.36	0.38	0.48
Ba	288	374	211	223	197	263	389	515
Th	0.4	0.5	0.3	0.3	0.4	0.3	0.5	3.0
Nb	5	6	3	3	3	3	7	8
Y	30	29	24	27	26	25	26	32
Hf	2.4	3.1	2.1	2.2	2.3	2.1	2.9	3.8
Ta	0.3	0.4	0.2	0.2	0.2	0.2	0.4	0.5
U	0.1	0.2	0.1	0.1	0.2	0.1	0.2	1.1
Pb	2	2	1	1	2	2	3	6
Rb	3.1	5.0	1.7	2.4	3.6	2.0	4.9	31.9
Cs	0.0	0.0	0.0	0.0	0.1	0.0	0.1	1.8
Sr	364	512	423	414	390	438	530	446
Zr	84	113	75	76	80	76	107	135

All data XRF and ICP-MS obtained by the Washington State University GeoAnalytical Laboratory, Pullman Washington. Major element data by X-ray fluorescence. ICP-MS prep done by Mark Ford (OSU) at Washington State University GeoAnalytical Laboratory for samples ending in MF. Total iron Is expressed as FeO*. Data in XRF section in bold italic are used in this paper. Data in ICP-MS section in bold italic is from XRF data, ICP-MS was not done on this sample. Ages preceded by a ~ or < are estimated, others do not show error in 40Ar/39Ar data presented in Table 1.

Table 3.3: Un-normalized major and trace element compositions of volcanic rocks from the northern margin of The High Lava Plains

Sample	HTB	HTB	HTB	HTB	HTB	HTB	HTB	HLP
Number	0623	0613	0511	0503c	0501	0516	0701	0704
Location	E. of Hampton Butte	Cougar Butte Southwest side	Cougar Butte	S. side Hampton Butte	Hampton Butte summit	Ash	Hampton Tuff	Potato Hills
Longitude (NAD 27)	120° 15.05′	120° 17.91′	120° 17.71′	120° 17.17′	120° 16.95′	120° 17.79′	120° 16.51′	120° 13.65′
Latitude	43° 46.05′	43° 43.80′	43° 43.84′	43° 46.39′	43° 46.44′	43° 44.49′	43° 45.51′	43° 45.49′
Age Ma (approx)	7.81	28	28	30	30.39	< 3.8	3.8	80 and 6.5
Classification	Andesite lava	Dacite	Dacite	Rhyodacite	Rhyodacite	Alkali rhyolite ash and pumice	Rhyolite tuff	Alkali rhyolite
SiO2 (Wt%)	58.80	65.64	65.71	67.16	67.66	69.67	72.36	73.64
TiO2	0.84	0.36	0.36	0.44	0.51	0.19	0.27	0.06
Al2O3	17.05	16.84	16.91	14.86	15.44	13.02	12.92	12.69
FeO*	6.21	2.45	2.48	3.20	3.54	2.02	3.12	0.64
MnO'	0.12	0.04	0.05	0.07	0.05	0.07	0.08	0.06
MgO	3.55	1.37	1.23	0.95	0.87	0.15	0.20	0.05
CaO	6.56	4.40	4.52	2.96	3.35	0.77	0.96	0.41
Na2O	3.56	4.66	4.83	3.62	4.44	2.95	4.80	3.80
K2O	2.04	1.36	1.33	3.48	2.40	4.44	3.17	4.43
P2O5	0.35	0.15	0.15	0.15	0.15	0.03	0.03	0.01
Total %	99.08	97.28	97.57	96.87	98.41	93.30	97.90	95.80
Trace elements by XRF								
Ni	***36***	***5***	***12***	***7***	***9***	***3***	***0***	***0***
Cr	56.9	19.3	19.0	9.8	13.0	1.7	2.7	3.2
V	***137***	***60***	***60***	***36***	***49***	***6***	***15***	***1***
Ba	866	770	721	751	672	1170	1171	29
Th	2.2	1.3	2.7	6.7	5.5	10.5	7.7	13.1
Nb	9	2	2	11	9	16	17	13
Y	22	8	6	17	16	63	79	76
Pb	8	8	10	9	8	18	13	18
Rb	27.7	15.9	14.3	66.7	56.5	89.9	70.0	119.4
Sr	***486***	***1019***	***1027***	***381***	***405***	***59***	***93***	***4***
Sc	18.4	6.5	7.2	4.9	5.9	7.0	9.4	7.3
Zr	177	73	75	144	142	348	397	74
Ga	18	19	19	19	19	19	20	17
Cu	67	34	37	6	14	7	5	3
Zn	77	51	46	56	53	83	101	41
La	25.5	11.0	7.6	17.8	19.4	39.5	32.3	10.0
Ce	52	17	19	37	38	84	64	35
Nd	24.5	9.3	6.2	14.2	17.6	45.7	40.2	20.3
Trace elements by ICP-MS (ppm)								
La	25.0	11.2	9.8	20.4	19.7	n.d.	35.2	13.9
Ce	48	19	18	38	35	n.d.	64	36
Pr	6.0	2.5	2.2	4.4	4.3	n.d.	9.8	5.1
Nd	23.7	9.8	8.4	16.2	16.4	n.d.	41.4	22.3
Sm	4.98	1.95	1.62	3.38	3.46	n.d.	10.4	7.83
Eu	1.47	0.64	0.55	0.86	0.86	n.d.	2.14	0.18
Gd	4.44	1.62	1.38	3.10	3.19	n.d.	11.3	9.38
Tb	0.69	0.23	0.19	0.52	0.52	n.d.	2.08	1.89
Dy	4.10	1.31	1.09	3.19	3.15	n.d.	13.5	12.8
Ho	0.81	0.25	0.21	0.65	0.64	n.d.	2.89	2.75
Er	2.22	0.67	0.56	1.84	1.77	n.d.	8.43	8.04
Tm	0.32	0.10	0.08	0.28	0.27	n.d.	1.28	1.26
Yb	2.06	0.58	0.49	1.80	1.70	n.d.	8.17	8.33
Lu	0.33	0.09	0.08	0.29	0.28	n.d.	1.31	1.33
Ba	874	786	716	763	664	***1170***	***1191***	29
Th	2.5	1.5	1.5	6.0	5.2	***10.5***	7.3	13.0
Nb	9	2	2	11	10	***16***	17	14
Y	22	7	6	18	17	***63***	77	75
Hf	4.3	2.0	1.9	4.1	3.8	n.d.	10.9	4.6
Ta	0.6	0.2	0.1	1.1	0.9	n.d.	1.1	1.2
U	1.0	0.8	0.8	2.1	1.9	n.d.	2.8	6.7
Pb	8	8	9	8	8	18	13	18
Rb	27.4	15.1	13.9	65.4	53.5	***89.9***	69.9	120.5
Cs	0.6	0.4	0.4	2.4	1.4	n.d.	1.9	5.3
Sr	487	1011	968	372	382	***59***	92	3
Zr	171	72	70	140	135	***348***	397	76

All data XRF and ICP-MS obtained by the Washington State University GeoAnalytical Laboratory, Pullman Washington. Major element data by X-ray fluorescence. ICP-MS prep done by Mark Ford (OSU) at Washington State University GeoAnalytical Laboratory for samples ending in MF. Total iron Is expressed as FeO*. Data in XRF section in bold italic is used in this paper. Data in ICP-MS section in bold italic is from XRF data, ICP-MS was not done on this sample. Ages preceded by a ~ or < are estimated, others do not show error in 40Ar/39Ar data presented in Table 1.

these selected elements, with the exception of the Cougar Butte sample in plot of strontium verses rubidium (Figure 3.5). Plots of the incompatible elements yttrium, ytterbium, zircon and thorium against incompatible rubidium shows a general concordance with the trend established by the other samples with the exception of the more depleted amount of zircon when compared to rubidium (Figure 3.5). Rubidium, nickel, strontium, and scandium from the Potato Hills sample, plotted against silica, show concordance with trends established by the other plotted samples (Figure 3.7).

3.3.3.3 Dry Mountain: The Basalt of Dry Mountain falls within the overlapping range of 90% of the samples from Jordan (2004) and the high alumina olivine tholeiites of Draper (1991) (Figure 3.9). Like the plateau-forming basalts that are at the base of Hampton Butte the sample from the summit of Dry Mountain is both metaluminous silica saturated, subalkaline, and part of the tholeiitic trend (Figure 3.8). DMT-0601 contains the lowest silica of the samples analyzed and more of the most compatible HREE (Er, Tm, Yb, Lu) than any other basalt analyzed (Table 2 and Figure 3.10).

3.3.3.4 Andesite (HTB-0623): The subalkaline metaluminous silica oversaturated andesite conforms to the trend of combined older and younger rocks on the plot of major elements (Figure 3.4). On a TAS plot with samples from the High Lava Plains the andesite of Hampton Buttes follows the trend of other northern margin samples an is lower in total alkalis compared to the majority of combined samples (Figure 3.3) A REE plot reveals a depletion of the light rare earth elements without a depleted europium signature (Figure 3.2). There is a general concordance with the

trend of the compatible elements strontium and nickel plotted against incompatible rubidium (Figure 3.5).

3.3.3.5 Basalt at Hampton Butte (HTB-0630, HTB-0631, HTB-0629, and HTB-0523): The four samples, arranged from left to right in the header, represent the four layers found in outcrop arranged in order of increasing un-normalized SiO_2 values (Table 2). Stratigraphically the order of samples, from oldest to youngest is HTB-0631, HTB-0630, HTB-0523, and HTB-0629. All samples of this normative olivine basalt are subalkaline metaluminous silica saturated. There is a close petrologic relationship between the samples and a close correlation with the high alumina olivine tholeiite (HAOT) basalt from the High Lava Plains of Draper (1991) and Jordan

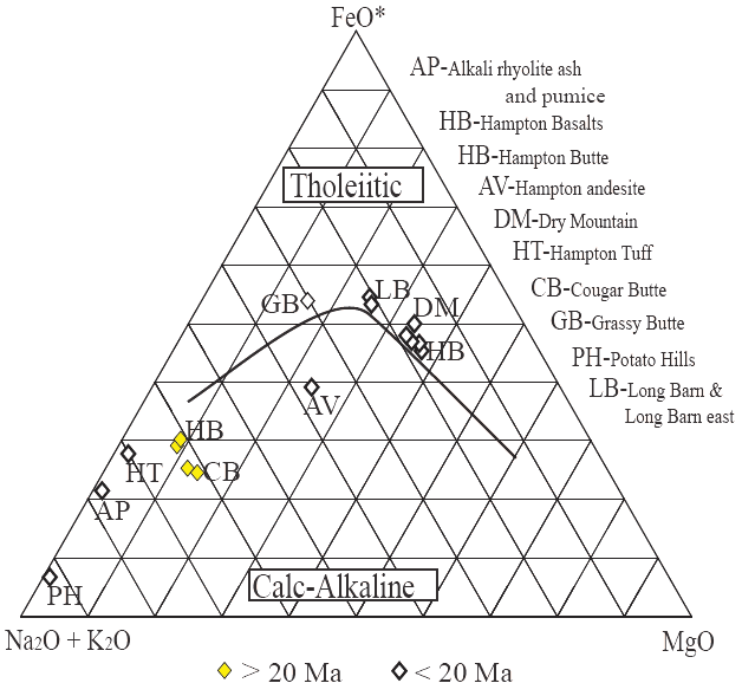

Figure 3.8: Ternary plot of collected samples showing the relationship of samples older than 20 million years to those less than 20 million years old. The younger andesite vent (HTB-0623), Hampton Tuff (HTB-0701), and Ash (HTB-0516) follow the calc-alkaline trend with the older samples.

(2004) (Figure 3.8, 3.9). Cerium, lead, and zinc values for Hampton Butte basalts and those of Draper (1991) and Jordan (2004) from outside the buttes are close enough to nearly form a single point on a spider diagram (Figure 3.10, Table 2).

3.3.3.6 Basalt of Long Barn (HTB-O710MF, HTB-0712MF): Both samples are of olivine basalt from outside the mapped area, collected on the eastern side of Hampton Buttes (Plate 2). Unlike the other samples from Hampton Buttes both HTB-0710MF and HTB-0712MF are alkaline (Figure 3.1). HTB-0710MF (Long Barn Butte) is metaluminous silica undersaturated, HTB-0712MF, from a ridge 4.6 kilometers south-southwest of Long Barn Butte is metaluminous silica saturated . The higher silica Long Barn sample has slightly more of the compatible mid to heavy rare earth elements (Tb through Lu) and is more evolved than the sample from the ridge south-southeast of Long Barn Butte (Figure 3.8, Plate III). These samples have high iron and titanium with lower magnesium compared to other basalts in this study (Table 2, Figure 3.4) yet share a similar set of values compared to the basalts of Jordan (2004) in a spider diagram. Like the basalts at the base of Hampton Butte cerium, lead, and zinc values for Hampton Butte basalts, these from the east side of the buttes nearly form a single point on a spider diagram (Figure 3.10, Table 2).

3.3.3.7 Basaltic andesite of Grassy Butte (GB-0701): The subalkaline basaltic andesite of Grassy Butte, classified under the system of Shand (1927) as metaluminous silica saturated, stands out from the other samples for its higher percentage of the major elements, iron and titanium, and slightly lower aluminum (Figure 3.4, Table 3.2). Enrichment in the compatible elements vanadium and scandium when plot-

ted against the incompatible rare earth element rubidium, compared to the other samples, as well as the depletion of nickel (Figure 3.5 and 3.7). The Grassy Butte sample conforms to the tholeiitic trend as do the samples of basalt from Long Barn, Dry Mountain, and Hampton Buttes (Figure 3.8).

3.3.3.8 Hampton Tuff (HTB-0701): The rhyolite tuff of Hampton Butte is the youngest and only peraluminous rock found at Hampton Butte (Shand, 1927) (Table 3.1). It is also the most evolved, enriched in the compatible HREE and LREE elements and follows the trend of other margin samples by being lower in total alkalis compared to other High Lava Plains samples (Figure 3.1 and 3.2). Major element plots against silica show that the Hampton Tuff is slightly enriched in iron compared to the other samples but is similar to other tuffs (Devine Canyon Tuff, Rattlesnake Tuff) in that they too are peraluminous with high iron (Streck and Grunder, 1995). A notable deviation from the overall trends in compatible verses incompatible elements on Harker diagrams is the depletion of nickel common with the basaltic andesite of Grassy Butte (Figure 3.5 and 3.7).

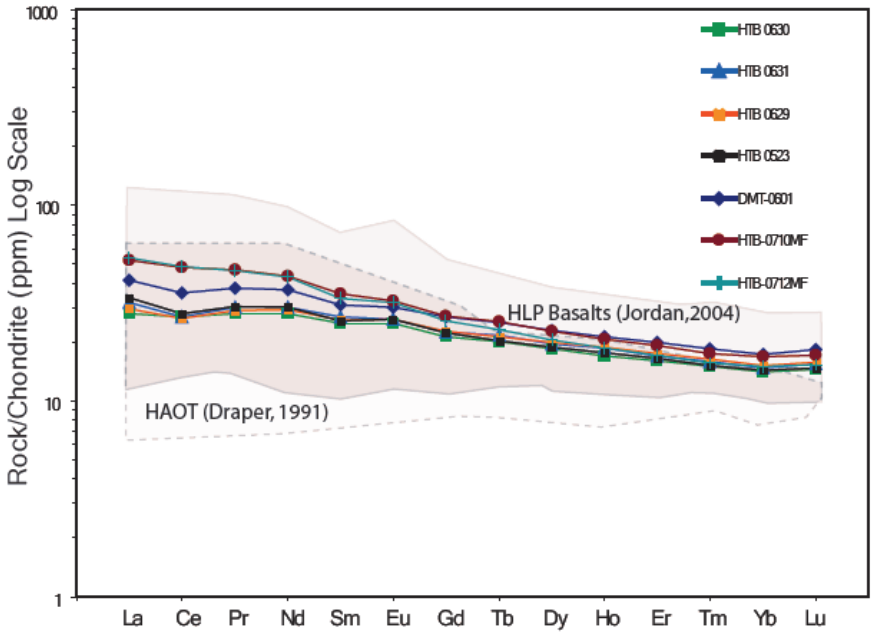

Figure 3.9: Spider diagram comparing High Lava Plains basalts of Draper (1991) and Jordan (2004) to samples collected along the northern margin for this thesis. Samples from the extreme eastern edge of Hampton Buttes (HTB-0710MF and HTB-0712MF) and Dry mountain (DMT-0601) are more enriched in the heavier REE than those of Draper (1991) and all are congruent with the High Lava Plains basalts of Jordan (2004).

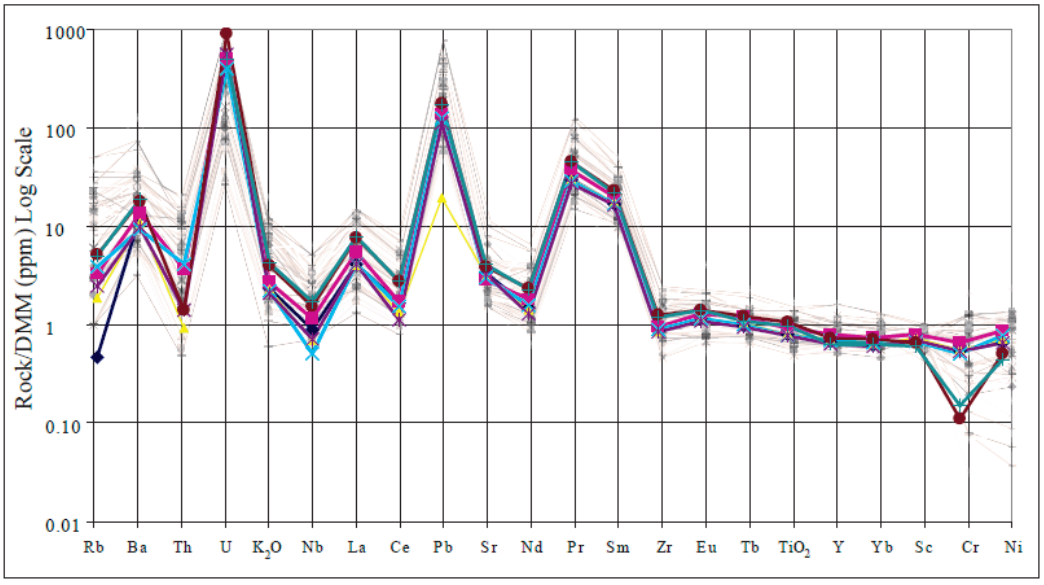

Figure 3.10: Basalts of the northern margin compared to those of Jordan (2004). The spider diagram shows the similarity between basalt from the High Lava Plains (colored lines) and those found along the northern margin. DMM values are from Workman and Hart, 2004. DMM in wt% used to calculate K_2O and TiO_2 are from Pierce, 1983.

4. ORIGINS OF VOLCANISM ALONG THE NORTHERN MARGIN

4.1 High Lava Plains

4.1.1 Timing of Volcanism: Volcanic rocks that predate the High Lava Plains volcanism includes the 17- 12 m.y. old Columbia River basalt group north and east of the High Lava Plains and coeval Steens Basalts, mainly to the south and southeast. These flood basalts lap onto older rock of Early to Mid Tertiary age that crop out on the north side of the High Lava Plains, such as at Hampton Buttes and to the south, in the northern Basin and Range as exposed in scarps at Steens Mountain, Hart Mountain, and Abert Rim (Hooper et al., 2002; Scarberry, 2008).

The High Lava Plains are a structurally transitional area between the Basin and Range and Blue Mountains that are dominated by intersecting NNE and NW striking normal faults (Plate II). A complex system of faulting transitions the east-west extension related normal faults of the Basin and Range to the combination of northeast to southwest extension related normal and strike-slip faults along the High Lava Plains (Trench, 2008; Scarberry et al., 2008).

The deeper-rooted accreted terrains of the Blue Mountains and the overlying Clarno and John Day Formations crop out as an irregular barrier that trends WNW across central Oregon, apparently serving as a backstop to the shallow northwest striking faults of the Brothers Fault Zone. Hampton Butte and Cougar Butte are part of this basement to the High Lava Plains. In central Oregon, clockwise rotation centered around an Euler pole located in the eastern Blue Mountains imparts dextral motion on faults of the Brothers Fault Zone that cut the High Lava Plains (Hammond

Figure 4.1: Euler pole locations proposed by Hammond and Thatcher (2005, solid square), Wells and Simpson (2001, solid circle), and McCaffrey et al. (2000, open circle). Clockwise rotation around a stable block imparts a right lateral strike-slip motion along the normal faults of the High Lava Plains (Trench, 2008). Northwest Basin and Range GPS velocities (arrows) with respect to North America (NA) from Hammond & Thatcher, 2005. Figure Modified from Trench (2008) after McCaffrey et al. (2000). The rectangle near the center of the figure is the study area.

and Thatcher, 2005; Trench, 2008) (Figure 4.1). Two additional pole locations along the Oregon - Washington border with clockwise rotation are also proposed by Wells and Simpson (2001) and McCaffrey et al. (2000).

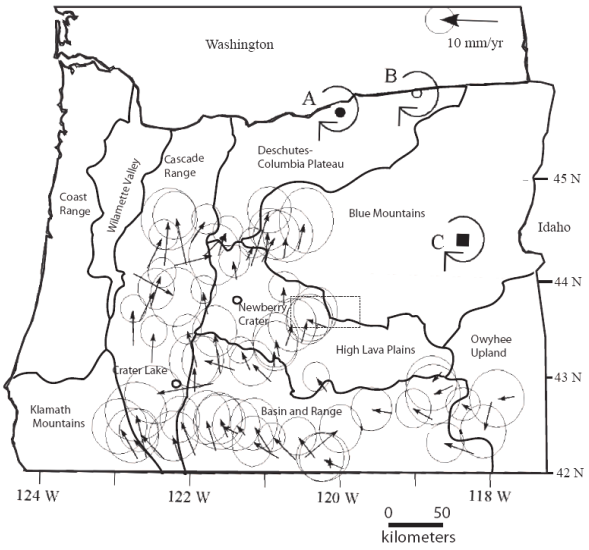

The presence of 7.75 (± 0.01) to 7.67 (± 1.31) Ma basalt banked on the south side of Hampton Butte indicates basaltic volcanism was occurring along that section of the High Lava Plains around 8 million years ago. Dry Mountain, a shield volcano composed of basalt also erupted around 7.91 (± 0.12) Ma, around the same time that a vents in Hampton Buttes were producing andesite (7.81 ± 0.12 Ma) and basalt, together forming a record of volcanism that at least extends from Hampton Buttes to Dry Mountain between 8 and 7 million years ago.

After a gap in activity from 8 - 4 Ma activity in the Hampton Buttes area resumed with the eruption of Grassy Butte ~ 4 Ma, followed shortly by the Hampton Tuff (~3.9 Ma). Since that time basalt, some dated as young as 1.3 ± 0.17 Ma (cf. Jordan, 2004), has covered much of the Hampton Tuff south of Hampton Buttes.

4.1.2 Timing of structural deformation: Northeast to southwest extension after the emplacement of Dry Mountain (7.91 ± 0.12 Ma) and Sheep Mountain (7.18 ± 0.01 Ma) has left both edifices divided by normal faults in an area where the pattern of transform faulting and extension is similar to the area surrounding the Hengill Triple Junction in Iceland, a region of recent seismicity, where seismic activity caused by right lateral transform and normal faulting is a result of tectonic shear and extension (Clifton et al., 2002) (Figure 4.2). A similar model is inferred for the High Lava Plains. The similarity between the High Lava Plains and The Hengill Triple Junction is further supported by a plot of normalized iron versus calcium (wt %) that reveals a similarity between the two suites of rocks (Figure 4.3).

Older rocks from within the High Lava Plains and immediately adjacent to it predominately fall outside the bimodal rift type and are outside the compositional zone of interest (Figure 4.3).Younger rocks of the High Lava Plains (< 20 Ma) tend to be widely scattered within the higher iron rift-zone related region shown by Jonasson, (2007) (Figure 4.3).

Dry Mountains age of 7.91 (± 0.12) Ma and the 7.18 (± 0.01) Ma age of Sheep Mountain defines the period of extension as having taken place after ~ 7 Ma. Timing is further constrained by faulting at Egli Ridge that postdates 7.13 ± 0.02 Ma basalts found there (Jordan, 2004) (Figure 4.4). Southeast of Dry Mountain, on faults traceable to it, basalt from un-faulted Oakerman Butte yielded a date of 5.44 Ma (Jordan et al., 2002), further constraining the episode of faulting to between 5.4 and 7.1 Ma. Wagontire Mountain's lack of major north-northwest trending faults, as are

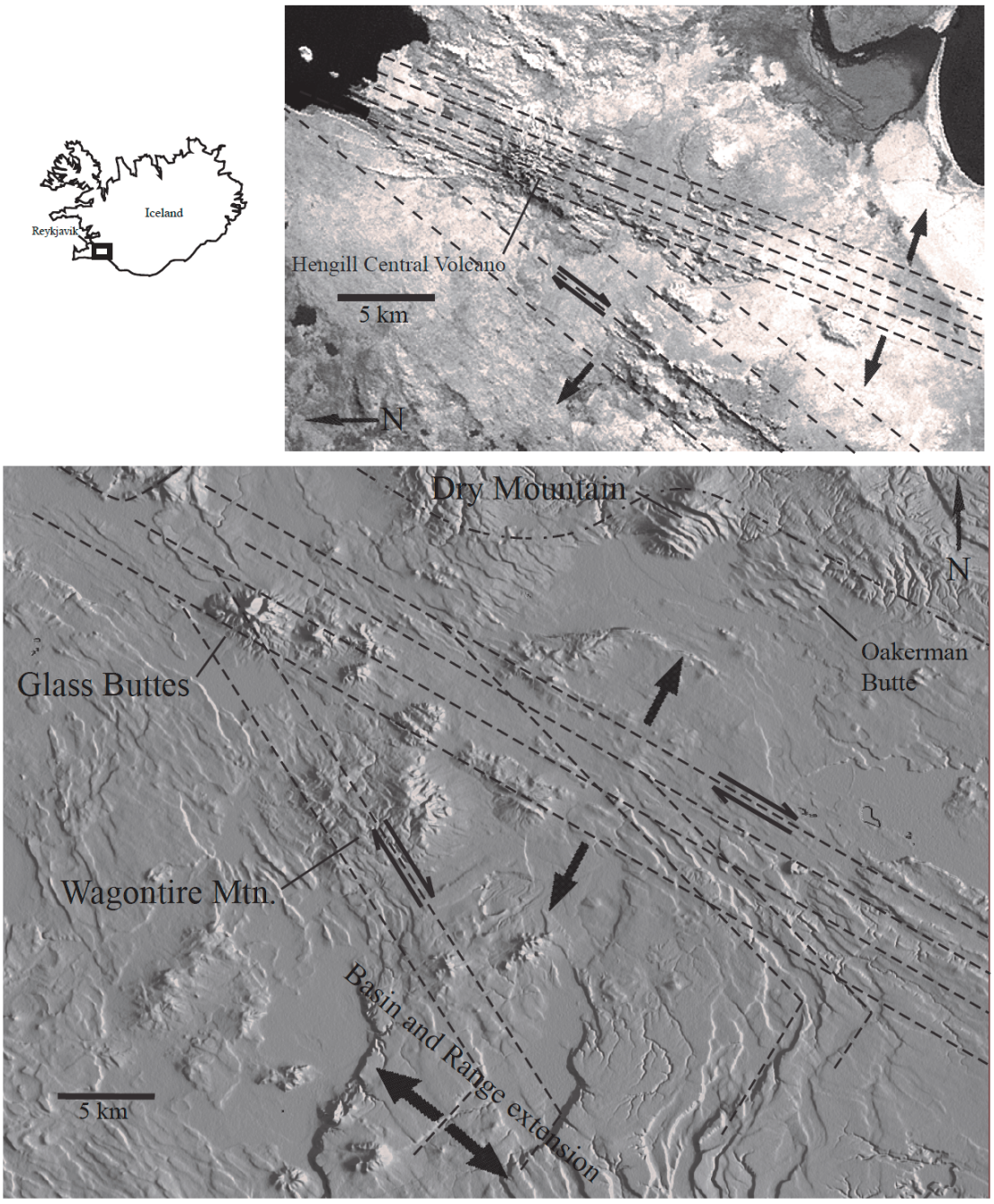

Figure 4.2: Top, left - Location of the Hengill triple junction, Reykjanes Peninsula, in southwest Iceland. Top, right and bottom - Dashed lines show fault trends (only) at the Hengill Triple Junction, and High Lava Plains at Dry Mountain. Heavy arrows approximate extension directions and others indicate presumed dextral motion on some of the normal faults. Scalloped northern margin of the High Lava Plains is indicated at the top of the lower illustration. (Top: After University of Maryland SDSU (2005), Bottom: After USGS, 2004)

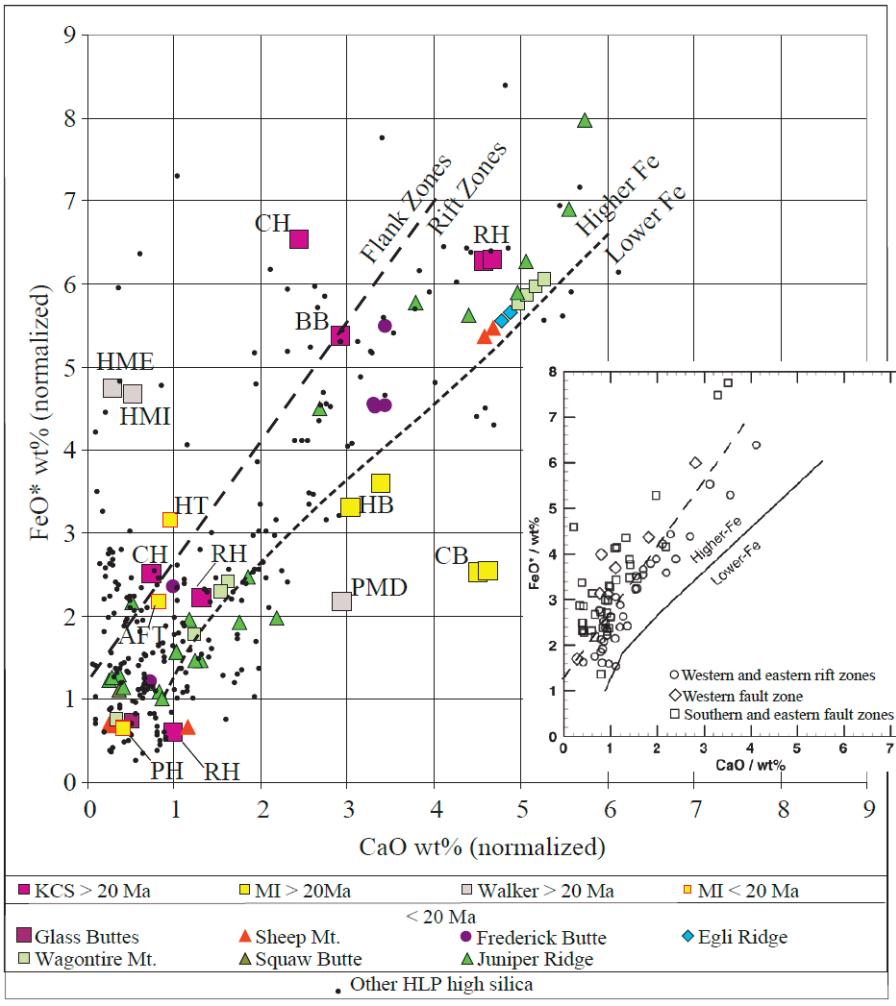

Figure 4.3: FeO vs. CaO for selected volcanic rocks from this study and of adjacent areas with SiO_2 > 60 wt %. Flank and rift zone divisions and inset are from Jonasson, (2007) based on Icelandic rocks with SiO_2 > 60 wt %. Icelandic rift zone rocks are all of the higher iron variety. FeO is even higher and CaO lower in flank zones compared to rift zones. Silicic rocks of the High Lava Plains are of both varieties, with the majority in the high FeO - rift zone. Potato Hills, Hampton and Cougar Buttes define the northern margin of the High Lava Plains at their locations (large yellow squares).

CH Coleman Hills, BB Beatys Butte, RH Rabbit Hills, HME Hart Mountain east, HMI Hart Mountain intrusive, PMD Pine Mountain Dome (Walker, 1981) HB Hampton Butte, CB Cougar Butte, PH Potato Hills, HT Hampton Tuff, AFT ashfall tuff (Iademarco, 2009) . Data from: Walker, 1981, Johnson, 1998, Johnson and Grunder, 2000, Jordan and Grunder,2004, Hart and Carlson, 1987, Hart, 1984, Jordan, et al., 2002, Berri, 1982, Johnson,1984, Langer, 1991, Mathis, 1993, MacLean, 1994, Johnson, 1995, Jordan, 2001, Scarberry, 2007, Ford, unpub., Streck & Grunder , unpub., Iademarco, unpub.

present in Dry Mountain and Sheep Mountain, and its 7.2 Ma age further confines the major rifting to the area between Sheep Mountain and Dry Mountain during that time period (Figure 4.4) (Plate 3).

At the eastern end of the study area Trench (2008) describes deformation as occurring between 7.05 and 5.68 Ma, at a rate of 0.1 mm/y, with total extension 161 m (± 5m). These dates are consistent with the 5.44 to 7.1 Ma ages figured further west on the High Lava Plains. They also coincide with those of Jordan et al. (2004) for increases in basaltic volcanism between 7.8 and 7.5 Ma and also from 5.9 to 5.3 Ma. Episodes of abundant mafic volcanism may indicate a period of rapid rifting and eruption of mantle derived tholeiitic basalts. Magmatism would be enhanced by extension and upwelling, and volcanism would be promoted by brittle dilation of the

Figure 4.4: Block diagrams of faulting and volcanic activity between Hampton Buttes and Dry Mountain **A)** Dry Mountain, Hampton basalts, Hampton andesite, Sheep Mountain and Wagontire Mountain are all active early in the time between 7.8 and 7.1 Ma. Later northwest to southeast extension causes normal faults to develop and cut Dry Mountain, Sheep Mountain, and the Hampton basalts. B) Rifting continues at a slower rate between 7.1 and 5.9 Ma. Basin and Range normal fault trends rotate clockwise slightly while the transition to the Brothers fault zone weakens the crust. C) Renewed volcanic activity between 5.9 and 4.2 Ma creates Egli Ridge, Glass Buttes, Oakerman Butte, and Grassy Butte. Combined northeast to southwest and Basin and Range extension continues to cause normal faulting of the Hampton basalts Egli Ridge, and Sheep Mountain but does not affect late placed Grassy and Oakerman Buttes. D) From 5.9 to 4.2 Ma, as rifting continues, basalt erupts, forming Grassy Butte (4.18 Ma). Silicic volcanism, the result of trapped and now fractionated basalt erupts, forming Frederick Butte (3.9 Ma) and the Hampton Tuff (3.9 Ma). Faulting continues and cuts Glass Buttes and the Hampton Tuff. Reactivated northwest trending faults cut Wagontire Mountain as Basin and Range faulting combined with Brothers Fault Zone faulting progresses towards Newberry Volcano. Black colored faults (lines) involve only NE/SW extension, blue and red colored faults include a Basin and Range extensional component.

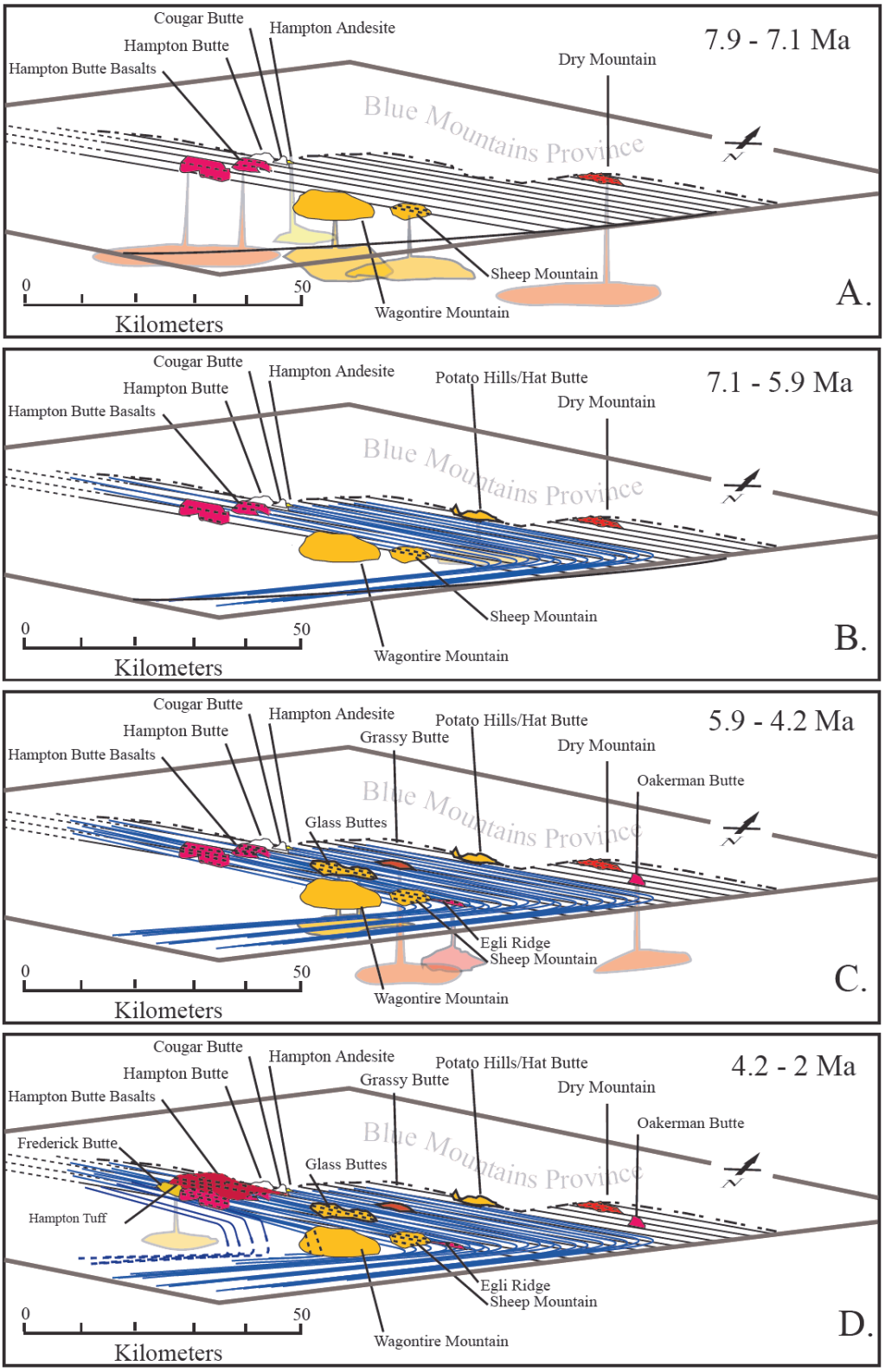

Figure 4.4: continued

upper crust. Accordingly the ~ 8 Ma pulse of volcanism should correspond to the larger tectonic event, consistent with the widespread distribution of such basalts.

The coincidence of the eruption of basalt at Dry Mountain and rhyolite at Sheep Mountain during the 7.8 to 7.5 Ma episode of basaltic volcanism may be best explained as result of early rifting at Dry Mountain having opened a channel for the rapid eruption of a partial melt of the mantle. Two older dates for basalt near Sheep Mountain are reported by Jordan et al., (2004); 35 kilometers to the southeast near Iron Mountain sample 148CHL98 is dated at 10.12 (± 0.13) Ma, and 35 kilometers south of Sheep Mountain near Little Juniper Mountain sample HP-33 is given an age of 8.23 (± 0.46) Ma. Rifting northeast to southwest and Basin and Range extension to the west-northwest, possibly driven by westward younging episodes of extension after the creation of Steens Mountain (~16 Ma), Jackass Mountain, and Poker Jim Ridge, may have been centered along the present High Lava Plains starting southeast of Iron Mountain and ending in the area of Hampton Butte (Plate 2). The combination of right lateral transform and normal faults propagating west, along the Brothers Fault Zone and northeast to southwest extension allowed basaltic magma to rapidly reach the surface through newly created rifts as they propagated to the northwest between about 8 and 10 Ma.

In a model developed for rift propagation in the Galapagos Islands (Sinton et al., 1983; Christie and Sinton, 1981) different magmatic suites result from ever increasing interconnected magma chambers that approach the steady supply system of

normal mid-ocean ridge segments. In the High Lava Plains, at the front of the propagating rifts, small isolated chambers at different levels in the crust provide reservoirs for magma evolution (Figure 4.5). Interconnection of the small chambers increases as magma supplies increase and propagation continues, followed by total connectivity through the chambers and a path for flow beneath the rifts (cf. Sinton et al., 1983; Christie and Sinton, 1981). Continuing rift propagation leads to eruption of more evolved magma compositions at the rift front (Mattsson and Oskarsson, 2005). In the High Lava Plains abundant basalts would erupt along the Brothers fault zone as well as to its south into the Basin and Range in areas affected by the combination east-west Basin and Range extension and northeast to southwest rifting, with no discernable progression of volcanism in any direction as the basalt exploited any weakness in the crust.

Silicic volcanism along the High Lava Plains does have an east to west progression beginning 16 Ma (Macleod, 1975; Jordan et al. 2002; Jordan et al., 2004; Jordan, 2005). With continued extension to the southwest during the 7.8 to 7.5 Ma episode small magma chambers that had fed the basaltic magmatism may have been sealed off by a combination of underplating and the plugging of vents by cooling magma (Figure 4.5) Until this happened reservoirs were replenished as mantle upwelling provided a continuing supply of fresh basalt to each axial chamber. As cooling and crystallization along reservoir walls shrinks the axial chamber volume, crystal settling and underplating by magma movement along the base of the crust isolates, at different times, each small axial magma chamber from its supply.

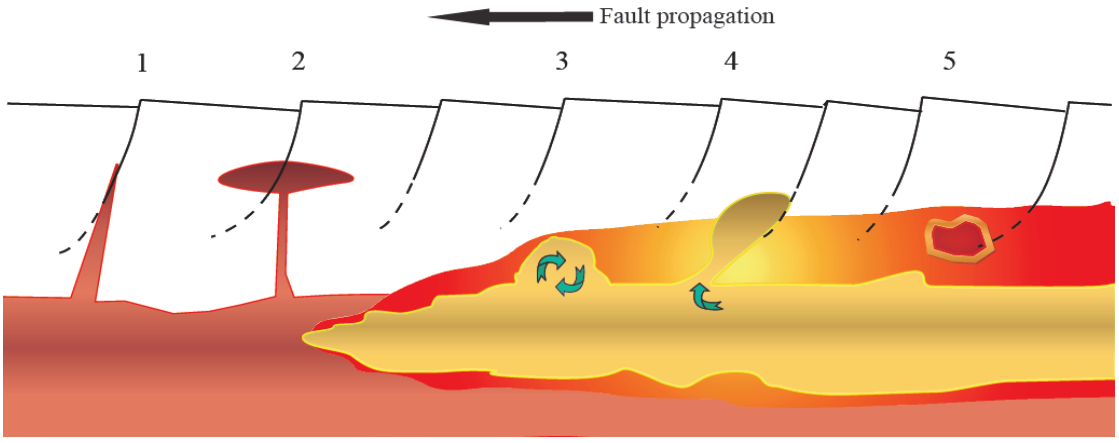

Figure 4.5: (No scale) Cartoon illustrating fault propagation from east to west in the Basin and Range at its juncture with the High Lava Plains combined with sub-lithospheric magma flow also from east to west and possible eruptive products.

1. Faulting provides a path for direct mantle decompression melts to reach the surface. Cooler surrounding crust inhibits assimilation. Produces eruptive products such as Dry Mountain.

2. Decompression melting of the mantle and fractionation in a magma chamber surrounded by cooler crust that promotes fractionation and inhibits assimilation produces the evolved high-silica magma as found at Glass Buttes.

3. Decompression mantle melt is combined continuously with fresh hot magma supplied by the sub-lithospheric flow in a chamber with inhibited fractionation due to the surrounding reheated crust. Little assimilation. The basalt at Hampton Butte.

4. Sub-lithospheric flow at a magma chamber nearly isolated from its magma supply by a narrowing opening due to crystallization. Contact with cooler surrounding rock promotes fractionation with less heat input by incoming magma. A more evolved magma such as the andesite of Hampton Buttes would be produced.

5. Complete closure of the channel between the chamber and sub-lithospheric magma flow by underplating and/or crystal accumulation allows assimilation of country rock heated by the magma.

Combined Basin and Range normal faulting and rifting along the High Lava Plains continues as new faults develop, or old faults are reactivated along the southern edge of the High Lava Plains. As northeast to southwest rifting continues, a new path to the surface for the now more silicic magma at westward propagating normal faults erupt, resulting in silicic volcanism at the surface. During the eruption, subsidence caused by the removal of magma on either side of the vent and the eventual solidification of magma below the vent, results in subsidence and elongated basin-like structures to either side. At Hampton Buttes this has resulted in a small basin directly to the south, between it and Frederick Butte. Waning extension causes both types of volcanism to slow, with sporadic isolated volcanism from basaltic to rhyolitic occurring where the axial magma chambers, depending on their depth, volume, and length of isolation make their way to the surface. Basaltic volcanism occurs where the isolation of the axial chambers is relatively recent and the magma has not had time to significantly differentiate. Eruptions are more silicic where the reservoir has been isolated from its source of magma for longer periods and had time to fractionate before eruption (Figures 4.4 and 4.5).

Basaltic volcanism between 5.3 and 5.9 Ma follows a similar pattern. During the third phase of extension, a major Basin and Range normal fault develops southeast of Wagontire Mountain opening northwest to southeast rifts that, in places follow older fault lines with the same trend. These reactivated sections of older faults ultimately intrude into the Brothers Fault Zone (Plate II). As happened during the previous episode of rifting, and noted by Jordan et al. (2004), a period of basaltic vol-

canism resulted that was preceded by random outbreaks of silicic and basaltic volcanism as the area continued to be subjected to extension. After 5.68 Ma at the eastern end of the study area 63 m (± 5 m) of extension accumulated at a rate of 0.01 mm/y (Trench, 2008). It is during this time that the fractionated and now silicic magma, emplaced and isolated during and after the previous mafic outburst was able to erupt due to the weakening of the overlying crust caused by continuing extension at the juncture of the northwest to southeast striking (reactivated) and High Lava Plains faults, forming Glass Buttes. Fault propagation and age progressive volcanism continues along the High Lava Plains to Frederick Butte (4.91 ± 0.73 Ma) where basalt erupted during the 5.9 to 5.3 Ma surge in basaltic volcanism that had been trapped in axial chambers and fractionated erupts as continued extension enables magma to reach to the surface (Figures 4.4 and 4.5). Age progressive volcanism extends out of the study area towards Newberry Volcano (cf. Jordan, 2005) (Plate II).

4.2 Petrology

4.2.1 Modeling Methods: Models for the development of selected samples from this study were developed by using the results of XRF and ICP-MS analyses and working back to derive a reasonable parental magma composition by adjusting the weight percent of each major element through the addition of minerals that would be removed during crystallization. The minerals are selected based on those commonly found in that rock type and are either added to or, in some cases, removed as necessary. Addition in these models simulates mass loss during differentiation. Mineral removal signals addition such as through assimilation or recharge. Mineral com-

positions are from Deer, Howie, and Zussman (1992). Partition coefficients are from tables published by Rollinson (1993) and were not adjusted except to another published value for that same rock type (first) or in a different rock type (second). A parental REE composition is derived by substitution with the listed partition coefficient until a reasonable match is made with the XRF or ICP-MS result.

4.3 Petrologic History

4.3.1 Basalts: The term HAOT (high alumina olivine tholeiite) was proposed by Hart et al. (1984) after they noticed a change in chemical composition following the eruption of the Columbia River and Steens flood basalts between 15 to 17 Ma. Hart and Carlson (1987) suggest that the transitional compositions of the basaltic rocks in southeastern Oregon are a mixture of primitive HAOT type mantle and Snake River olivine tholeiite (SROT). Compared to the Columbia River and Steens basalts, HAOT and SROT basalts have limited variation in composition yet have distinct isotopic and chemical signatures. McKee et al. (1983) and Bailey and Conrey (1992) recognize oceanic affinities in eastern Oregon basalts that have not been contaminated nor fractionated (Draper, 1991). Experimental work by Bartels et al. (1991) on HAOT basalt at Medicine Lake established that the basalt had equilibrated at a shallow (~35 km) level in the mantle. Maclean (1994) summed this up by stating that the regional basalts are most likely a result of mantle melts with little or no time in a crustal magma chamber rising rapidly through the crust and erupting.

Major element compositions (by wt %) of the samples collected for this thesis show that compared to the average composition of Hart et al. (1984) for HAOT basalt of the High Lava Plains those of the northern margin are depleted in magnesium, and usually iron while being enriched in silica, titanium, aluminum, sodium, potassium and phosphorous; in other words they are slightly evolved . Lower MgO is consistent with the fractionation of forsterite (Mg_2SiO_4). Fractionation of the calcic clinopyroxene, augite (Ca, Mg, Fe, Al)$_2$(Si, Al)$_2O_6$) would lead to the reduction of some iron and calcium. Both augite and olivine phenocrysts are present in the basalt of the northern margin. Titanium compatibility is low (0.02 into olivine) resulting in an increase in its percentage in the remaining melt (Figure 4.6). The tholeiitic differentiation trend defined by the basalt is consistent with a crystal fractionation trend (Figures 3.8, 4.7)

Grassy Butte (GB-0701) and the andesite of Hampton Buttes (HTB-0623) are the most evolved of the lower silica rocks sampled. HTB-0623 (andesite) is included as a part of the volcanism of the High Lava Plains due to its 7.81 (± 0.14) Ma age, consistent with the ages of other samples from this thesis and others belonging in a period of increased volcanism around that time. Plots of major minerals for Grassy Butte and HTB-0623 (andesite) show that the same minerals (except for ilmenite in the andesite) have been removed from the melt, with the andesite reaching 80% crystallization compared to 60% for the basaltic andesite of Grassy Butte (Appendix 3). Lower titanium in HTB-0623 (andesite) of Hampton Buttes can be correlated to the

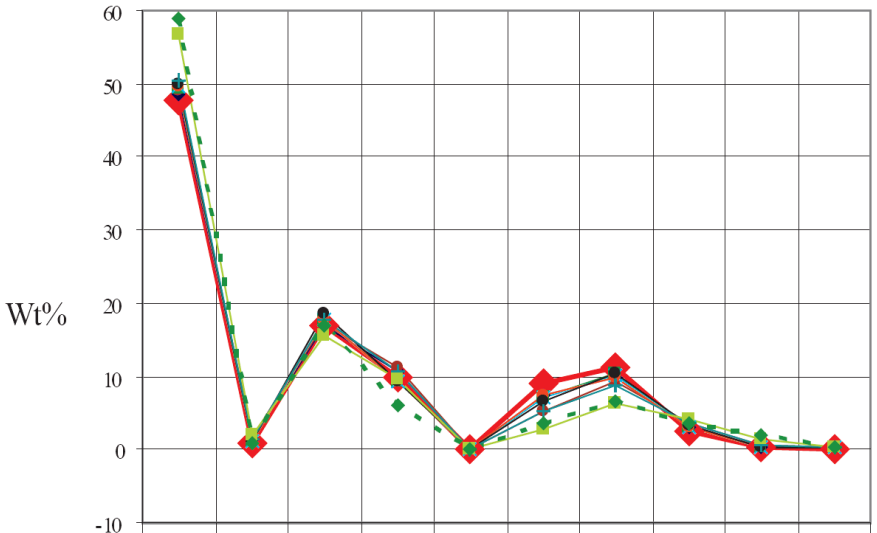

	SiO_2	TiO_2	Al_2O_3	FeO*	MnO	MgO	CaO	Na_2O	K_2O	P_2O_5
50 HAOT of Hart et al., 1984	47.66	1.0	16.91	9.88	0.17	9.06	11.2	2.53	0.23	0.13
DMT-0601	48.56	1.50	16.97	10.84	0.18	7.39	9.88	3.09	0.43	0.33
HTB-0710MF	49.11	1.72	17.37	11.33	0.20	5.17	9.23	3.70	0.65	0.40
HTB-630	49.47	1.26	17.87	9.25	0.16	7.04	10.36	3.19	0.34	0.24
HTB-0631	49.59	1.28	17.88	9.32	0.16	7.15	10.27	3.18	0.37	0.24
HTB-0629	49.66	1.25	17.86	9.21	0.16	7.47	9.78	3.16	0.35	0.22
HTB-0523	50.01	1.30	18.55	9.37	0.16	6.57	10.36	3.26	0.38	0.25
HTB-0712MF	50.41	1.56	17.90	10.82	0.18	5.26	8.81	3.70	0.68	0.42
GB-0701	56.65	1.97	15.56	9.71	0.19	2.78	6.30	4.09	1.31	0.32
HTB-0623 Andesite of Hampton Buttes	58.80	0.84	17.05	6.21	0.12	3.55	6.56	3.56	2.04	0.35

Figure 4.6: A comparison of basalt, basaltic andesite and andesite collected from along the northern margin of the High Lava Plains against the average of 50 samples used to define HAOT basalts by Hart et al. (1984). The fractionation of olivine and augite accounts for the decrease of magnesium and iron in the HTB basalt samples. Titanium does not partition well into either phase and becomes more concentrated in the melt. The basaltic andesite of Grassy Butte (GB-0701) fractionates more forsterite and calcic pyroxene during a brief respite in a crustal magma chamber before erupting. HTB-0623 also has a short residence in a crustal magma chamber, removing more magnesium and calcic pyroxene with the added fractionation of ilmenite ($FeTiO_{3)}$ further reducing titanium.

production of ilmenite ($FeTiO_3$), compared to dominantly magnetite in the other samples (Figure 4.6).

A rare earth element plot of the basalt samples collected reveals that fractionation has resulted in a small degree of the less compatible light rare earth elements enrichment and to a lesser degree the incorporation of the more compatible rare earth elements into the fractionating minerals (Figure 4.8). The basaltic andesite of Grassy Butte (4.18 ± 0.14) may originate from a more primitive source than the older basalts (Figure 4.8) due to the upwelling or flow of plume transported mantle material during the 5.9 to 5.3 Ma increase in basaltic activity proposed by Jordan et

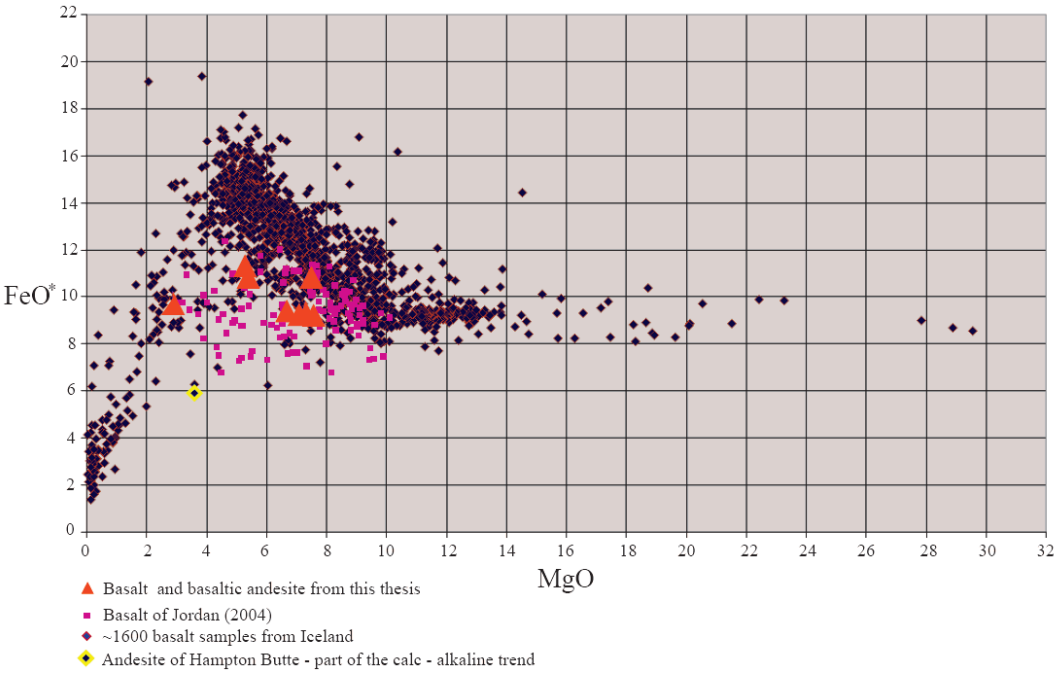

Figure 4.7: Comparison of samples from this thesis with SiO_2 less than 60 % to samples from Iceland. Thesis samples are of a lower iron variety compared to the Icelandic rocks but are distinctly part of the tholeiitic basalts from Jordan (2004). Black line represents the trend of over 1600 Icelandic basalts (modified from Gunn and Sarbas, 2002).

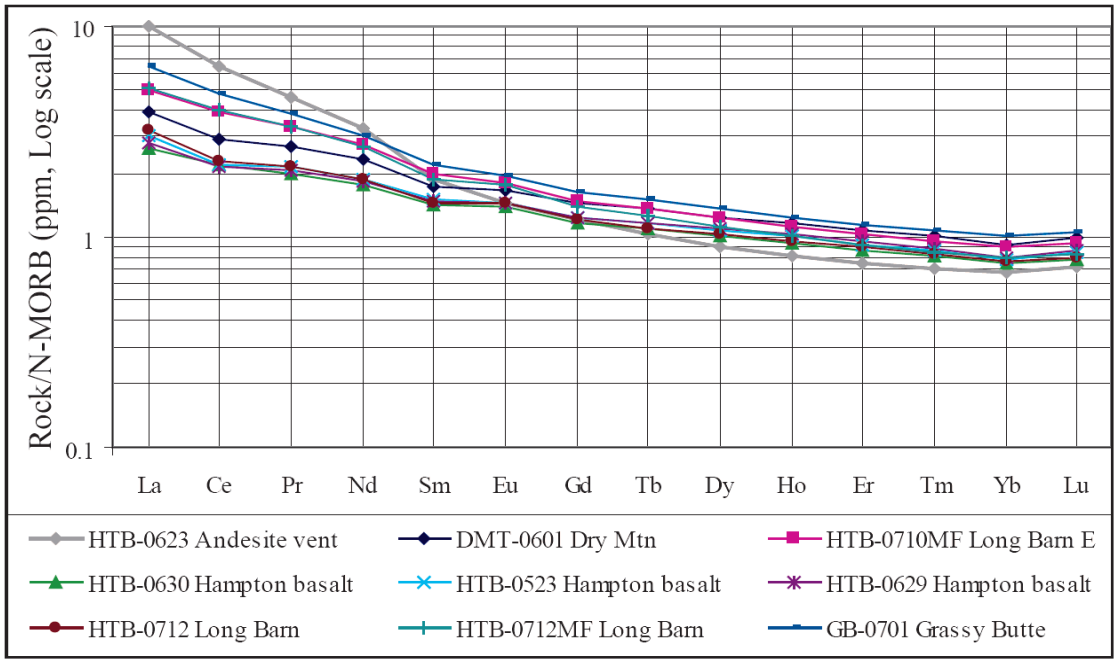

Figure 4.8: Rare earth element plot of samples collected for this study with SiO_2 less than 60 %. The small negative cerium anomalies may reflect the removal of magnetite (Di 1.3 – 3.0) (Schock,1979) from the melt prior to eruption or removal during weathering as Ce^{4+}. Normalizing values from Sun and McDonough (1989).

al. (2004). The rare earth element plot of results for HTB-0623, the Hampton andesite, reveals a decrease of the more compatible heavy rare earth elements and an increase of the more incompatible light rare earth elements in a smooth curved pattern suggesting fractional crystallization with little or no assimilation.

All of the High Lava Plains samples in this study with SiO_2 less than 60 % lack a negative europium anomaly and most are interpreted as having a slight positive europium anomaly (Figure 4.8). At 8 kilobars (~ 30 km) and higher, plagioclase is not a stable phase and the substitution of europium into plagioclase cannot take place, and result in a negative europium anomaly. According to Nielsen (1992) strontium is also incompatible in plagioclase at temperatures above 1220°C so any frac-

tionation that has taken place with these samples happened at over 10 kilobars and/or 1220°C. No decrease in strontium concentration with increasing silica content is evident therefore fractionation most likely took place at or over 29.6 kilometers and 1220°C (Table 3.2), consistent with origination near the base of the crust (Figures 1.4 b : 3.3: 4.12). A shallower depth is possible if water had suppressed the onset of plagioclase fractionation.

4.4 Silicic volcanism after 20 Ma

4.4.1 Potato Hills and Hat Butte: The 6.52 ± 0.07 Ma Potato Hills rhyolite are clearly part of the High lava Plains volcanism, originated in a manner consistent with the extensional bimodal model illustrated by Hildreth (1981) (Figure 4.9). The highly silicic rhyolites of the High Lava Plains are in contrast to the older (John Day age), lower silica differentiates of Hampton and Cougar Buttes. The Potato Hills rhyolite has the hallmarks of a highly differentiated high-silica rhyolite as indicated by the extreme Eu anomaly and low Sr, an origin consistent with extreme crystal fractionation, such as the early erupted Bishop Tuff (c.f. Hildreth, 1979). The flat REE pattern (Figure 3.2) suggests fractionation of a LREE-enriched trace phase such as allanite (Hildreth, 1979, Miller and Mittlefehldt, 1982). Although the Potato Hills rhyolite can be modeled from a basalt consistent with HAOT compositions (Appendix 3) it is not possible to be certain if its origin without knowing its silicic precursor. Streck and Grunder(2008) point out that the liquid line of descent is difficult to discern as late stage fractionation obscures rhyolite parentage.

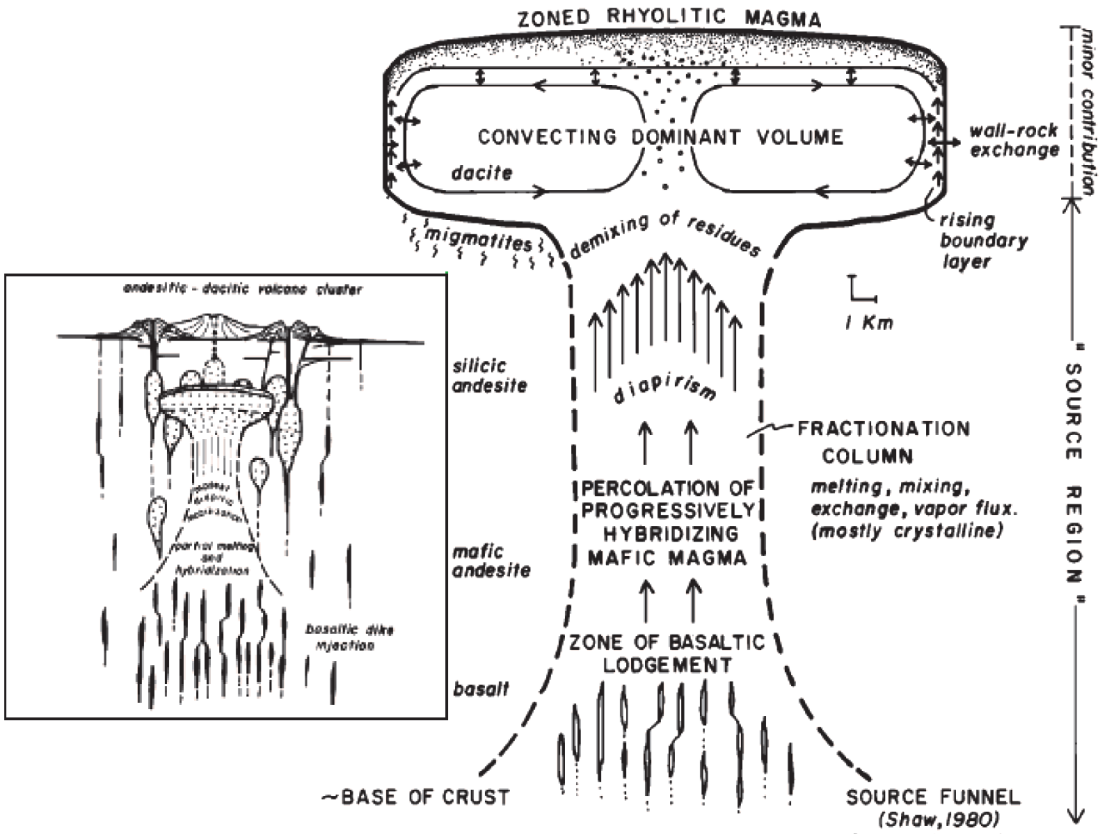

Figure 4.9: Basaltic magma provides the heat that progressively warms the crust, resulting in the large scale crustal diapirism. Circulation in a chamber such as this may account for the zoned and resorbed textures found in the rhyodacite at Hampton Butte. Inset: Andesitic to dacitic magma generation during an earlier stage of development.

4.4.2 Hampton Tuff : The 3.8 (± 0.8) Ma $^{40}Ar/^{39}Ar$ age of the Hampton Tuff (HTB-0701) sampled in Hampton Buttes is virtually same as the K-Ar age of 3.7 (± 0.6) Ma recalculated by Fiebelkorn et al. (1983) from Walker (1974) for the tuff of Espeland Draw (Plate II) 6.5 kilometers north northeast of Frederick Butte. Chemical similarities between the two samples and another taken eight kilometers north of Frederick Butte share similarities in major and rare earth elements. Johnson (1998) suggests that the Hampton Tuff may be related to rhyolite pumice and dacite taken from Frederick Butte (Table 4.1). If the tuff is related to the eruption of the dacite and pumice as suggested, the similarities between the Hampton Tuff, alkali rhyolite ash and pumice, and Tuff of Espeland Draw add more substance to the argument for their common origin.

Modeling of the XRF and ICP-MS results of the Hampton Tuff sample (HTB -0701) produces a parent inconsistent with the average of 50 basalts used to define high alumina olivine tholeiites by Hart et al. (1984), and tholeiitic basalts of this study (Figures 4.6). It appears that these older magmas had different mantle-derived parents or that HAOT basalt underwent a stage of differentiation to become parent to the Hampton Tuff. By mixing the normalized values of Hart et al. (1984) with a pyroxenite composition consistent with those of Vallier and Brooks (1995) and Zheng et al. (2009) at the base of the crust (Figure 4.10) the parent composition of the Hampton Tuff can be matched (Table 4.2). Fractionation of this mixture in the crust could yield not only the Hampton Tuff, but with some assimilation the composition of the alkali rhyolite ash and pumice (HTB-0516) and the Tuff of Espeland Draw

Table 4.1: Comparison of normalized major element values and un-normalized REE values for 2 samples collected from different locations in Hampton Buttes and 1 between the buttes and Frederick Butte by Johnson (1998) at Espeland Draw.

	HTB-0701 Hampton Tuff	FB 94-12 Tuff of Espeland Draw	HTB-0613 Alkali Rhyolite ash and pumice
SiO2 (wt %)	73.91	74.59	74.68
TiO2	0.27	0.22	0.20
Al2O3	13.19	13.43	13.95
FeO*	3.19	2.18	2.16
MnO	0.08	0.08	0.07
MgO	0.21	0.21	0.16
CaO	0.98	0.92	0.83
Na2O	4.90	4.18	3.16
K2O	3.24	4.14	4.75
P2O5	0.03	0.05	0.03
	100.00	100.00	100.00
Total before normalization	100.00	99.02	93.30
Rb (ppm)	70	77	90
Ba	1171	1149	1170
Sr	93	58	59
Zr	397	305	348
Nb	17	15	16
Ni	0	10	3
V	15	5	6
La	32	49	nd
Ce	64	69	nd
Y	79	8	63

(Figure 4.1). Slight fractionation and and/or assimilation would also result in basalt consistent with the compositions of Jordan (2004) (Figure 4.11).

4.5 Silicic volcanism before 20 Ma

4.5.1 Hampton and Cougar Buttes:

The close proximity of the buttes to one another (5 km) and the timing necessitates investigating if there is a petrologic link between the two; with attention to the make up of the crust through which both magmas needed to pass to reach the surface. Reverse modeling of the Hampton Butte rhyodacite (HTB-0501) and Cougar Butte Dacite shows that the parent for both rocks are likely the same. Of the two modeled parents, the model for HTB-0613 is the more primitive of the samples. Using modeled parental magma compositions for the buttes produces a root mean squared error (RMSE), comparing the calculated parental magmas at seventy percent crystallization, of 0.920 (Table 4.3). The result is close but the gap can be further resolved by forward modeling to 10% crystallization from the calculated parent of Cougar Butte using a differ-

Table 4.2: The mixing of a basalt with the average composition of Hart et al. (1984) and a pyroxenite can produce the parent composition of the Hampton Tuff.

	Hart (normalized)		Modeled pyroxenite		Parent of Hampton Tuff (modeled)	R
66.9%	48.25	+ 33.1%	50.86	= 49.12	49.12	0.00
	1.01		4.58	2.19	2.19	0.00
	17.12		2.94	12.43	12.42	0.00
	10.00		16.02	11.99	12.00	0.00
	0.17		0.82	0.39	0.39	0.00
	9.17		15.66	11.32	11.32	0.00
	11.34		4.65	9.13	9.12	0.00
	2.56		2.30	2.47	2.48	0.00
	0.23		1.71	0.72	0.72	0.00
	0.13		0.46	0.24	0.24	0.00
Total	100.00		100.00	100.00	100.00	
					$\sum R^2$	0.00

ent combination of phases and weight percentages while keeping the same distribution coefficients (Appendix 3) (Table 4.3). By doing this the RMSE between a ten percent crystallization of the Cougar Butte (HTB-0613) parent and the calculated parent of Hampton Butte (HTB-0501) is minimized to 0.358 (Table 4.4). Rare earth element concentrations can be modeled by using the reverse modeled rare earth elements of Cougar Butte as a starting point for modeling through the link to the parent of Hampton Butte. Adjusting the distribution coefficients produces a result that allows for the assimilation of trace elements from the crust (Table 4.5 and 4.6). Differences in chemical make-

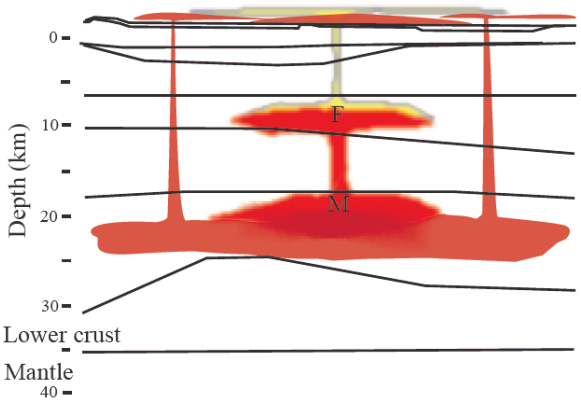

Figure 4.10: Hypothetical cross section near Hampton Buttes illustrating mixing of a tholeiitic magma and pyroxenite at the base of the crust followed by a mid-crust fractionation, producing the Hampton Tuff. M - mixing F - fractionation

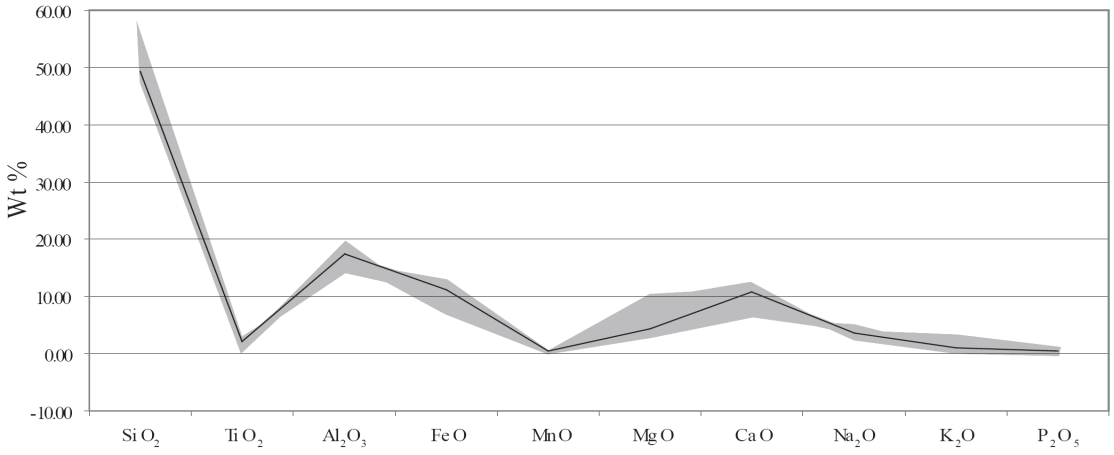

Figure 4.11: Comparison of a basalt modeled from mixture of 66.9 % of the average HAOT basalt of Hart et al. (1984) and 33.1 % of a calculated pyroxenite consistent with pyroxenite compositions in Vallier and Brooks (1995) and Zheng et al. (2009) compared to the range of 113 High Lava Plains basalts from Jordan (2004).

up of Hampton Butte (rhyodacite) and Cougar Butte (dacite), derived from the same parent, can be explained by the changing mineral fractionation. The early fractionation of the Cougar Butte calculated parent to the calculated parent of Hampton Butte by removal of large amounts plagioclase and olivine reduced the silica content of the melt and to a lesser amount the aluminum, calcium, and magnesium, leaving the restite depleted in these elements relative to Cougar Butte. Enrichment, compared to the parent of Cougar Butte, can be seen in iron and potassium (Figure 4.3). Removal of larger concentrations of silica through crystallization of olivine and plagioclase (compared to iron depletion) slightly increased the iron available for the second stage of the Hampton Butte fractionation (Hampton Butte calculated parent to the rhyodacite) with the concentration of potassium increasing in the same manner (Table 4.3). It is to be borne in mind that these models are simplifications in that all crystals are removed or added in one step, although not all will be in equilibrium simultane-

Table 4.3: Comparison of results from least squares mass-balance calculations modeling parent compositions for Hampton Butte (HTB-0501) and Cougar Butte (HTB-0613). Rubidium, strontium, and barium parent compositions were determined by reverse modeling from the XRF results, as were the major elements. Phases are those removed from the melt. Total iron reported as FeO.

	HTB-0501					HTB-0613					Residual	
	Parent of HTB-0501 (calc)	Phases (calc)	wt % (calc)	(Calc)	(XRF)	Parent of HTB-0613 (calc)	Phases (calc)	wt % (calc)	(Calc)	(XRF)	Parent of HTB-0501 (-) Parent of HTB-0613	R^2
SiO2 (wt%)	49.33	T-mag	12	67.66	67.66	48.78	T-mag	12	65.64	65.64	-0.553	0.306
TiO2	1.97	Plag	37	0.51	0.51	1.87	Plag	37	0.34	0.36	-0.100	0.010
Al2O3	13.28	Hbld	5	15.44	15.44	13.70	Hbld	05	16.81	16.84	0.420	0.176
FeO	12.18	Apatite	1	3.55	3.54	11.75	Apatite	1	2.44	2.45	-0.430	0.185
MnO	0.35	Ol	29	0.05	0.05	0.35	Biotite	1	0.03	0.04	0.003	0.000
MgO	11.61	Cpx	6	0.87	0.87	11.79	Ol	29	1.35	1.37	0.185	0.032
CaO	7.20	**Total**	**100**	3.35	3.35	7.47	Cpx	16	4.40	4.40	0.270	0.076
Na2O	2.66			4.44	4.44	2.71	**Total**	**100**	4.65	4.66	0.050	0.002
K2O	0.89			2.40	2.40	0.58			1.37	1.36	-0.242	0.059
P2O5	0.34			0.15	0.15	0.34			0.15	0.15	0.000	0.000
				$\sqrt{\sum R^2}$ =	**0.01**				$\sqrt{\sum R^2}$ =	**0.04**	$\sqrt{\sum R^2}$ =	0.920
Rb (ppm)	5			17	54	5			-	15		
Sr	691			318	382	691			-	1011		
Ba	346			581	664	321			-	786		

ously. Although they are a simplification, they remain a robust test of the path independent differentiation.

Retallack et al. (1999) report paleosols with high concentrations of barium and low rubidium from the Clarno and John Day Formations that may underlie the region below Hampton Buttes (Table 4.5). High silica rocks (>58 wt% SiO_2) of the High Lava Plains from Ford (in progress), Scarberry (2008) and Walker (1981) average 84 ppm rubidium for 263 analysis, the Hampton and Cougar butte rocks from the northern margin average 36 ppm of rubidium with a high of 65.4 ppm for Hampton Butte and a low of 13.9 at Cougar Butte (Table 2.2). For the same number of analysis barium averages 732 ppm in the samples from Hampton Buttes compared to 710 ppm from the High Lava Plains. Strontium values for the same samples from the High Lava Plains average 221 ppm, for Hampton Buttes samples the average is 683 ppm

Table 4.4: Results of modeling the link from the calculated parent of Hampton Butte to the calculated parent of Cougar Butte after 10% crystallization of the calculated Cougar Butte Parent.

	Parent of HTB-0613 (calc)	Phases (calc)	wt % (calc)	10 % crystallization of HTB-0613	R^2	Parent of HTB-0501 (calc)
SiO_2	48.78	T-mag	12	49.33	0.000	49.33
TiO_2	1.87	Plag	37	1.97	0.000	1.97
Al_2O_3	13.70	Hbld	5	13.28	0.000	13.28
FeO*	11.75	Apatite	1	11.95	0.051	12.18
MnO	0.35	Biotite	1	0.32	0.001	0.35
MgO	11.79	Ol	29	11.68	0.005	11.61
CaO	7.47	Cpx	16	7.31	0.003	7.20
Na_2O	2.71			2.70	0.002	2.66
K_2O	0.58			0.67	0.046	0.89
P_2O_5	0.34			0.24	0.010	0.34
		Total	**1.00**	$\sqrt{\sum R^2}$=	**0.358**	
Rb	5			5		5
Sr	691			691		691
Ba	321			327		346

with Cougar Butte having an over 2.5 to 1 concentration of strontium compared to Cougar Butte. If Hampton Butte and Cougar Butte share a common parent and evolution it is necessary to explain the differences in rare earth element abundances.

Using element abundances and partition coefficients it is possible to explain the large differences and similarities in the three elements. Most of the time rubidium and barium are incompatible elements and tend to be enriched in the melt as crystal-

Table 4.5: Selected trace element analysis (ppm) by AA and XRF of John Day and Clarno paleosols from G.J. Retallack et al. (1999) that now cap the underlying crust.

Paleosol	Hz	JODA #	As	Ba	Ce	Co	Cr	Cu	Ga	La	Li	Nb	Ni	Pb	Rb	Sc	Sr	Th	V	Y	Zv	Zr
John Day																						
Luca	Bt	5392	-	1007	15	-	14	40	28	7	-	13.2	5	12	179	31	80	0	94	39	95	168
Clarno																						
Basalt	A	5719	-	411	66	-	460	37	16	20	-	23.5	159	4	29	27	559	3	201	20	69	148
Type	A	5085	2.0	587	35	-	18	17	17	18	-	8	26	8	45	10	257	5	30	11	57	113
Patat	A	5086	-	526	44	-	7	18	20	7	-	11.4	7	5	34	12	372	5	39	14	34	134
Patat	Bw	5087	-	811	51	-	14	7	25	21	-	11.8	2	12	51	13	334	3	63	15	87	143
Patat	Bw	5088	-	690	58	-	13	23	22	18	-	13.4	8	2	51	17	397	7	66	13	58	149
Patat	C	5089	-	1111	66	-	14	23	20	30	-	16.6	10	68	15	15	418	8	89	16	95	196

Analyses by Christine McBirney, using atomic absorption (AA) with errors from 10 replicates of standard rock W2 and Diane Johnson, using X-ray florescense, with errors from Mt. Rainier andesite analysis.

Table 4.6: Calculated bulk distribution coefficients for reverse modeled HTB-0501, HTB-0613, and the link between the modeled parental rubidium, strontium, and barium compositions. Bulk distribution coefficients are modeled using partition coefficients from Rollinson (1993). Arrows indicate direction of calculations. Major element modeling results are in table 4.3. Appendix 3 lists distribution coefficients used and detailed calculation results.

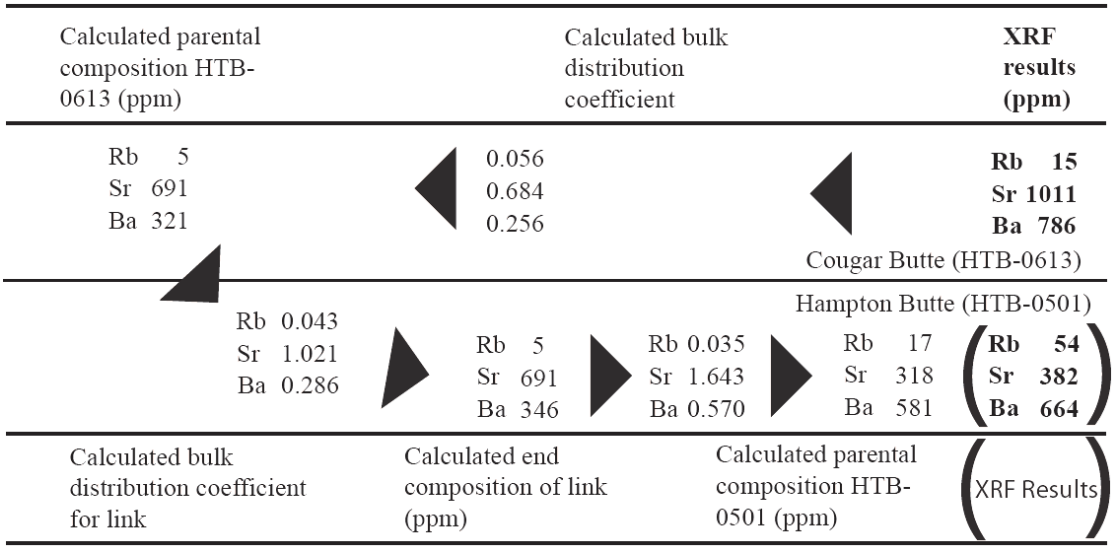

lization progresses. If phlogopite or biotite is present the behavior of these elements in a melt change. In phlogopite, rubidium is 3 times more compatible than barium (3.06 to 1.090) and in biotite barium is twice as compatible as rubidium (6.360 to 3.260). Strontium has a wide range of partition coefficients, ranging from 0.01 in garnet to 15.633 in plagioclase of high silica rhyolites (Rollinson, 1993).

If both samples have the same parent, the difference in rubidium could be explained by the fractionation of phlogopite or biotite in the evolution of the Cougar Butte dacite removing rubidium from the system. Phlogopite can exist in magnesium rich medium-to high-grade metamorphic rocks such as altered peridotites. Such metamorphic rocks were suggested to be in the lower crust of the High lava Plains by Catchings and Mooney (1988) (Figure 4.11). However no phlogopite is found in the

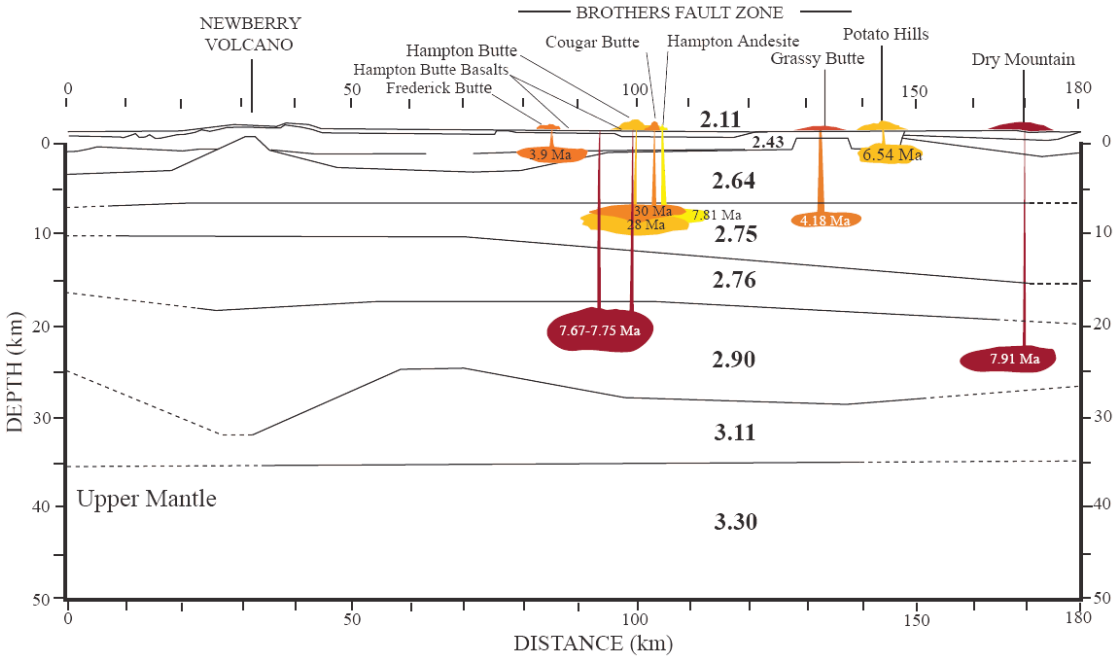

Figure 4.12: Position of magma reservoirs based on the calculated density of the magma using "Magma", a software program developed at Los Alamos National Laboratory. Reservoirs are positioned at approximately a neutrally buoyant location in the cross section of Catchings and Mooney (1988).Data used for the calculations is in Table 4.7.

Table 4.7: Data used and results from "Magma" software program . Reservoirs are positioned at approximately a neutrally buoyant location in the cross section of Catchings and Mooney (1988) in Figure 4.12.

Sample #	Location	Rock type	Pressure (bars)	Temperature (°C)	Liquidus (°C)	Crystals (Vol%)	Crystal size (mm)	Water added (wt%)	Bulk density (g/cm^3)
HTB-0701	Hampton Tuff	Rhyolite	2000	1097	897	15	1	2.1	2.5
HTB-0523	Hampton Basalts	Basalt	5000	1286	1186	10	0.5	0.0	2.9
HTB-0501	Hampton Butte	Rhyodacite	2500	1186	986	30	1	1.6	2.7
HTB-0511	Cougar Butte	Dacite	2500	1207	1007	30	0.1	2.3	2.7
HTB-0623	Hampton Buttes	Andesite	2500	1318	118	10	0.2	0.0	2.7
GB-0701	Grassy Butte	Basaltic Andesite	2500	1288	1088	10	0.5	0.9	2.7
HLP-0704	Potato Hills	Rhyolite	2000	1016	816	20	2	4.2	2.4
DMT-0601	Dry Mountain	Basalt	5000	1348	1148	5	0.2	0.83	2.9

samples examined. Biotite, as a scavenger of rubidium, would potentially remove substantial barium at the same time, but a large difference in barium between the two samples does not exist (Table 2.2). Lower strontium values in the older Hampton Butte samples compared to the Cougar Butte strontium indicate a bigger role for plagioclase in its removal. If the parent for the two rocks is the same than the fractionation path for each is different, biotite reducing rubidium in the Cougar Butte Dacite and plagioclase playing a bigger role in the removal of barium from the melt. If there is a common parent for the two buttes there needs to be two separate fractionation paths (Figure 4.13).

Strontium isotope values obtained by Ford (in progress) for Hampton Butte and Cougar Butte are 0.7035 and 0.7036 respectively. According to Rollinson (1993), $^{87}Sr/^{86}Sr$ between 0.702 and 0.704 with Rb/Sr 0.2 to 0.4 indicates a mid continental crustal source. However, the Rb/Sr ratios for the Hampton Butte (0.18 and 0.14) and Cougar Butte (0.14 and 0.15) samples are outside Rollinsons parameters with either lower rubidium or higher strontium than other crustally sourced rocks. Using a compilation of data by Saunders et al. (1988) and Weaver, (1991) Rollinson (1993) also formulated a table of incompatible trace element ratios in mantle and crust reservoirs (Table 4.8). A comparison of incompatible trace element ratios for Hampton Butte samples (HTB-0501, 0503c) reveals a closer match with ratios from other crustal sourced rocks compared to those that are mantle sourced, possibly a result of assimilating the incompatible trace elements from surrounding rock during fractionation. (Table 4.5 and 4.9). The higher ratios in the Cougar Butte samples

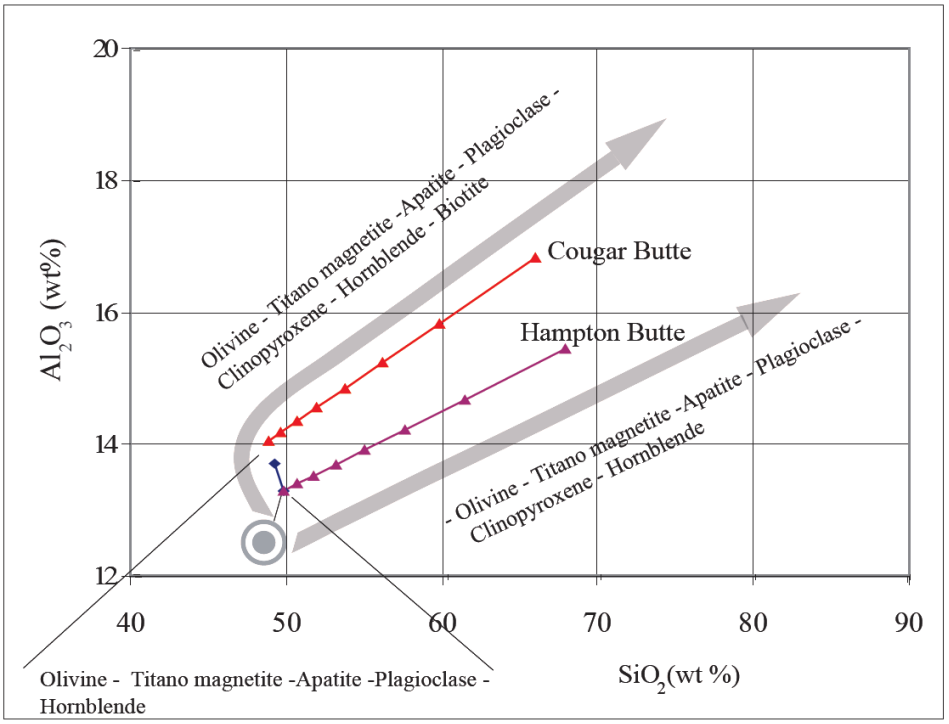

	T-mag	Plag	Hornblende	Apatite	Olivine	CPX	Biotite
Hampton Butte HTB-0501	12%	37%	5%	1%	29%	16%	0.0%
Link - Cougar Butte parent to Hampton Butte parent	4.5%	55.5%	8.5%	3%	27%	0.0 %	0.0%
Cougar Butte HTB-0613	12%	37%	5%	1%	29%	16%	1%

Figure 4.13: Plot of aluminum verses silica, as a tracer for crystallization of hornblende. Both HTB-0501 (Hampton Butte) and HTB-0613 (Cougar Butte) can be produced by the same parent by removing the same phases and phase percentages if a link between the calculated parent of Cougar Butte and that of Hampton Butte is made. By adjusting phase percentages and adding biotite to the Cougar Butte path, at 10 percent crystallization a reasonable link can be made.

Table 4.8: Incompatible trace element ratios in crust and mantle reservoirs (from compilations by Saunders et al., 1988, and Weaver, 1991) modified from Rollinson, 1993.

Incompatible trace element ratios in crust and mantle reservoirs (from compilations by Saunders et al., 1988, and Weaver, 1991) modified from Rollinson, 1993

	Zr/Nb	La/Nb	Ba/Nb	Ba/Th	Rb/Nb	K/Nb	Th/Nb	Th/La	Ba/La
Primitive mantle	15	1.0	9	77	0.1	323	0.117	0.1	9.6
N-MORB	30	1.0	2.0-8	60	0.4	210-350	0.0-0.1	0.1	4
E-MORB			5.0-9			205-230	0.1		
Continental crust	17	2.0	54	124	4.7	1341	0.4	0.2	25
HIMU-OIB	3.0-5.0	1.0	5-7	49-77	0.4	77-179	0.1	0.1	6.8-8.7
EMI-OIB	4.0-12	1.0	11-18	103-154	0.9-1.0	213-432	0.1	0.1	13.-17
EMII-OIB	5-7	1.0-1.1	7-13	67-84	0.6-0.9	248-378	0.1-0.2	0.1-0.2	8.0-11

(HTB-0613, HTB-0511) may result from the assimilation of the more incompatible elements in the crust during the ascent of the Cougar Butte magma or mixing with the residue of the Hampton Butte magma chamber.

The possibility of the more evolved Hampton Butte rock being an evolutionary product related to the younger dacite is supported by examining a model that allows an older rock to apparently have a younger parent. Hildreth (1981) presents evidence that large eruptions of non-basaltic magma are the result of large compositionally, thermally zoned magma chambers being tapped, and that small-scale eruptions result from the eruption of evolving heterogeneous magma systems (Figure 4.9).

Table 4.9: Incompatible trace element ratios for samples collected for this thesis.

Older Than 20 Ma

	Zr/Nb	La/Nb	Ba/Nb	Ba/Th	Rb/Nb	K/Nb	Th/Nb	Th/La	Ba/La
Older Than 20 Ma									
HTB 0613	41	6.0	427	592	9.0	3896	1.0	0.0	70
HTB 0511	44	4.0	423	267	8.0	4021	2.0	0.0	95
HTB 0501	16	2.0	74	122	6.0	1339	1.0	0.0	35
HTB 0503c	13	2.0	68	112	6.0	1635	1.0	0.0	42
HLP 0704	6	1.0	2.3	2	9.0	1779	1.0	1.0	3
Younger than 20 Ma									
DMT 0601	21	3.0	68	366	0.0	504	0.0	0.0	25
HTB 0710MF	20	3.0	67	1294	1.0	565	0.0	0.0	23
HTB 0630	30	3.0	80	723	1.0	631	0.0	0.0	24
HTB 0631	31	3.0	88	1150	1.0	711	0.0	0.0	27
HTB 0629	44	5.0	106	223	2.0	937	1.0	0.0	23
HTB 0523	24	3.0	80	n.d.	0.0	552	0.0	0.0	31
HTB 0712MF	17	3.0	63	n.d.	1.0	527	0.0	0.0	24
GB 0701	19	2.0	69	246	4.0	881	0.0	0.0	29
HTB 0623	21	3.0	102	393	3.0	1211	0.0	0.0	34
HTB 0516	21	2.0	72	111	6.0	1459	1.0	0.0	30
HTB 0701	24	1	71	152	4.0	982	1.0	0.0	36

Zoned plagioclase in the rhyodacite of Hampton Butte is evidence of changing composition of the magma chamber that was beneath Hampton Butte and the resorbtion texture observed is an indication of changing temperatures within it. The model of Hildreth (1981) explains the process that produces these textures and provides an explanation of how the younger dacite of Cougar Butte can be the parent of the rhyodacite at Hampton Butte. Also, while the two buttes are not quite coeval, similar magma may have recurred at depth for protracted time.

The injection of basaltic dikes at the base of the crust provides the heat to drive partial melting and hybridization that increases as the mafic magma percolates upward. Diapirism results from the intrusion of magma into the overlying crust and in the more advanced systems convection cells form in the magma chamber at the upper level (Figure 4.9). Magma, contaminated by surrounding rock as it rises and fractionates will ultimately be the result of input from the mantle and different levels in the crust (Hildreth, 1981). At Hampton Buttes, these layers most likely include Early to Late Cretaceous near-shore deltaic, and fluvial deposits, and the Clarno and John Day Formations, which contribute to the magmas make-up. The partially resorbed and zoned plagioclase in the rhyodacite of Hampton Butte show the affect of circulation in the convection cell at the top of a more evolved magmatic system as it alternately moves between areas with differing compositions and temperatures (Figure 4.9). The break down of amphibole to irregular fragments and granular masses of plagioclase, clinopyroxene, and magnetite (Figure 2.1) observed in thin section indicates a short but sufficient amount of residence time at pressures less than

1.3 to 2 kilobars, the pressure stability field of hornblende, for the amphibole to break down before erupting (cf. Rutherford and Devine, 2003).

An alternative model is that the rhyodacite of Hampton Butte resulted from differentiation in a zoned magma chamber with the rhyodacite, the most evolved magma at the top, and dacite, its parent, layered below it. Following the eruption of the upper portion of the magma chamber, the void left by the erupting rhyodacite is filled by the denser dacite. Ideally, the eruption would remove all the rhyolite leaving the magma chamber now filled with the denser dacite. This is unlikely, since no dacite can be found capping the rhyodacite of Hampton Buttes; it is more likely that a very small amount of the more evolved magma remained in the chamber, mixing with the incoming parent to the Cougar Butte Dacite (Figure 4.9). Minor fractionation and assimilation ultimately could lead to the composition of the Hampton Butte rhyodacite (Table 4.10).

Table 4.10: Results of modeling from the calculated parent of the Cougar Butte dacite to the Hampton Butte rhyodacite. Results show that fractionation of the Cougar Butte dacite composition can produce a rhyolite similar to the Hampton rhyodacite. Mineral compositions are from Deer, Howie, and Zussman (1992), Distribution coefficients are from Rollinson, (1993).

Model of HTB-0613 (Cougar Butte) to HTB-0501 (Hampton Butte)

	Parent (Calc)	70.0% Plag	3.0% Hornblende	8.0% Alk. Fldspr	10.0% Quartz	9.0% CPX
SiO_2	65.64	53.89	36.34	67.27	100.00	50.40
TiO_2	0.36		0.94			0.87
Al_2O_3	16.84	29.20	14.06	18.35		3.92
FeO	2.45	0.93	28.00	0.92		6.41
MnO	0.04	0.93	0.75			0.13
MgO	1.37		3.14			15.45
CaO	4.40	11.14	11.82	0.15		21.86
Na_2O	4.66	4.85	1.14	6.45		0.29
K_2O	1.36	0.29	2.66	7.05		
P_2O_5	0.15					
	97.28	101.23	98.85	100.19	100.00	99.33
Rb	15					
Sr	1011					
Ba	786					

Results at 20 % Crystallization

	Parent (Calc)	Modeled	XRF	Residual	R^2
SiO_2	65.64	67.37	67.66	-0.29	0.08
TiO_2	0.36	0.42	0.51	-0.09	0.01
Al_2O_3	16.84	15.38	15.44	-0.06	0.00
FeO	2.45	2.53	3.54	-1.02	1.03
MnO	0.04	-0.13	0.05	-0.18	0.03
MgO	1.37	1.34	0.87	0.47	0.22
CaO	4.40	2.97	3.35	-0.38	0.14
Na_2O	4.66	4.83	4.44	0.39	0.15
K_2O	1.36	1.49	2.40	-0.90	0.82
P_2O_5	0.15	0.19	0.15	0.04	0.00
	97.28	96.40	98.41	$\sqrt{\sum R^2}$= 1.58	
Rb	15	19	54		
Sr	1011	885	382		
Ba	786	820	664		

5. Conclusions

Between Hampton Buttes and Dry Mountain the northern margin of the High Lava Plains is an irregular boundary described by the geomorphic character of the terrain formed, for the most part, by volcanism of the High Lava Plains where it banks on to the older deposits of the Blue Mountains Province. Hampton Buttes is the predominate marker along the High Lava Plains northern margin and preserves a record of the interaction between the older rocks of the John Day Formation that lie to the north, and younger extension related rock to the south.

Mapping, dating, and geochronology work done in the area of Hampton Butte divide the rocks into two main suites. The first is a suite related to the John Day Formation and underlying Clarno Formation. They are the extensive 30.39 ± 0.25 Ma Hampton Butte rhyodacite dome and flow complex, and smaller 28 ± 0.12 Ma Cougar Butte dacitic dome complex. This suite expands known sources of John Day volcanism, and bridges High Lava Plains and Basin and Range rocks with Blue Mountains rock of John Day age.

The second younger suite consists of rocks of basaltic composition ranging from 7.91 ± 0.12 Ma to 7.67 ± 1.31 Ma (Hampton Basalts, Dry Mountain), a 7.81 ± 0.12 Ma andesite (Hampton andesite), a basaltic andesite (Grassy Butte) that is 4.18 ± 0.14 Ma, and a 3.8 ± 0.6 Ma rhyolite tuff (Hampton Tuff). I interpret the rocks of basaltic composition to belong a pulse of basaltic volcanism along the High Lava Plains occurring between 7.9 and 7.5 Ma. The basaltic andesite (Grassy Butte) and

the Hampton Tuff I attribute to the release of fractionated and/or mixed magmas during the propagation of faults westward along the High Lava Plains.

The High Lava Plains suite conforms with other iron-rich silicic rocks and HAOT character of regional basalts of the High Lava Plains, which are similar to the bimodal suite of Iceland. The extensional tectonics of Iceland that are coupled with transform fault zones are analogous to the High Lava Plains in character but not scale.

The northern boundary of the High Lava Plains is defined by the lapping of tholeiitic basalts onto the John Day Formation basement of Hampton and Cougar Buttes. The northern margin is also defined by the limit of abundant northwest-striking faults that form a scalloped boundary that I interpret as a series of en-echelon transform fault sets coupled with normal faults as the normal faults of the Basin and Range province merge with the Brothers Fault Zone.

The 30.39 ± 0.25 Ma age of Hampton Butte and 28 ± 0.12 Ma age for Cougar Butte solidly places both as volcanism at the time of John Day Formation and fills a gap between John Day volcanism to the north and John Day age volcanism further south described by Scarberry (2006). Around 8 million years ago during a regional peak in basaltic volcanism tholeiitic basalt lapped onto the side of Hampton Butte but disappears beneath younger basalt south of the butte, a result of faulting less than 3.8 million years ago that lowered Cougar Butte, and isolated the 8 million year old basalt of Hampton Butte higher than the area to the south later covered by younger silicic and basaltic volcanism. The Hampton Tuff (3.8 ± 0.6 Ma) most likely origi-

nated at Frederick Butte and serves as an aid in constraining faulting, being cut by the normal faults that form the southern limit of Hampton Buttes.

Further east along the northern margin Grassy Butte, and Dry mountain mark the northernmost vents currently known along the High Lava Plains between Dry Mountain and Hampton Buttes. Potato Hills and adjacent Hat Butte represent the northernmost limit of High Lava Plains volcanism between the two. Like the basalts of Hampton Butte, both Grassy Butte and Dry Mountain can be modeled to a parent that is consistent with a rapidly erupted partial mantle melt with little or no assimilation (Appendix 3).

Dry Mountain is bordered to the north by the Izee terrain of the Blue Mountains Province, a Mesozoic fore-arc basin (Orr, 1996). The Rattlesnake Tuff, slightly younger than Dry Mountain, forms a bridge that links the two tuff's but covers the Dry Mountain-Blue Mountains Province contact, making the tuffs' northern edge (in this area) the northern extent of High Lava Plains volcanism. The new age (7.91 ± 0.12 Ma) and chemistry for a sample from Dry Mountain's summit clearly show that this vent is a tholeiitic basalt that is a partial melt of the mantle (Table 3.1 and 3.2). Extension to the west-southwest has divided the mountain since its eruption and no evidence is found of right lateral transform motion at Dry Mountain since then. Although no evidence of transform motion has been found along the High Lava Plains the pattern of faulting strongly infers that it has happened, and silicic volcanism along the margin in the brothers fault zone as a result propagates west through extension caused by a combination of plume, slab counter flow, and tectonic forces opening or re-opening routes for basalt or fractionated magma to reach the surface.

Others have noted that basaltic volcanism of the High Lava Plains is the result of the rapid rise and eruption of partial melts of the mantle, a reasonable hypothesis that data and modeling presented here supports. (Carlson and Hart 1989). The more silicic volcanism along the northern margin in the High Lava Plains may be the result of basaltic magma trapped in axial magma chambers isobarically fractionating then moving to the surface and erupting during a pulse of extension. Subsequent more minor episodes of extension would cause the eruption of anything from a basalt to a rhyolite, depending on how long the magma has been trapped in a magma chamber and the chamber's position relative to the rifting zone.

Bibliography

Atwater, 1970. Implications of plate tectonics for the Cenozoic tectonic evolution of western North America. Geological Society of America Bulletin, 81: 3513-3536

Bailey, D.G., and Conrey R.M., 1992. Common parent magma for Miocene to Holocene mafic volcanism in the northwestern United States. In: Geology [Boulder]. Geological Society of America (GSA) : Boulder, CO, United States, United States, pp. 1131-1134.

Baksi, A.K., 1989. Reevaluation of the timing and duration of extrusion of the Imnaha, Picture Gorge, and Grande Ronde basalts, Columbia River Basalt Group. 0072-1077, Geological Society of America (GSA) : Boulder, CO, United States, United States.

Barrash, W., Bond, J. and Venkatakrishnan, R., 1983. Structural evolution of the Columbia Plateau in Washington and Oregon. American Journal of Science, 283: 935-897.

Bartels, K.S., Kinzler, R.J. and Grove, T.L., 1991. High pressure phase relations of primitive high-alumina basalts from Medicine Lake Volcano, Northern California, Contributions to Mineralogy and Petrology. Springer International : Heidelberg-New York, International, International, pp. 253-270.

Bowman, F.J., 1940.The geology of the north half of Hampton quadrangle, Oregon. Masters Thesis, Oregon State University, Corvallis, Oregon, 71 pp.

Brooks, H.C. and Vallier, T.L., 1978. Mesozoic rocks and tectonic evolution of eastern Oregon and western Idaho, Pacific Coast Paleogeography Symposium. Pacific Section, Society of Economic Paleontologists and Mineralogists : Los Angeles, CA, United States, United States, pp. 133.

Camp, V.E., Ross, M.E. and Hanson, W.E., 2003. Genesis of flood basalts and Basin and Range volcanic rocks from Steens Mountain to the Malheur River Gorge, Oregon. Bulletin of the Geological Society of America, 115(1): 105-128.

Carlson, R.W. and Hart, W.K., 1987. Crustal Genesis on the Oregon Plateau. J. Geophys. Res., 92(B7): 6191-6208.

Carlson, R.W., T. L. Grove, and J. M. Donnelly-Nolan 2008. Concentrating the slab-fluid input to Newberry volcano, Geochim. Cosmochim. Acta,72(12, Suppl. 1): A136.

Catchings, R.D. and Mooney, W.D., 1988. Crustal structure of east central Oregon; relation between Newberry Volcano and regional crustal structure. Journal of Geophysical Research, 93: 10,081.

Christie, D.M. and Sinton, J.M., 1981. Evolution of abyssal lavas along propagating segments of the Galapagos spreading center. Earth and Planetary Science Letters, 56: 321-335.

Clifton, A.E., Sigmundsson, F., Feigl, K.L., Gunnar, G. and Árnadóttir, T., 2002. Surface effects of faulting and deformation resulting from magma accumulation at the Hengill triple junction, SW Iceland, 1994-1998. Journal of Volcanology and Geothermal Research, 115(1-2): 233-255.

Couch, R.W. and Lowell, R.P., 1971. Earthquakes and seismic energy release in Oregon, Ore Bin. Oregon Department of Geology and Mineral Industries : Portland, OR, United States, United States, pp. 84-61.

Dickinson, W.R., 1979. Cenozoic plate tectonic setting of the Cordilleran region in the United States. Pacific Coast Paleogeography Symposium: 13-1.

Dickinson, W.R., Helmold, K.P. and Stein, J.A., 1979. Mesozoic lithic sandstones in central Oregon. Journal of Sedimentary Petrology, 49(2): 501-506.

Dickinson, W.R. and Thayer, T.P., 1978. Paleogeographic and paleotectonic implications of Mesozoic stratigraphy and structure in the John Day inlier of central Oregon. Pacific Coast Paleogeography Symposium: 147.

Draper, D.S., 1991. Late Cenozoic Bimodal Magmatism in the Northern Basin and Range Province of Southeastern Oregon. Journal of Volcanology and Geothermal Research, 47(3-4): 299-328.

Duncan, R.A., and Hogan, L.G., 1994, Radiometric dating of young MORB using the 40Ar-39Ar incremental heating method: Geophysical Research Letters, v. 21, p. 1927-1930.

Fiebelkorn, R.B., Walker, G.W., MacLeod, N.S., McKee, E.H. and Smith, J.G., 1983. Isochron/West Index to K-Ar determinations for the State of Oregon. Isochron/West, 37.

Grunder, A.L., Johnson, J.A. and Streck, M.J., 1995. Basalt-rhyolite volcanism of the high lava plains, mirror of the Snake River plain. International Union of Geodesy and Geophysics, General Assembly, 21, Week A: 444.

Gunn, B.M., and Sarbas, B., 2002, An assessment of the composition of oceanic island basalts and fractionates, *in* Sarbas, B., ed., Eos, Transactions, American Geophysical Union, Volume 83: United States, American Geophysical Union : Washington, DC, United States, p. 1434-1434.

Hamilton, W., and Myers, W. B., 1966. Cenozoic Tectonics of the Western United States. Rev. Geophys., 4: 509-549.

Hammond, W.C. and Thatcher, W., 2005. Northwest Basin and Range tectonic deformation observed with the Global Positioning System, 1999-2003. Journal of Geophysical Research B: Solid Earth, 110(10): 1-12.

Hart, W.K., Aronson, J.L. and Mertzman, S.A., 1984. Areal distribution and age of low-K, high-alumina olivine tholeiite magmatism in the northwestern Great Basin. Geological Society of America Bulletin, 95: 195-186.

Hart, W.K. and Mertzman, S.A., 1982. K-Ar ages of basalts from south-central and southeastern Oregon. Isochron/West: 23-26.

Hemphill-Haley, M.A., D., P.W., Carver, G.A. and Burke, R.M., 2000. Paleoseismicity of the Alvord Fault, Steens Mountain, southeastern Oregon. In: J.S. Noller, Sowers, J. M., and Lettis, W. R., eds. (Editor), Quaternary Geochronology, Methods and Applications, pp. 537-540.

Hildreth, W., 1979. The Bishop Tuff; evidence for the origin of compositional zonation in silicic magma chambers, Special Paper - Geological Society of America. Geological Society of America (GSA) : Boulder, CO, United States, United States, pp. 43-75.Shelf 4, p. 537-540.

Hildreth, W., 1981. Gradients in silicic magma chambers; implications for lithospheric magmatism, Journal of Geophysical Research. American Geophysical Union : Washington, DC, United States, United States, pp. 10153-10192.

Hooper, P.R., Binger, G. B., Lees, K.R., 2002. Ages of the Steens and Columbia River flood basalts and their relationship to extension-related calc-alkalic volcanism in eastern Oregon. Bulletin of the Geological Society of America, 114 (1): 43-50.

Johnson, J.A., 1995. Geologic evolution of the Duck Creek Butte eruptive center, High Lava Plains, southeastern Oregon, Oregon State University, United States, 122 pp.

Johnson, J.A. and Grunder, A.L., 2000. The making of intermediate composition magma in a bimodal suite; Duck Butte eruptive center, Oregon, USA. Journal of Volcanology and Geothermal Research, 95: 175.

Jónasson, K., 2007. Silicic volcanism in Iceland: Composition and distribution within the active volcanic zones. Journal of Geodynamics, 43(1): 101-117.

Jordan, B.T., 2005. Age-progressive volcanism of the Oregon High Lava Plains; overview and evaluation of tectonic models. Special Paper - Geological Society of America, 388: 503.

Jordan, B.T., Grunder, A.L. and Duncan, R.A., 2004. Geochronology of age-progressive volcanism of the Oregon High Lava Plains; implications for the plume interpretation of Yellowstone. Journal of Geophysical Research, 109.

Jordan, B.T., Streck, M.J. and Grunder, A.L., 2002. Bimodal volcanism and tectonism of the High Lava Plains, Oregon. Special Paper - Oregon, Department of Geology and Mineral Industries, 36: 23.

Koppers, A.A.P., 2002, ArArCALC--software for 40Ar/39Ar age calculations: Computers & Geosciences, v. 28, p. 605-619.

Lawrence, R.D., 1976. Strike-slip faulting terminates the Basin and Range Province in Oregon. Geological Society of America Bulletin, 87: 850-846.

Linneman, S.R. and Myers, J.D., 1990. Magmatic inclusions in Holocene rhyolites of Newberry Volcano, central Oregon. Journal of Geophysical Research, 95: 17.

Livaccari, R.F., 1979. Late Cenozoic tectonic evolution of the western United States. Geology Boulder, 7: 75-72.

MacLean, J.W., 1994. Geology and geochemistry of Juniper Ridge, Horsehead Mountain and Burns Butte; implications for the petrogenesis of silicic magma on the High Lava Plains, southeastern Oregon, Oregon State University, Corvallis, 122 pp.

MacLeod, N.S., Walker, G.W. and McKee, E.H., 1975. Open-File Report - U. S. Geological Survey Geothermal significance of eastward increase in age of upper Cenozoic rhyolitic domes in southeastern Oregon. Open-File Report - U. S. Geological Survey.

Mattsson, H.B. and Oskarsson, N., 2005. Petrogenesis of alkaline basalts at the tip of a propagating rift: Evidence from the Heimaey volcanic centre, south Iceland. Journal of Volcanology and Geothermal Research, 147(3-4): 245-267.

McCaffrey, R., Long, M. D., Goldfinger, C., Zwick, P. C., Nabelek, J. L., Johnson, C. K. & Smith, C. , 2000. Rotation and plate locking at the southern Cascadia subduction zone. Geophysical Research Letters, 27((19)): 3117-3120.

McDonough, W.F., 1995. The composition of the Earth. In: S.S. Sun (Editor), Chemical Geology. Elsevier : Amsterdam, Netherlands, Netherlands, pp. 223-253.

McKee, E.H., Duffield, W.A. and Stern, R.J., 1983. Late Miocene and early Pliocene basaltic rocks and their implications for crustal structure, northeastern California and South-central Oregon. Geological Society of America Bulletin, 94: 292-304.

Miller, C.F., 1982. Depletion of light rare-earth elements in felsic magmas. In: D.W. Mittlefehldt (Editor), Geology [Boulder]. Geological Society of America (GSA) : Boulder, CO, United States, United States, pp. 129-133.

Nathenson, M. and Guffanti, M., 1988. Geothermal gradients in the conterminous United States. Journal of Geophysical Research, 93(B6): 6437-6450.

Nielsen, R.L., 1992. BIGD.FOR: A FORTRAN program to calculate trace-element partition coefficients for natural mafic and intermediate composition magmas. Computers & Geosciences, 18(7): 773-788.

Pearce, J.A., 1983, Role of the sub-continental lithosphere in magma genesis at active continental margins Shiva geology series: United Kingdom, Shiva Publ. : Nantwich, United Kingdom, 230-249 p.

Retallack, G.J., Bestland, E.A. and Fremd, T.J., 1999. Eocene and Oligocene Paleosols of Central Oregon. Special Paper 344: Eocene and Oligocene Paleosols of Central Oregon, 344(0): 1-192.

Robinson, P.T., Walker, G.W. and McKee, E.H., 1990. Eocene(?), Oligocene, and lower Miocene rocks of the Blue Mountains region. 1044-9612, U. S. Geological Survey : Reston, VA, United States, United States.

Robyn, T.L. and Hoover, J.D., 1982. Late Cenozoic Deformation and Volcanism in the Blue Mountains of Central Oregon - Microplate Interactions. Geology, 10 (11): 572-576.

Rollinson, H.R.,1993. Using Geochemical Data: Evaluation, Presentation, Interpretation. Harlow, Essex, England : Longman Scientific & Technical ; New York : Copublished in the U.S. with J. Wiley & Sons.

Roth, J.B., Fouch, M.J., James, D.E. and W., C.R., 2008. Three-dimensional seismic velocity structure of the northwestern United States. Geophys. Res. Lett., 35 (L15304).

Rutherford, M.J. and Devine, J.D., 2003. Magmatic Conditions and Magma Ascent as Indicated by Hornblende Phase Equilibria and Reactions in the 1995-2002 Soufriere Hills Magma. J. Petrology, 44(8): 1433-1453.

Rytuba, J.J. and McKee, E.H., 1984. Peralkaline ash flow tuffs and calderas of the McDermitt volcanic field, Southeast Oregon and north central Nevada. Journal of Geophysical Research, 89: 8616-8628.

Saunders, A.D., Norry, M.J. and Tarney, J., 1988. Origin of MORB and chemically-depleted mantle reservoirs; trace element constraints. Journal of Petrology, 1988: 415-445.

Scarberry, 2008. Extension and volcanism : tectonic development of the northwestern margin of the Basin and Range Province in southern Oregon, Oregon State University, Corvallis, Oregon, 223 pp.

Schock, H.H., 1979. Distribution of rare-earth and other trace elements in magnetites, Chemical Geology. Elsevier : Amsterdam, Netherlands, Netherlands, pp. 119-133

Shand, S.J., 1927. The Eruptive Rocks. John Wiley, New York.

Sinton, J.M., Wilson, D.S., Christie, D.M., Hey, R.N. and Delaney, J.R., 1983. Petrologic consequences of rift propagation on oceanic spreading ridges. Earth and Planetary Science Letters, 62(2): 193-207.

Streck, M.J. and Grunder, A.L., 1995. Crystallization and welding variations in a widespread ignimbrite sheet; the Rattlesnake Tuff, eastern Oregon, USA. Bulletin of Volcanology, 57: 169-151.

Streck, M.J., and Grunder, A.L., 2007. Phenocryst-poor rhyolites of bimodal, tholeiitic provinces: The Rattlesnake Tuff and implications for mush extraction models. Bulletin of Volcanology Petrogenesis and Volcanology of Anorogenic Rhyolites, 70(3): 385-401.

Streck, M.J., Johnson, J.A. and Grunder, A.L., 1999. Field guide to the Rattlesnake Tuff and High Lava Plains near Burns, Oregon. Oregon Geology, 61: 64.

Streck M.J. Grunder A.L, Phenocryst-poor rhyolites of bimodal, tholeiitic provinces: The Rattlesnake Tuff and implications for mush extraction models: Bulletin of Volcanology, v. 70 n3, p. 385-401

Swanson, D.A. and Robinson, P.T., 1968. Base of the John Day Formation in and near the Horse Heaven mining district, north-central Oregon, pp. d161-D154.

Taylor, E.M., 1977. The Clarno Formation; a record of early Tertiary volcanism in central Oregon. Abstracts with Programs - Geological Society of America, 9: 768-768.

Trench, 2008. The termination of the Basin and Range Province into a clockwise rotating region of transtension and volcanism, central Oregon ,Oregon State University, Corvallis, Oregon.

University of Maryland SDSU (2005), VCF, UMD Tiles, 220r015_7k20000710_z26_nn61, Global Land Cover Facility, University of Maryland, College Park, Maryland.

USGS, 2004. Shuttle Radar Topography Mission,3 Arc Second scene SRTM_u03_n055e282, e283, e284, e220, e221, e222, Unfilled Unfinished 2.0. Global Land Cover Facility, University of Maryland, College Park, Maryland, February 2000.

Vallier, T.L. and Brooks, H.C., 1995. Geology of the Blue Mountains region of Oregon, Idaho, and Washington; petrology and tectonic evolution of pre-Tertiary rocks of the Blue Mountains region. U. S. Geological Survey Professional Paper.

Walker, G.W., 1974. Some implications of late Cenozoic volcanism to geothermal potential in the high lava plains of south-central Oregon. 01961497, U. S. Geological Survey : Reston, VA, United States, United States.

Walker, G.W. and Nolf, B., 1981. Roadlog for High Lava Plains, Brothers fault zone to Harney Basin, Oregon. 0364-6017, U. S. Geological Survey : Reston, VA, United States, United States.

Walker, G.W. and Robinson, P.T., 1990a. Cenozoic tectonism and volcanism of the Blue Mountains region. US Geological Survey Professional Paper, 1437: 119-135.

Walker, G.W. and Robinson, P.T., 1990b. Paleocene(?), Eocene, and Oligocene(?) rocks of the Blue Mountains region. US Geological Survey Professional Paper, 1437: 13-27.

Washington State University GeoAnalytical Lab, 2009. Technical Notes, Pullman, WA. http://www.sees.wsu.edu/Geolab/contact.html

Waters, A.C., 1954. John Day Formation west of its type locality (Oregon). Geological Society of America Bulletin, 65: 1320-1320.

Watkins, N.D. and Baksi, A.K., 1974. Magnetostratigraphy and oroclinal folding of the Columbia River, Steens, and Owyhee basalts in Oregon, Washington, and Idaho. American Journal of Science, 274: 148-189.

Weaver, C.S. and Shedlock, K.M., 1991. Open-File Report - U. S. Geological Survey Estimates of seismic source regions from considerations of the earthquake distribution and regional tectonics in the Pacific Northwest. 0196-1497, U. S. Geological Survey : Reston, VA, United States, United States.

Wells, R.E. and Simpson, R.W., 2001. Northward migration of the Cascadia forearc in the northwestern U. S. and implications for subduction deformation. Earth, Planets and Space, 53: 275-283.

Workman, R.K., and Hart, S.R., 2005, Major and trace element composition of the depleted MORB mantle (DMM): Earth and Planetary Science Letters, v. 231, p. 53-72.

Zheng, J.P. et al., 2009. Age and composition of granulite and pyroxenite xenoliths in Hannuoba basalts reflect Paleogene underplating beneath the North China Craton. Chemical Geology, 264(1-4): 266-280.

Appendices

Appendix 1
Results of geochronology calculations done at Oregon State University Noble Gas Mass Spectrometry Lab using ArArCalc, an Excel® spreadsheet by Koppers (2006).

Potato Hills (HLP-0701)

Incremental Heating			36Ar(a)	37Ar(ca)	38Ar(cl)	39Ar(k)	40Ar(r)	Age ± 2σ (Ma)	40Ar(r) (%)	39Ar(k) (%)	K/Ca ± 2σ
08C1389	500 °C	4	0.089374	0.015231	0.000702	0.010006	0.247627	70.75 ± 137.68	0.93	1.19	0.282 ± 0.067
08C1390	600 °C	4	0.257471	0.036701	0.001444	0.057546	0.602991	30.29 ± 67.81	0.79	6.84	0.674 ± 0.090
08C1392	675 °C	4	0.361514	0.055101	0.002841	0.090424	2.186787	69.17 ± 45.33	2.01	10.74	0.706 ± 0.074
08C1393	750 °C	4	0.465254	0.081863	0.004325	0.133441	2.773282	59.60 ± 55.67	1.98	15.85	0.701 ± 0.066
08C1394	800 °C	4	0.033805	0.005029	0.000468	0.010862	0.368545	96.30 ± 60.56	3.56	1.29	0.929 ± 0.125
08C1395	850 °C	4	0.251435	0.062231	0.002495	0.098445	2.397187	69.63 ± 41.91	3.13	11.70	0.680 ± 0.077
08C1398	900 °C	4	0.215691	0.053419	0.001850	0.075828	1.721369	65.00 ± 52.46	2.63	9.01	0.610 ± 0.068
08C1399	950 °C	4	0.179725	0.055522	0.001984	0.094593	2.399749	72.49 ± 23.07	4.32	11.24	0.733 ± 0.076
08C1400	1000 °C	4	0.132626	0.049488	0.001692	0.068182	1.888030	78.98 ± 31.95	4.60	8.10	0.592 ± 0.074
08C1401	1050 °C	4	0.104590	0.039023	0.000995	0.052349	1.207524	66.03 ± 29.70	3.76	6.22	0.577 ± 0.060
08C1402	1125 °C	4	0.068620	0.032043	0.001066	0.041776	1.207341	82.35 ± 20.25	5.62	4.96	0.561 ± 0.071
08C1452	1200 °C	4	0.071503	0.020940	0.000950	0.038406	1.189251	88.10 ± 19.41	5.33	4.56	0.789 ± 0.070
08C1466	1300 °C	4	0.066261	0.013565	0.000631	0.036316	0.904121	71.16 ± 40.04	4.41	4.31	1.151 ± 0.110
08C1468	1400 °C	4	0.054817	0.009149	0.000783	0.033525	1.129184	95.62 ± 21.75	6.52	3.98	1.576 ± 0.194
		S	2.352687	0.529304	0.022227	0.841701	20.222987				

Information on Analysis		Results	40(r)/39(k) ± 2σ		Age ± 2σ (Ma)		MSWD	39Ar(k) (%,n)	K/Ca ± 2σ
HLP-0704 (AKA HTB-0704)plag HLP Plag Potato Hills MI		Weighted Plateau	27.8539	± 3.0176 ± 10.83%	79.44	± 8.43 ± 10.61%	0.63	100.00 14	0.658 ± 0.108
					External Error	± 8.53	2.16	Statistical T Ratio	
					Analytical Error	± 8.42	1.0000	Error Magnification	
Project = HLP Irradiation = OSU3E07 J = 0.0016161 ± 0.0000047 FCT-3 = 28.030 ± 0.003 Ma		Total Fusion Age	24.0263	± 4.9571 ± 20.63%	68.72	± 13.92 ± 20.25%		14	0.684 ± 0.023
					External Error	± 13.96			
					Analytical Error	± 13.91			

Normal Isochron			39(k)/36(a) ± 2σ	40(a+r)/36(a) ± 2σ	r.i.
08C1389	500 °C	4	0.1 ± 0.0	298.3 ± 5.5	0.5092
08C1390	600 °C	4	0.2 ± 0.0	297.8 ± 5.3	0.7783
08C1392	675 °C	4	0.3 ± 0.0	301.5 ± 4.1	0.8267
08C1393	750 °C	4	0.3 ± 0.0	301.5 ± 5.8	0.8928
08C1394	800 °C	4	0.3 ± 0.0	306.4 ± 7.2	0.5628
08C1395	850 °C	4	0.4 ± 0.0	305.0 ± 6.0	0.8977
08C1398	900 °C	4	0.4 ± 0.0	303.5 ± 6.7	0.9006
08C1399	950 °C	4	0.5 ± 0.0	308.9 ± 4.5	0.7983
08C1400	1000 °C	4	0.5 ± 0.0	309.7 ± 6.2	0.8018
08C1401	1050 °C	4	0.5 ± 0.0	307.0 ± 5.5	0.7351
08C1402	1125 °C	4	0.6 ± 0.0	313.1 ± 4.7	0.7881
08C1452	1200 °C	4	0.5 ± 0.0	312.1 ± 4.0	0.8858
08C1466	1300 °C	4	0.5 ± 0.0	309.1 ± 8.2	0.9674
08C1468	1400 °C	4	0.6 ± 0.0	316.1 ± 5.1	0.8488

Results		40(a)/36(a) ± 2σ		40(r)/39(k) ± 2σ		Age ± 2σ (Ma)		MSWD
Isochron		292.4821	± 3.9646 ± 1.36%	34.0477	± 8.7398 ± 25.67%	96.63	± 24.16 ± 25.00%	0.49
						External Error	± 24.21	
						Analytical Error	± 24.15	
Statistics		Statistical F Ratio	1.75		Convergence		0.0000002777	
		Error Magnification	1.0000		Number of Iterations		6	
		n	14		Calculated Line		Weighted York-2	

08C1389.AGE >>> HTB-0704 plag HLP 3E16-07 >>> HLP PROJECT

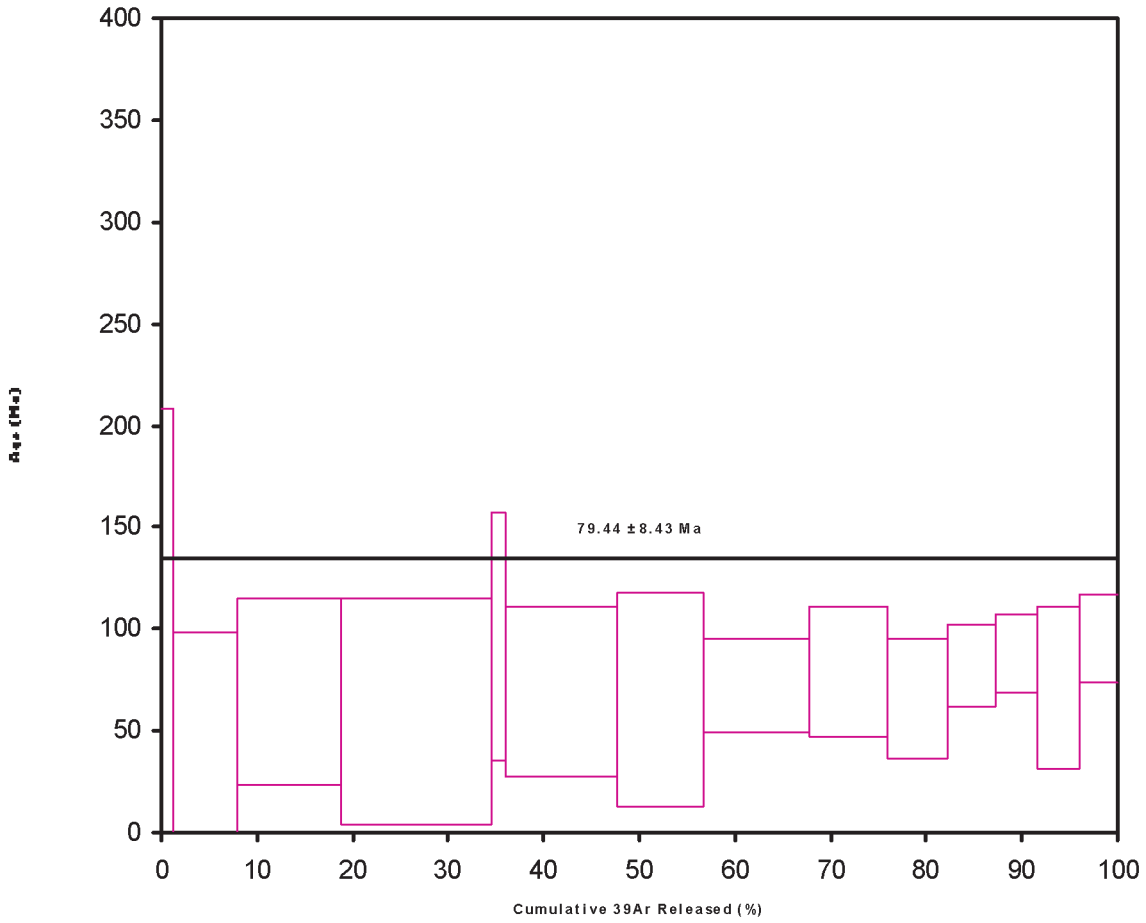

Ar-Ages in Ma

WEIGHTED PLATEAU
79.44 ± 8.43
TOTAL FUSION
68.72 ± 13.92
NORMAL ISOCHRON
96.63 ± 24.16
INVERSE

Sample Info

Plagioclase
Potato Hills
lademarco

IRR = OSU3E07
J = 0.0016161 ±

Appendix 1 (continued)

Potato Hills (HLP-0701a)

Incremental Heating			36Ar(a)	37Ar(ca)	38Ar(cl)	39Ar(k)	40Ar(r)	Age ± 2s (Ma)	40Ar(r) (%)	39Ar(k) (%)	K/Ca ± 2s
09C2034	500 °C		0.002226	0.004314	0.000030	0.008857	0.004283	1.52 ± 4.22	0.65	0.72	0.883 ± 0.067
09C2035	600 °C		0.002166	0.041873	0.000059	0.070598	0.132990	5.91 ± 0.23	17.20	5.71	0.725 ± 0.039
09C2036	700 °C	4	0.015841	0.098645	0.000242	0.169090	0.334583	6.20 ± 2.11	6.67	13.67	0.737 ± 0.039
09C2037	800 °C	4	0.006789	0.139789	0.000154	0.268824	0.554121	6.46 ± 0.19	21.64	21.73	0.827 ± 0.044
09C2039	875 °C	4	0.001621	0.088117	0.000090	0.180591	0.373083	6.48 ± 0.10	43.78	14.60	0.881 ± 0.047
09C2040	950 °C	4	0.003825	0.085936	0.000099	0.169569	0.353861	6.54 ± 0.21	23.84	13.71	0.848 ± 0.047
09C2041	1100 °C	4	0.002540	0.052145	0.000028	0.095713	0.208506	6.83 ± 0.97	21.74	7.74	0.789 ± 0.043
09C2042	1175 °C	4	0.000604	0.021014	0.000016	0.044566	0.093686	6.59 ± 0.25	34.42	3.60	0.912 ± 0.050
09C2044	1250 °C	4	0.001633	0.080424	0.000075	0.154593	0.323715	6.56 ± 0.10	40.15	12.50	0.827 ± 0.044
09C2045	1325 °C	4	0.000990	0.025813	0.000043	0.052748	0.108481	6.45 ± 0.31	27.05	4.26	0.879 ± 0.051
09C2046	1400 °C	4	0.000683	0.012201	0.000032	0.021710	0.045009	6.50 ± 0.73	18.23	1.76	0.765 ± 0.044
		S	0.038917	0.650271	0.000869	1.236859	2.532319				

Information on Analysis	Results	40(r)/39(k) ± 2s	Age ± 2s (Ma)	MSWD	39Ar(k) (%,n)	K/Ca ± 2s
HLP-0704A 1D4-09 plagioclase High LP MI	**Weighted Plateau**	2.0801 ± 0.0191 (± 0.92%)	6.52 ± 0.07 (± 1.06%) External Error ± 0.12 Analytical Error ± 0.06	0.37 2.31 1.0000	93.58 9 Statistical T Ratio Error Magnification	0.822 ± 0.039
Project = HLP Irradiation = OSU1D09 J = 0.0017409 ± 0.0000047 FCT-3 = 28.030 ± 0.003 Ma	**Total Fusion Age**	2.0474 ± 0.0978 (± 4.77%)	6.42 ± 0.31 (± 4.80%) External Error ± 0.32 Analytical Error ± 0.31		11	0.818 ± 0.016

Normal Isochron			39(k)/36(a) ± 2s	40(a+r)/36(a) ± 2s	r.i.
09C2034	500 °C		4.0 ± 0.1	297.4 ± 5.4	0.8680
09C2035	600 °C		32.6 ± 0.3	356.9 ± 2.8	0.7849
09C2036	700 °C	4	10.7 ± 0.3	316.6 ± 7.7	0.9872
09C2037	800 °C	4	39.6 ± 0.4	377.1 ± 3.0	0.7729
09C2039	875 °C	4	111.4 ± 1.4	525.7 ± 6.3	0.9531
09C2040	950 °C	4	44.3 ± 0.5	388.0 ± 3.9	0.9278
09C2041	1100 °C	4	37.7 ± 1.5	377.6 ± 14.9	0.9894
09C2042	1175 °C	4	73.8 ± 1.5	450.6 ± 8.9	0.9586
09C2044	1250 °C	4	94.7 ± 0.9	493.8 ± 4.7	0.9666
09C2045	1325 °C	4	53.3 ± 0.9	405.1 ± 7.0	0.9581
09C2046	1400 °C	4	31.8 ± 0.8	361.4 ± 9.1	0.9637

Results		40(a)/36(a) ± 2s	40(r)/39(k) ± 2s	Age ± 2s (Ma)	MSWD
Isochron		295.0572 ± 3.0557 (± 1.04%)	2.0857 ± 0.0445 (± 2.13%)	6.54 ± 0.14 (± 2.20%) External Error ± 0.18 Analytical Error ± 0.14	0.41
Statistics	Statistical F Ratio	2.01	Convergence	0.0000000099	
	Error Magnification	1.0000	Number of Iterations	17	
	n	9	Calculated Line	Weighted York-2	

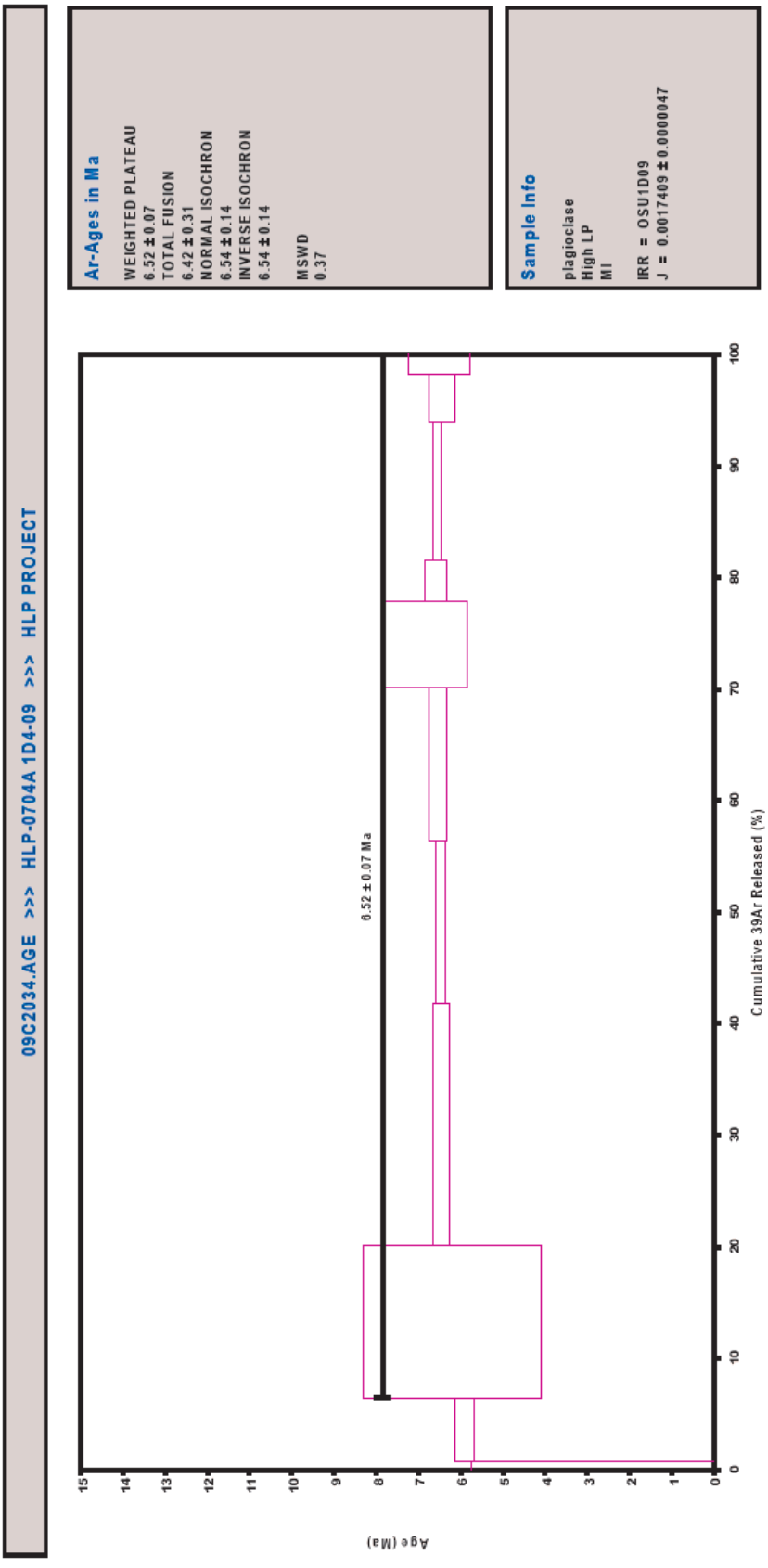
09C2034.AGE >>> HLP-0704A 1D4-09 >>> HLP PROJECT
Ar-Ages in Ma
WEIGHTED PLATEAU
6.52 ± 0.07
TOTAL FUSION
6.42 ± 0.31
NORMAL ISOCHRON
6.54 ± 0.14
INVERSE ISOCHRON
6.54 ± 0.14
MSWD
0.37
Sample Info
plagioclase
High LP
MI
IRR = OSU1D09
J = 0.0017409 ± 0.0000047
6.52 ± 0.07 Ma
Age (Ma)
Cumulative 39Ar Released (%)

Appendix 1 (continued)

Hampton Butte (HTB-0501)

Incremental Heating			36Ar(a)	37Ar(ca)	38Ar(cl)	39Ar(k)	40Ar(r)	Age ± 2σ (Ma)	40Ar(r) (%)	39Ar(k) (%)	K/Ca ± 2σ
06C1659	600 °C		0.00041	0.04154	0.00014	0.01439	0.10683	28.16 ± 1.82	47.13	1.25	0.149 ± 0.005
06C1660	700 °C		0.00005	0.12315	0.00000	0.02914	0.25773	33.49 ± 1.14	94.08	2.52	0.102 ± 0.003
06C1661	800 °C		0.00008	0.45368	0.00003	0.10120	0.84445	31.62 ± 0.30	97.24	8.76	0.096 ± 0.003
06C1662	875 °C	4	0.00031	0.84408	0.00000	0.16494	1.32159	30.37 ± 0.29	93.58	14.28	0.084 ± 0.003
06C1663	950 °C	4	0.00027	1.52793	0.00003	0.23246	1.85091	30.18 ± 0.20	95.89	20.12	0.065 ± 0.002
06C1664	1000 °C	4	0.00027	1.28772	0.00000	0.14701	1.17060	30.19 ± 0.33	93.71	12.73	0.049 ± 0.002
06C1665	1050 °C	4	0.00011	1.13796	0.00000	0.11916	0.96406	30.67 ± 0.36	96.79	10.32	0.045 ± 0.001
06C1666	1100 °C	4	0.00014	0.92211	0.00002	0.09462	0.76253	30.55 ± 0.38	94.71	8.19	0.044 ± 0.001
06C1667	1150 °C	4	0.00018	0.62148	0.00000	0.06657	0.53845	30.66 ± 0.44	91.15	5.76	0.046 ± 0.002
06C1668	1225 °C	4	0.00023	0.60587	0.00000	0.06400	0.51546	30.53 ± 0.42	88.56	5.54	0.045 ± 0.001
06C1669	1400 °C	4	0.00090	1.16593	0.00017	0.12162	0.98372	30.66 ± 0.41	78.62	10.53	0.045 ± 0.001
		S	0.00294	8.73144	0.00039	1.15512	9.31632				

Information on Analysis	
Sample	HTB-0501
Material	plagioclase
Location	hampton butte
Analyst	mi
Project	HLP
Irradiation	OSU1D06
J-value	0.002119
Standard	28.03

Results	40(r)/39(k) ± 2σ	Age ± 2σ (Ma)	MSWD	39Ar(k) (%,n)	K/Ca ± 2σ
Weighted Plateau	8.0167 ± 0.0403 ± 0.50%	30.39 ± 0.25 ± 0.82%	1.76	87.47 8	0.049 ± 0.007
	External Error ± 0.54		2.36	Statistical T ratio	
	Analytical Error ± 0.15		1.3270	Error Magnification	
Total Fusion Age	8.0653 ± 0.0298 ± 0.37%	30.57 ± 0.23 ± 0.75%		11	0.057 ± 0.001
	External Error ± 0.54				
	Analytical Error ± 0.11				

Normal Isochron			39(k)/36(a) ± 2σ	40(a+r)/36(a) ± 2σ	r.i.
06C1659	600 °C		35 ± 2	559 ± 32	0.988
06C1660	700 °C		532 ± 284	4998 ± 2674	1.000
06C1661	800 °C		1251 ± 312	10737 ± 2672	1.000
06C1662	875 °C	4	539 ± 66	4612 ± 568	0.999
06C1663	950 °C	4	868 ± 112	7208 ± 927	1.000
06C1664	1000 °C	4	554 ± 76	4710 ± 649	0.999
06C1665	1050 °C	4	1104 ± 215	9228 ± 1796	0.999
06C1666	1100 °C	4	658 ± 127	5601 ± 1082	0.999
06C1667	1150 °C	4	377 ± 51	3341 ± 451	0.999
06C1668	1225 °C	4	284 ± 27	2586 ± 249	0.998
06C1669	1400 °C	4	134 ± 6	1383 ± 63	0.992

Results	40(a)/36(a) ± 2σ	40(r)/39(k) ± 2σ	Age ± 2σ (Ma)	MSWD
No Convergence	311.5366 ± 22.0625 ± 7.08%	7.9783 ± 0.0586 ± 0.73%	30.24 ± 0.30 ± 0.98%	1.38
			External Error ± 0.56	
			Analytical Error ± 0.22	

Statistics				
	Statistical F ratio	2.10	Convergence	0.0000376856
	Error Magnification	1.1744	Number of Iterations	500
	n	8	Calculated Line	Weighted York-2

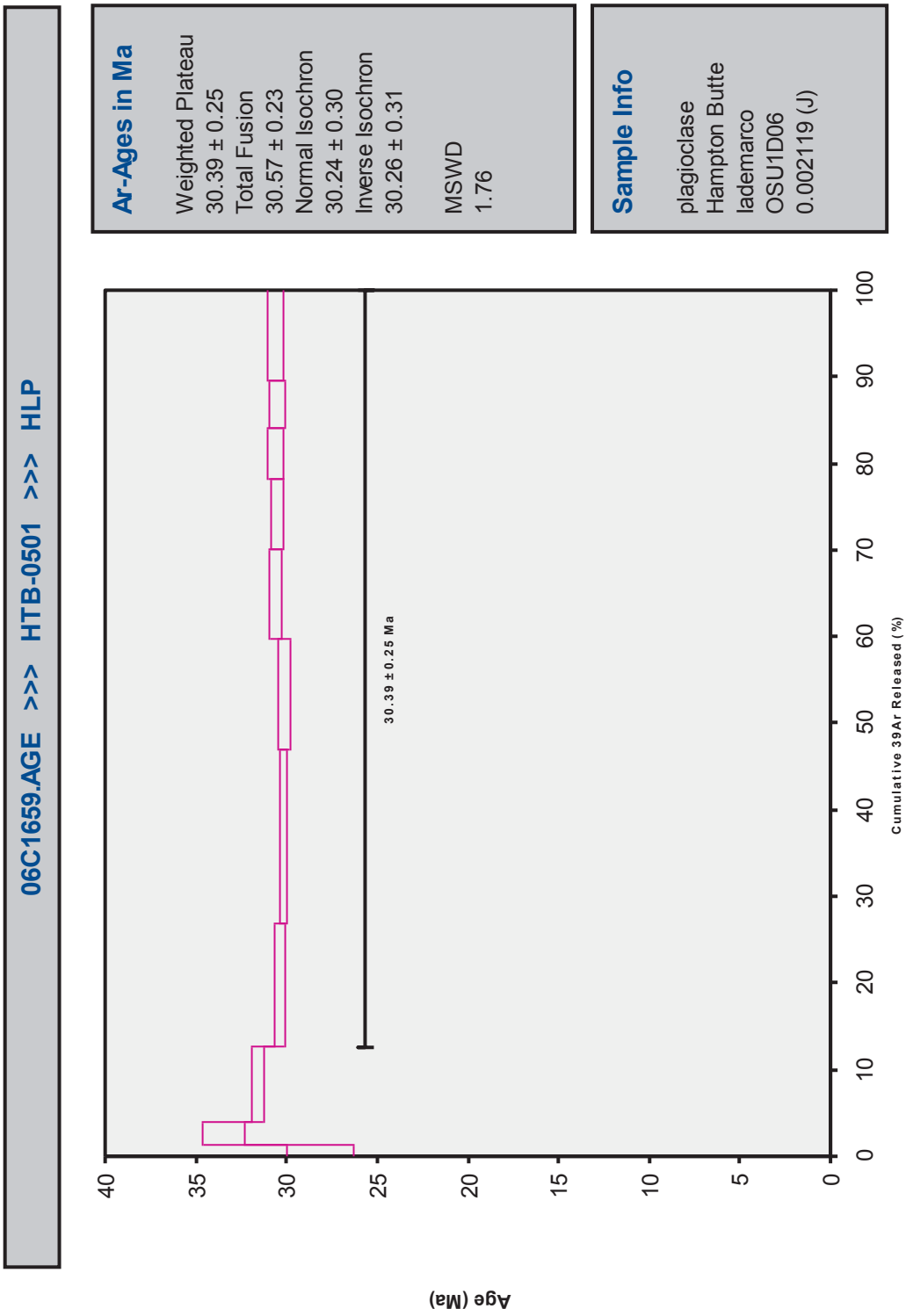
06C1659.AGE >>> HTB-0501 >>> HLP
Ar-Ages in Ma
Weighted Plateau
30.39 ± 0.25
Total Fusion
30.57 ± 0.23
Normal Isochron
30.24 ± 0.30
Inverse Isochron
30.26 ± 0.31
MSWD
1.76
Sample Info
plagioclase
Hampton Butte
lademarco
OSU1D06
0.002119 (J)
30.39 ± 0.25 Ma
Age (Ma)
Cumulative 39Ar Released (%)
0
5
10
15
20
25
30
35
40
0
10
20
30
40
50
60
70
80
90
100

Appendix 1 (continued)

Cougar Butte (HTB-0613)

Incremental Heating			36Ar(a)	37Ar(ca)	38Ar(cl)	39Ar(k)	40Ar(r)	Age ± 2σ (Ma)	40Ar(r) (%)	39Ar(k) (%)	K/Ca ± 2σ
08C913	500 °C		0.003804	0.014887	0.000039	0.004598	0.060318	38.84 ± 10.39	5.09	1.93	0.133 ± 0.009
08C914	600 °C	4	0.001405	0.056228	0.000027	0.015823	0.151118	28.36 ± 1.48	26.69	6.65	0.121 ± 0.008
08C915	700 °C	4	0.000549	0.108866	0.000021	0.027399	0.261560	28.34 ± 0.69	61.71	11.51	0.108 ± 0.007
08C917	800 °C	4	0.000409	0.176798	0.000021	0.040952	0.392215	28.44 ± 0.27	76.42	17.21	0.100 ± 0.006
08C918	875 °C	4	0.000262	0.146035	0.000010	0.030852	0.298799	28.75 ± 0.34	79.40	12.96	0.091 ± 0.006
08C919	950 °C	4	0.000857	0.192738	0.000006	0.039125	0.387838	29.42 ± 0.59	60.49	16.44	0.087 ± 0.006
08C921	1025 °C		0.001187	0.169734	0.000027	0.030097	0.297379	29.33 ± 0.50	45.89	12.65	0.076 ± 0.005
08C922	1100 °C		0.001193	0.126181	0.000018	0.019662	0.200614	30.28 ± 1.11	36.27	8.26	0.067 ± 0.004
08C923	1175 °C		0.001054	0.087432	0.000002	0.012750	0.134878	31.38 ± 1.37	30.23	5.36	0.063 ± 0.004
08C925	1250 °C		0.000722	0.058347	0.000014	0.008039	0.085821	31.67 ± 1.97	28.69	3.38	0.059 ± 0.004
08C926	1325 °C		0.000590	0.035865	0.000011	0.004674	0.050093	31.79 ± 2.17	22.32	1.96	0.056 ± 0.004
08C927	1400 °C		0.000682	0.033625	0.000014	0.004006	0.047506	35.14 ± 2.71	19.09	1.68	0.051 ± 0.003
		S	0.012714	1.206735	0.000210	0.237977	2.368138				

Information on Analysis	Results	40(r)/39(k) ± 2σ	Age ± 2σ (Ma)	MSWD	39Ar(k) (%,n)	K/Ca ± 2σ
HTB-0613 pl HLP 3E14-07 plag hampton butte mi	Weighted Plateau	9.6420 ± 0.1050 ± 1.09%	28.63 ± 0.34 ± 1.18% External Error ± 0.57 Analytical Error ± 0.31	2.64 2.78 1.6256	64.78 5 Statistical T Ratio Error Magnification	0.099 ± 0.011
Project = HLP Irradiation = OSU3E07 J = 0.0016588 ± 0.0000040 FCT-3 = 28.030 ± 0.003 Ma	Total Fusion Age	9.9511 ± 0.1055 ± 1.06%	29.54 ± 0.34 ± 1.15% External Error ± 0.58 Analytical Error ± 0.31		12	0.085 ± 0.002

Normal Isochron			39(k)/36(a) ± 2σ	40(a+r)/36(a) ± 2σ	r.i.
08C913	500 °C		1.2 ± 0.0	311.4 ± 4.5	0.8174
08C914	600 °C	4	11.3 ± 0.2	403.1 ± 7.7	0.9669
08C915	700 °C	4	49.9 ± 1.9	771.8 ± 29.8	0.9927
08C917	800 °C	4	100.0 ± 2.6	1253.4 ± 32.3	0.9801
08C918	875 °C	4	117.6 ± 4.7	1434.9 ± 56.6	0.9876
08C919	950 °C	4	45.6 ± 1.4	747.9 ± 22.4	0.9844
08C921	1025 °C		25.4 ± 0.4	546.1 ± 7.6	0.9608
08C922	1100 °C		16.5 ± 0.3	463.7 ± 9.7	0.9791
08C923	1175 °C		12.1 ± 0.2	423.5 ± 8.0	0.9500
08C925	1250 °C		11.1 ± 0.3	414.4 ± 10.4	0.9855
08C926	1325 °C		7.9 ± 0.2	380.4 ± 7.5	0.9083
08C927	1400 °C		5.9 ± 0.1	365.2 ± 6.6	0.8605

Results	40(a)/36(a) ± 2σ	40(r)/39(k) ± 2σ	Age ± 2σ (Ma)	MSWD
Error Chron	296.5506 ± 10.8841 ± 3.67%	9.6237 ± 0.1826 ± 1.90%	28.57 ± 0.55 ± 1.94% External Error ± 0.72 Analytical Error ± 0.54	3.33

Statistics				
	Statistical F Ratio	2.60	Convergence	0.0000000876
	Error Magnification	1.8236	Number of Iterations	73
	n	5	Calculated Line	Weighted York-2

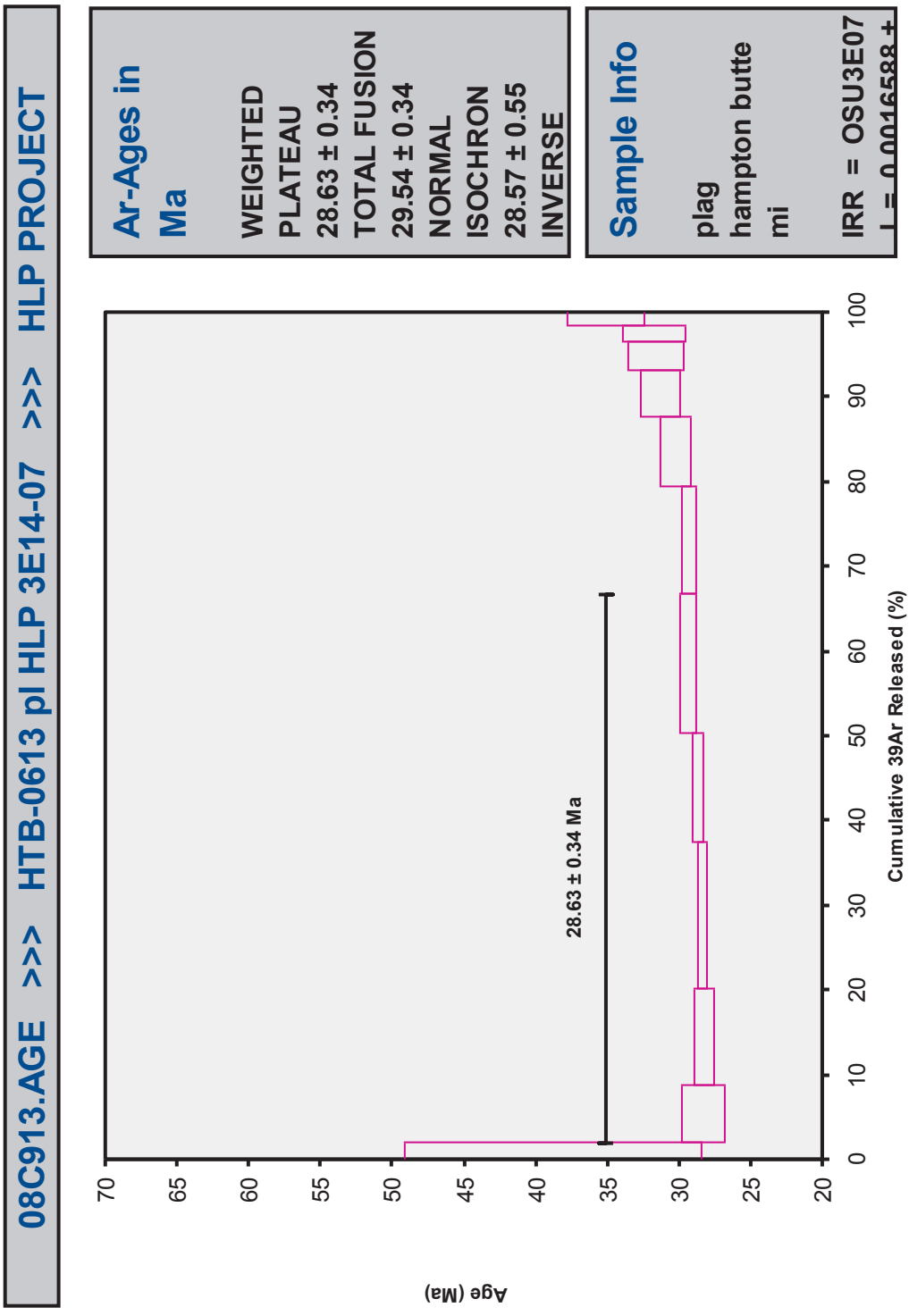
08C913.AGE >>> HTB-0613 pl HLP 3E14-07 >>> HLP PROJECT
Ar-Ages in Ma
WEIGHTED PLATEAU
28.63 ± 0.34
TOTAL FUSION
29.54 ± 0.34
NORMAL ISOCHRON
28.57 ± 0.55
INVERSE
Sample Info
plag
hampton butte
mi
IRR = OSU3E07
28.63 ± 0.34 Ma
Age (Ma)
Cumulative 39Ar Released (%)
70
65
60
55
50
45
40
35
30
25
20
0
10
20
30
40
50
60
70
80
90
100

Appendix 1 (continued)

Dry Mountain (HTB-0601)

Incremental Heating			36Ar(a)	37Ar(ca)	38Ar(cl)	39Ar(k)	40Ar(r)	Age ± 2σ (Ma)	40Ar(r) (%)	39Ar(k) (%)	K/Ca ± 2σ
07C1792	400 °C		0.002114	0.014381	0.000030	0.026110	0.074129	7.53 ± 0.99	10.61	1.16	0.781 ± 0.043
07C1793	500 °C		0.002781	0.032477	0.000091	0.099416	0.316780	8.45 ± 0.44	27.82	4.40	1.316 ± 0.075
07C1794	600 °C	4	0.003427	0.120916	0.000381	0.354828	1.081863	8.08 ± 0.20	51.65	15.71	1.262 ± 0.069
07C1796	700 °C	4	0.002195	0.238341	0.000454	0.440162	1.312252	7.91 ± 0.13	66.91	19.49	0.794 ± 0.043
07C1797	775 °C	4	0.002289	0.334437	0.000499	0.399480	1.200659	7.97 ± 0.10	63.96	17.69	0.514 ± 0.029
07C1798	850 °C	4	0.002391	0.362981	0.000466	0.307439	0.902017	7.78 ± 0.14	56.07	13.61	0.364 ± 0.020
07C1800	925 °C	4	0.002185	0.302084	0.000340	0.207264	0.605193	7.74 ± 0.20	48.38	9.18	0.295 ± 0.016
07C1801	1000 °C		0.002273	0.228945	0.000256	0.138220	0.378338	7.26 ± 0.29	36.03	6.12	0.260 ± 0.014
07C1802	1075 °C		0.001862	0.164114	0.000197	0.095977	0.274675	7.59 ± 0.32	33.30	4.25	0.251 ± 0.013
07C1803	1150 °C		0.001989	0.145185	0.000132	0.075707	0.212565	7.45 ± 0.50	26.56	3.35	0.224 ± 0.012
07C1805	1225 °C		0.001683	0.111657	0.000106	0.053756	0.155745	7.68 ± 0.55	23.85	2.38	0.207 ± 0.012
07C1806	1300 °C		0.001211	0.082871	0.000063	0.035503	0.103737	7.75 ± 0.71	22.47	1.57	0.184 ± 0.010
07C1808	1400 °C		0.000940	0.058248	0.000056	0.024682	0.069361	7.45 ± 0.63	19.98	1.09	0.182 ± 0.010
		S	0.027338	2.196638	0.003071	2.258545	6.687315				

Information on Analysis	Results	40(r)/39(k) ± 2σ	Age ± 2σ (Ma)	MSWD	39Ar(k) (%,n)	K/Ca ± 2σ
DMT-0601 GM HLP 4C20-06 groundmass hlp mi	Weighted Plateau	2.9828 ± 0.0381 ± 1.28%	7.91 ± 0.12 ± 1.53% External Error ± 0.17 Analytical Error ± 0.10	2.65 2.78 1.6271	75.68 5 Statistical T Ratio Error Magnification	0.401 ± 0.187
Project = HLP Irradiation = OSU4C06 J = 0.0014731 ± 0.0000062 FCT-3 = 28.030 ± 0.003 Ma	Total Fusion Age	2.9609 ± 0.0245 ± 0.83%	7.85 ± 0.09 ± 1.18% External Error ± 0.16 Analytical Error ± 0.06		13	0.012 ± 0.000

Normal Isochron			39(k)/36(a) ± 2σ	40(a+r)/36(a) ± 2σ	r.i.
07C1792	400 °C		12.3 ± 0.2	330.6 ± 5.1	0.9419
07C1793	500 °C		35.7 ± 0.7	409.4 ± 8.0	0.9446
07C1794	600 °C	4	103.6 ± 2.6	611.2 ± 14.1	0.9085
07C1796	700 °C	4	200.6 ± 3.8	893.4 ± 17.3	0.8574
07C1797	775 °C	4	174.6 ± 3.2	820.1 ± 14.4	0.9214
07C1798	850 °C	4	128.6 ± 2.8	672.8 ± 14.4	0.9545
07C1800	925 °C	4	94.9 ± 2.2	572.5 ± 13.2	0.9555
07C1801	1000 °C		60.8 ± 1.4	462.0 ± 10.0	0.9259
07C1802	1075 °C		51.5 ± 1.1	443.0 ± 9.0	0.9552
07C1803	1150 °C		38.1 ± 0.9	402.4 ± 9.5	0.9456
07C1805	1225 °C		31.9 ± 0.7	388.1 ± 8.5	0.9400
07C1806	1300 °C		29.3 ± 0.8	381.2 ± 9.9	0.9276
07C1808	1400 °C		26.3 ± 0.6	369.3 ± 7.8	0.9707

Results	40(a)/36(a) ± 2σ	40(r)/39(k) ± 2σ	Age ± 2σ (Ma)	MSWD
Error Chron	289.8338 ± 22.2517 ± 7.68%	3.0201 ± 0.1570 ± 5.20%	8.01 ± 0.42 ± 5.25% External Error ± 0.44 Analytical Error ± 0.42	3.28

Statistics				
	Statistical F Ratio	2.60	Convergence	0.0000000269
	Error Magnification	1.8115	Number of Iterations	32
	n	5	Calculated Line	Weighted York-2

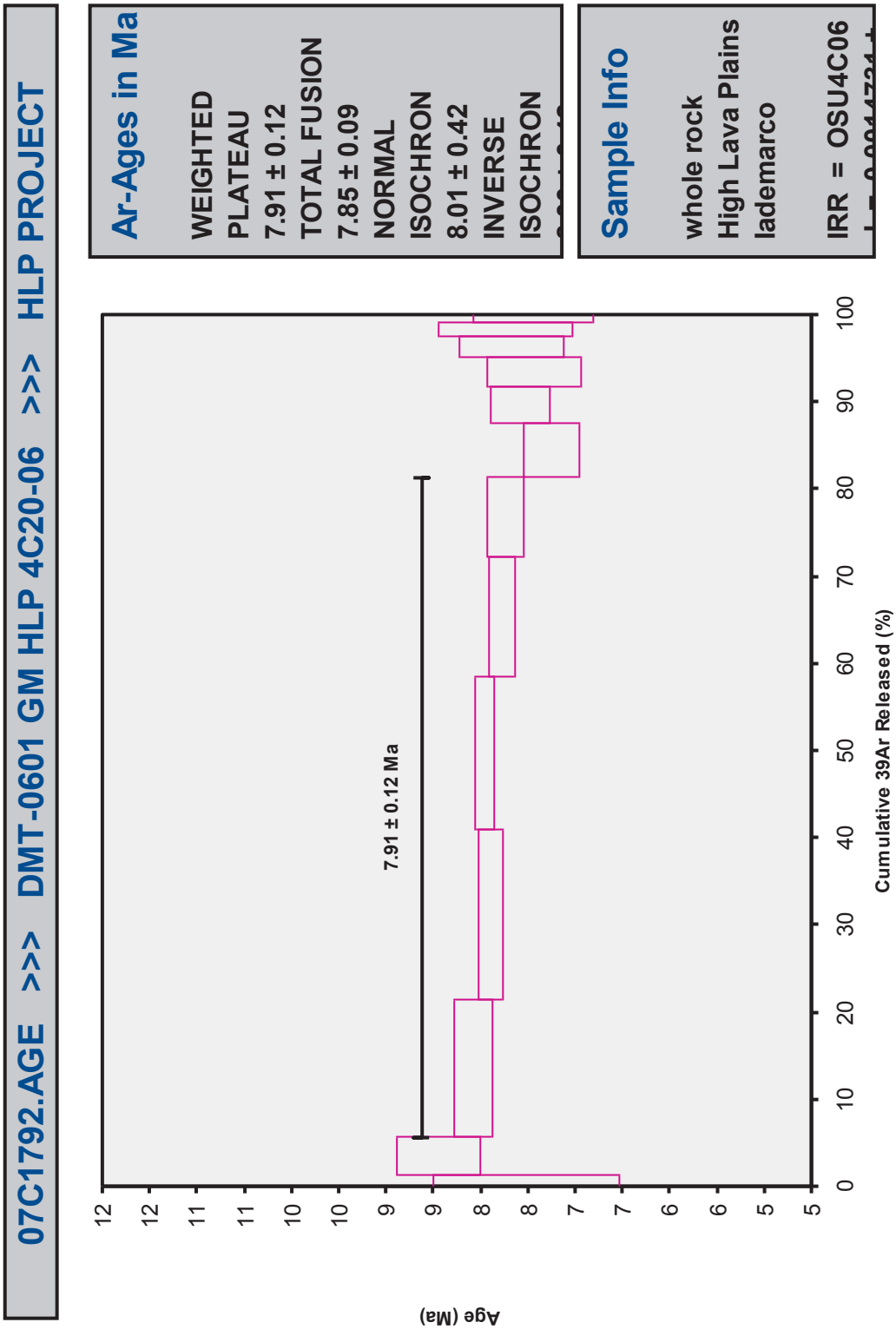
07C1792.AGE >>> DMT-0601 GM HLP 4C20-06 >>> HLP PROJECT
Ar-Ages in Ma
WEIGHTED
PLATEAU
7.91 ± 0.12
TOTAL FUSION
7.85 ± 0.09
NORMAL
ISOCHRON
8.01 ± 0.42
INVERSE
ISOCHRON
Sample Info
whole rock
High Lava Plains
lademarco
IRR = OSU4C06
7.91 ± 0.12 Ma
Age (Ma)
Cumulative 39Ar Released (%)
0
10
20
30
40
50
60
70
80
90
100
5
6
7
8
9
10
11
12

Appendix 1 (continued)

Hampton Basalt (HTB-0523) 1st run

Incremental Heating			36Ar(a)	37Ar(ca)	38Ar(cl)	39Ar(k)	40Ar(r)	Age ± 2σ (Ma)	40Ar(r) (%)	39Ar(k) (%)	K/Ca ± 2σ
06C1606	500 °C	4	0.18036	0.27399	0.00128	0.05136	0.17953	13.21 ± 76.96	0.34	2.80	0.081 ± 0.003
06C1607	600 °C	4	0.08341	0.23796	0.00017	0.03998	0.22004	20.76 ± 75.28	0.88	2.18	0.072 ± 0.003
06C1608	700 °C	4	0.12488	1.30167	0.00136	0.15076	1.19174	29.75 ± 26.04	3.13	8.21	0.050 ± 0.002
06C1609	775 °C	4	0.07609	1.82771	0.00091	0.22419	1.08424	18.26 ± 10.39	4.60	12.20	0.053 ± 0.002
06C1610	850 °C	4	0.05833	2.36606	0.00150	0.29952	1.05391	13.30 ± 3.56	5.76	16.30	0.054 ± 0.002
06C1611	925 °C	4	0.04205	1.31371	0.00132	0.16307	0.45741	10.61 ± 4.25	3.55	8.88	0.053 ± 0.002
06C1612	1000 °C	4	0.05463	0.93730	0.00213	0.12256	0.41456	12.79 ± 9.54	2.50	6.67	0.056 ± 0.002
06C1613	1100 °C	4	0.05003	1.33620	0.00457	0.17394	0.70726	15.36 ± 4.81	4.57	9.47	0.056 ± 0.002
06C1614	1200 °C	4	0.02647	2.95082	0.01267	0.27843	0.89666	12.18 ± 1.67	10.28	15.16	0.041 ± 0.001
06C1615	1400 °C	4	0.04922	9.79275	0.00952	0.33319	1.26695	14.37 ± 3.41	8.01	18.14	0.015 ± 0.000
		S	0.74548	22.33816	0.03544	1.83700	7.47231				

Information on Analysis		Results	40(r)/39(k) ± 2σ	Age ± 2σ (Ma)	MSWD	39Ar(k) (%,n)	K/Ca ± 2σ
Sample	HTB-0523	Weighted Plateau	3.3920 ± 0.3304 ± 9.74%	12.82 ± 1.25 ± 9.73%	0.72	100.00	0.029 ± 0.013
Material	whole rock					10	
Location	HTB		External Error ± 1.26		2.26	Statistical T ratio	
Analyst	mi		Analytical Error ± 1.24		1.0000	Error Magnification	
Project	HLP	Total Fusion Age	4.0677 ± 1.0333 ± 25.40%	15.37 ± 3.89 ± 25.30%		10	0.035 ± 0.001
Irradiation	OSU1D06						
J-value	0.002103		External Error ± 3.90				
Standard	28.03		Analytical Error ± 3.89				

Normal Isochron			39(k)/36(a) ± 2σ	40(a+r)/36(a) ± 2σ	r.i.
06C1606	500 °C	4	0 ± 0	296 ± 6	0.891
06C1607	600 °C	4	0 ± 0	298 ± 10	0.728
06C1608	700 °C	4	1 ± 0	305 ± 9	0.961
06C1609	775 °C	4	3 ± 0	310 ± 9	0.985
06C1610	850 °C	4	5 ± 0	314 ± 5	0.919
06C1611	925 °C	4	4 ± 0	306 ± 5	0.907
06C1612	1000 °C	4	2 ± 0	303 ± 6	0.966
06C1613	1100 °C	4	3 ± 0	310 ± 5	0.941
06C1614	1200 °C	4	11 ± 0	329 ± 5	0.950
06C1615	1400 °C	4	7 ± 0	321 ± 7	0.964

Results	40(a)/36(a) ± 2σ	40(r)/39(k) ± 2σ	Age ± 2σ (Ma)	MSWD
Isochron	297.1385 ± 3.1383 ± 1.06%	3.1350 ± 0.5853 ± 18.67%	11.85 ± 2.21 ± 18.62%	0.66
			External Error ± 2.22	
			Analytical Error ± 2.21	

Statistics				
	Statistical F ratio	1.94	Convergence	0.0000000135
	Error Magnification	1.0000	Number of Iterations	6
	n	10	Calculated Line	Weighted York-2

06C1606.AGE >>> HTB-0523 >>> HLP

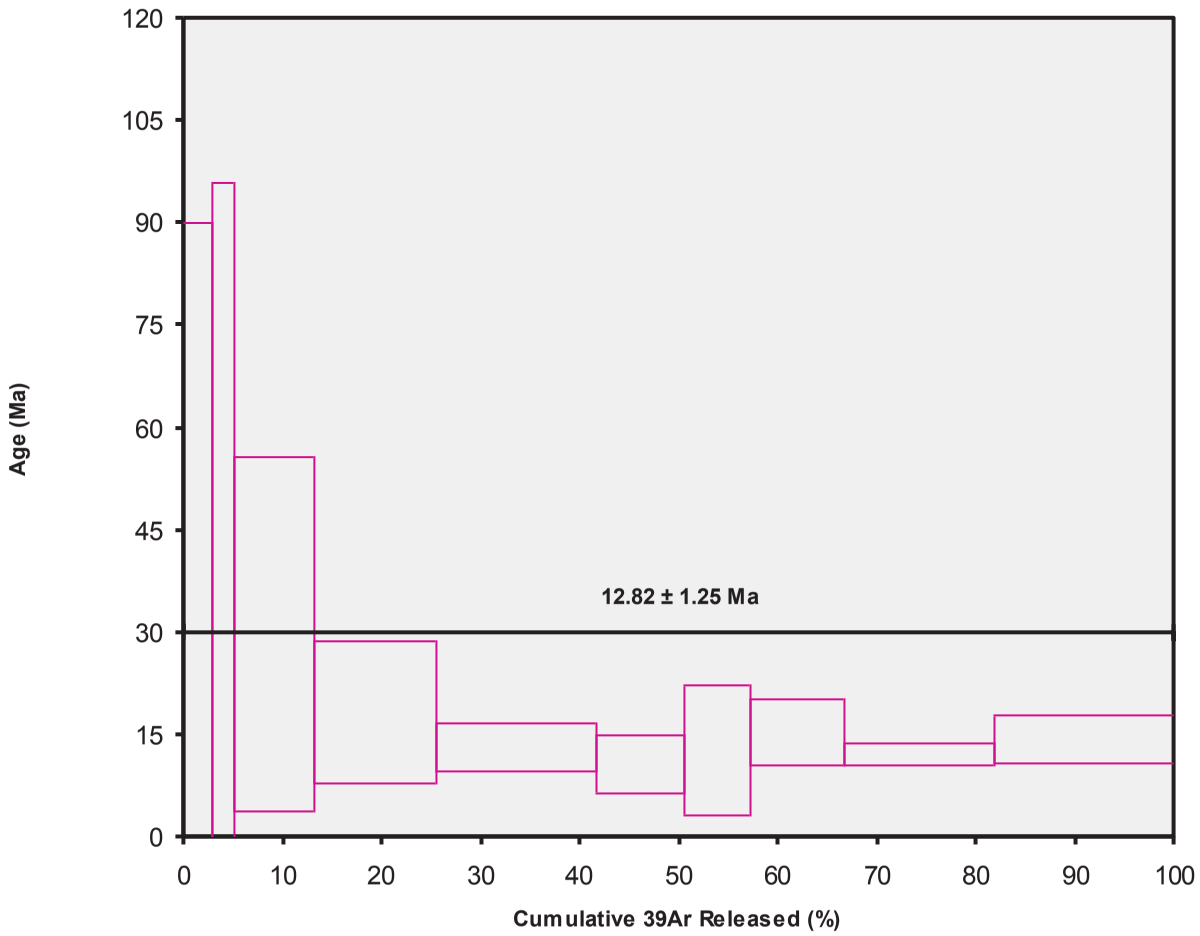

Ar-Ages in Ma

Weighted Plateau
12.82 ± 1.25
Total Fusion
15.37 ± 3.89
Normal Isochron
11.85 ± 2.21
Inverse Isochron
11.84 ± 2.16

MSWD
0.72

Sample Info

whole rock
Hampton Basalt 1st run
lademarco
OSU1D06
0.002103 (J)

Appendix 1 (continued)

Hampton Basalt (HTB-0523) 2nd run

Incremental Heating			36Ar(a)	37Ar(ca)	38Ar(cl)	39Ar(k)	40Ar(r)	Age ± 2σ (Ma)	40Ar(r) (%)	39Ar(k) (%)	K/Ca ± 2σ
08C902	500 °C		0.000292	0.089261	0.000000	0.000969	0.005986	17.67 ± 11.91	6.49	5.15	0.005 ± 0.000
08C903	600 °C	4	0.000045	0.426850	0.000000	0.003473	0.011061	9.12 ± 2.95	45.36	18.48	0.003 ± 0.000
08C904	800 °C	4	0.000039	0.438985	0.000000	0.003414	0.007350	6.18 ± 2.53	38.82	18.16	0.003 ± 0.000
08C905	800 °C	4	0.000046	0.466943	0.000000	0.003441	0.008158	6.80 ± 3.09	37.35	18.30	0.003 ± 0.000
08C907	900 °C	4	0.000041	0.284529	0.000000	0.001983	0.004079	5.90 ± 4.32	25.01	10.55	0.003 ± 0.000
08C908	1025 °C	4	0.000068	0.297199	0.000000	0.001979	0.006635	9.61 ± 3.43	24.78	10.53	0.003 ± 0.000
08C909	1150 °C	4	0.000111	0.214919	0.000000	0.001399	0.005114	10.47 ± 4.75	13.47	7.44	0.003 ± 0.000
08C910	1300 °C	4	0.000219	0.229635	0.000000	0.001466	0.003464	6.77 ± 5.17	5.07	7.80	0.003 ± 0.000
08C911	1400 °C		0.000346	0.105265	0.000000	0.000676	0.004615	19.49 ± 9.29	4.32	3.60	0.003 ± 0.000
		S	0.001209	2.553586	0.000000	0.018800	0.056464				

Information on Analysis	Results	40(r)/39(k) ± 2σ	Age ± 2σ (Ma)	MSWD	39Ar(k) (%,n)	K/Ca ± 2σ
HTB-0523 plag HLP 3E17-07 plag hampton butte mi	Weighted Plateau	2.6772 ± 0.4583 ± 17.12%	7.67 ± 1.31 ± 17.10% External Error ± 1.32 Analytical Error ± 1.31	1.02 2.45 1.0120	91.25 7 Statistical T Ratio Error Magnification	0.003 ± 0.000
Project = HLP Irradiation = OSU3E07 J = 0.0015923 ± 0.0000051 FCT-3 = 28.030 ± 0.003 Ma	Total Fusion Age	3.0034 ± 0.4879 ± 16.24%	8.61 ± 1.40 ± 16.22% External Error ± 1.40 Analytical Error ± 1.39		9	0.003 ± 0.000

Normal Isochron			39(k)/36(a) ± 2σ	40(a+r)/36(a) ± 2σ	r.i.
08C902	500 °C		3.3 ± 0.2	316.0 ± 14.8	0.9111
08C903	600 °C	4	77.0 ± 20.7	540.8 ± 145.3	0.9992
08C904	800 °C	4	87.1 ± 22.7	483.1 ± 125.9	0.9994
08C905	800 °C	4	74.3 ± 20.2	471.7 ± 128.3	0.9995
08C907	900 °C	4	47.9 ± 11.7	394.1 ± 96.4	0.9984
08C908	1025 °C	4	29.0 ± 3.4	392.8 ± 46.3	0.9929
08C909	1150 °C	4	12.6 ± 0.9	341.5 ± 24.1	0.9841
08C910	1300 °C	4	6.7 ± 0.3	311.3 ± 12.7	0.9492
08C911	1400 °C		2.0 ± 0.1	308.8 ± 6.7	0.6911

Results	40(a)/36(a) ± 2σ	40(r)/39(k) ± 2σ	Age ± 2σ (Ma)	MSWD
Isochron	299.9324 ± 13.2567 ± 4.42%	2.4200 ± 0.6181 ± 25.54%	6.94 ± 1.77 ± 25.50% External Error ± 1.77 Analytical Error ± 1.77	1.09

Statistics				
	Statistical F Ratio	2.21	Convergence	0.0000000135
	Error Magnification	1.0438	Number of Iterations	17
	n	7	Calculated Line	Weighted York-2

Appendix 1 (continued)

Hampton Basalt (HTB-0631)

Incremental Heating			36Ar(a)	37Ar(ca)	38Ar(cl)	39Ar(k)	40Ar(r)	Age ± 2σ (Ma)	40Ar(r) (%)	39Ar(k) (%)	K/Ca ± 2σ
07C1380	500 °C		0.007213	0.102717	0.000054	0.024046	0.099420	10.85 ± 4.14	4.46	3.71	0.101 ± 0.004
07C1381	600 °C		0.000305	0.096418	0.000005	0.017778	0.057457	8.49 ± 0.64	38.89	2.74	0.079 ± 0.003
07C1382	700 °C		0.000293	0.560343	0.000000	0.091792	0.286543	8.20 ± 0.16	76.75	14.17	0.070 ± 0.003
07C1383	800 °C	4	0.000213	0.816848	0.000000	0.140318	0.417950	7.82 ± 0.14	86.88	21.66	0.074 ± 0.003
07C1384	875 °C	4	0.000103	0.867515	0.000000	0.127239	0.380094	7.85 ± 0.16	92.57	19.64	0.063 ± 0.003
07C1385	950 °C	4	0.000112	1.091382	0.000000	0.106033	0.309605	7.67 ± 0.14	90.28	16.36	0.042 ± 0.002
07C1386	1025 °C	4	0.000121	0.625579	0.000073	0.049799	0.143067	7.55 ± 0.23	80.02	7.69	0.034 ± 0.001
07C1387	1100 °C	4	0.000194	0.221218	0.000083	0.016121	0.049107	8.00 ± 0.82	46.12	2.49	0.031 ± 0.001
07C1388	1225 °C	4	0.002282	3.529306	0.000187	0.054580	0.167782	8.07 ± 0.88	19.92	8.42	0.007 ± 0.000
07C1389	1400 °C		0.000613	0.669391	0.000000	0.020259	0.097917	12.68 ± 0.73	35.10	3.13	0.013 ± 0.001
		S	0.011449	8.580717	0.000402	0.647965	2.008941				

Information on Analysis	Results	40(r)/39(k) ± 2σ	Age ± 2σ (Ma)	MSWD	39Ar(k) (%,n)	K/Ca ± 2σ
HTB-0631 WR HLP 4A27-06 WR Hampton Butte MI	Weighted Plateau	2.9509 ± 0.0372 ± 1.26%	7.75 ± 0.12 ± 1.55% External Error ± 0.17 Analytical Error ± 0.10	1.57 2.57 1.2521	76.25 6 Statistical T Ratio Error Magnification	0.010 ± 0.010
Project = HLP Irradiation = OSU4A06 J = 0.0014589 ± 0.0000066 FCT-3 = 28.030 ± 0.003 Ma	Total Fusion Age	3.1004 ± 0.0700 ± 2.26%	8.14 ± 0.20 ± 2.43% External Error ± 0.24 Analytical Error ± 0.18		10	0.001 ± 0.000

Normal Isochron			39(k)/36(a) ± 2σ	40(a+r)/36(a) ± 2σ	r.i.
07C1380	500 °C		3.3 ± 0.1	309.3 ± 5.5	0.8758
07C1381	600 °C		58.2 ± 2.8	483.6 ± 23.1	0.9965
07C1382	700 °C		312.8 ± 18.0	1272.0 ± 72.5	0.9890
07C1383	800 °C	4	658.5 ± 70.1	2257.0 ± 240.1	0.9977
07C1384	875 °C	4	1237.9 ± 298.2	3993.4 ± 961.9	0.9994
07C1385	950 °C	4	943.4 ± 140.0	3050.1 ± 452.2	0.9986
07C1386	1025 °C	4	412.6 ± 50.6	1481.0 ± 181.4	0.9989
07C1387	1100 °C	4	83.1 ± 7.3	548.5 ± 47.7	0.9915
07C1388	1225 °C	4	23.9 ± 0.7	369.0 ± 10.0	0.9845
07C1389	1400 °C		33.1 ± 1.0	455.4 ± 13.8	0.9613

Results	40(a)/36(a) ± 2σ	40(r)/39(k) ± 2σ	Age ± 2σ (Ma)	MSWD
No Convergence	298.8413 ± 10.9086 ± 3.65%	2.9350 ± 0.0458 ± 1.56%	7.71 ± 0.14 ± 1.80% External Error ± 0.18 Analytical Error ± 0.12	1.83

Statistics				
	Statistical F Ratio	2.37	Convergence	0.0000002064
	Error Magnification	1.3510	Number of Iterations	500
	n	6	Calculated Line	Weighted York-2

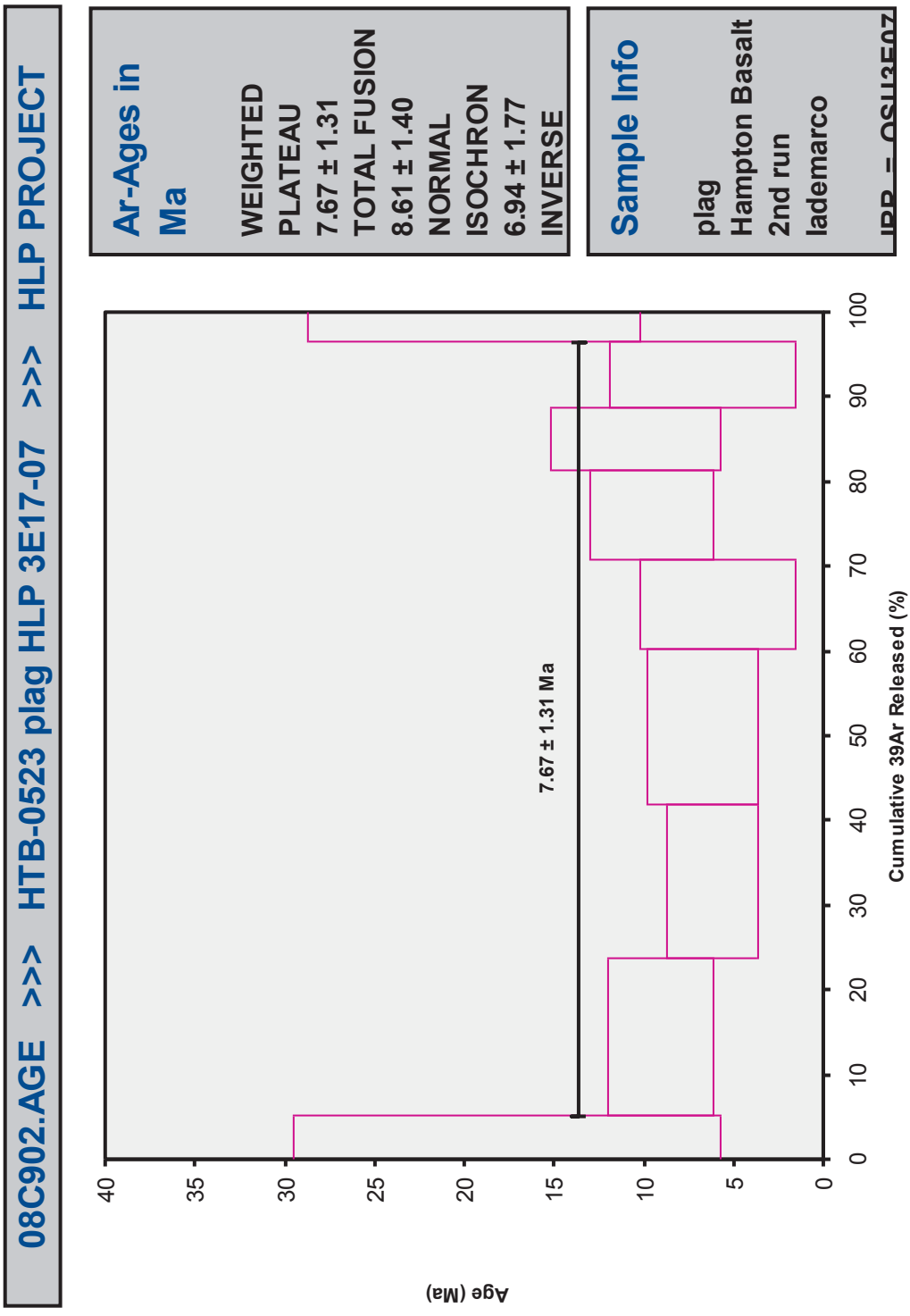
08C902.AGE >>> HTB-0523 plag HLP 3E17-07 >>> HLP PROJECT
Ar-Ages in Ma
WEIGHTED PLATEAU
7.67 ± 1.31
TOTAL FUSION
8.61 ± 1.40
NORMAL ISOCHRON
6.94 ± 1.77
INVERSE
Sample Info
plag
Hampton Basalt
2nd run
lademarco
IRR = OSU3E07
7.67 ± 1.31 Ma
Age (Ma)
Cumulative 39Ar Released (%)
0
5
10
15
20
25
30
35
40
0
10
20
30
40
50
60
70
80
90
100

Appendix 1 (continued)

Hampton andesite (HTB-0623)

Incremental Heating			36Ar(a)	37Ar(ca)	38Ar(cl)	39Ar(k)	40Ar(r)	Age ± 2σ (Ma)	40Ar(r) (%)	39Ar(k) (%)	K/Ca ± 2σ
07C1447	500 °C		0.005463	0.158441	0.000154	0.065748	0.258248	10.27 ± 1.35	13.79	8.14	0.178 ± 0.008
07C1448	600 °C	4	0.001005	0.139808	0.000018	0.036011	0.109005	7.92 ± 0.61	26.85	4.46	0.111 ± 0.005
07C1449	700 °C	4	0.000727	0.468754	0.000036	0.082975	0.254322	8.02 ± 0.31	54.19	10.28	0.076 ± 0.003
07C1450	800 °C	4	0.000396	0.728323	0.000009	0.110598	0.323663	7.66 ± 0.32	73.41	13.70	0.065 ± 0.003
07C1451	875 °C	4	0.000188	0.581878	0.000002	0.082127	0.247637	7.89 ± 0.16	81.66	10.17	0.061 ± 0.003
07C1452	950 °C	4	0.000227	0.553570	0.000039	0.057865	0.169299	7.65 ± 0.20	71.64	7.17	0.045 ± 0.002
07C1453	1025 °C	4	0.000211	0.289154	0.000047	0.026483	0.079436	7.85 ± 0.40	55.99	3.28	0.039 ± 0.002
07C1454	1100 °C	4	0.000135	0.105187	0.000028	0.008977	0.026451	7.71 ± 0.79	39.80	1.11	0.037 ± 0.002
07C1455	1225 °C	4	0.002998	3.169774	0.000280	0.216849	0.638096	7.70 ± 0.29	41.86	26.86	0.029 ± 0.001
07C1456	1400 °C	4	0.001880	1.968527	0.000119	0.119692	0.365939	8.00 ± 0.40	39.71	14.83	0.026 ± 0.001
		S	0.013230	8.163416	0.000730	0.807327	2.472095				

Information on Analysis	Results	40(r)/39(k) ± 2σ	Age ± 2σ (Ma)	MSWD	39Ar(k) (%,n)	K/Ca ± 2σ
HTB-0623 HLP 4A28-06 WR HLP mi	Weighted Plateau	2.9860 ± 0.0359 ± 1.20%	7.81 ± 0.12 ± 1.51% External Error ± 0.17 Analytical Error ± 0.09	0.97 2.31 1.0000	91.86 9 Statistical T Ratio Error Magnification	0.038 ± 0.011
Project = HLP Irradiation = OSU4A06 J = 0.0014533 ± 0.0000067 FCT-3 = 28.030 ± 0.003 Ma	Total Fusion Age	3.0621 ± 0.0616 ± 2.01%	8.01 ± 0.18 ± 2.21% External Error ± 0.22 Analytical Error ± 0.16		10	0.001 ± 0.000

Normal Isochron			39(k)/36(a) ± 2σ	40(a+r)/36(a) ± 2σ	r.i.
07C1447	500 °C		12.0 ± 0.3	342.8 ± 7.2	0.9510
07C1448	600 °C	4	35.8 ± 1.0	404.0 ± 11.3	0.9683
07C1449	700 °C	4	114.1 ± 5.2	645.2 ± 29.3	0.9871
07C1450	800 °C	4	279.0 ± 31.4	1112.0 ± 125.0	0.9977
07C1451	875 °C	4	436.9 ± 37.4	1613.0 ± 138.0	0.9980
07C1452	950 °C	4	255.4 ± 16.6	1042.7 ± 67.6	0.9944
07C1453	1025 °C	4	125.4 ± 8.0	671.6 ± 42.9	0.9968
07C1454	1100 °C	4	66.3 ± 4.5	490.9 ± 33.1	0.9904
07C1455	1225 °C	4	72.3 ± 1.9	508.3 ± 13.4	0.9784
07C1456	1400 °C	4	63.7 ± 2.1	490.2 ± 16.0	0.9822

Results	40(a)/36(a) ± 2σ	40(r)/39(k) ± 2σ	Age ± 2σ (Ma)	MSWD
Isochron	297.3387 ± 6.7398 ± 2.27%	2.9690 ± 0.0578 ± 1.95%	7.77 ± 0.17 ± 2.15% External Error ± 0.21 Analytical Error ± 0.15	1.08

Statistics				
	Statistical F Ratio	2.01	Convergence	0.0000000287
	Error Magnification	1.0382	Number of Iterations	147
	n	9	Calculated Line	Weighted York-2

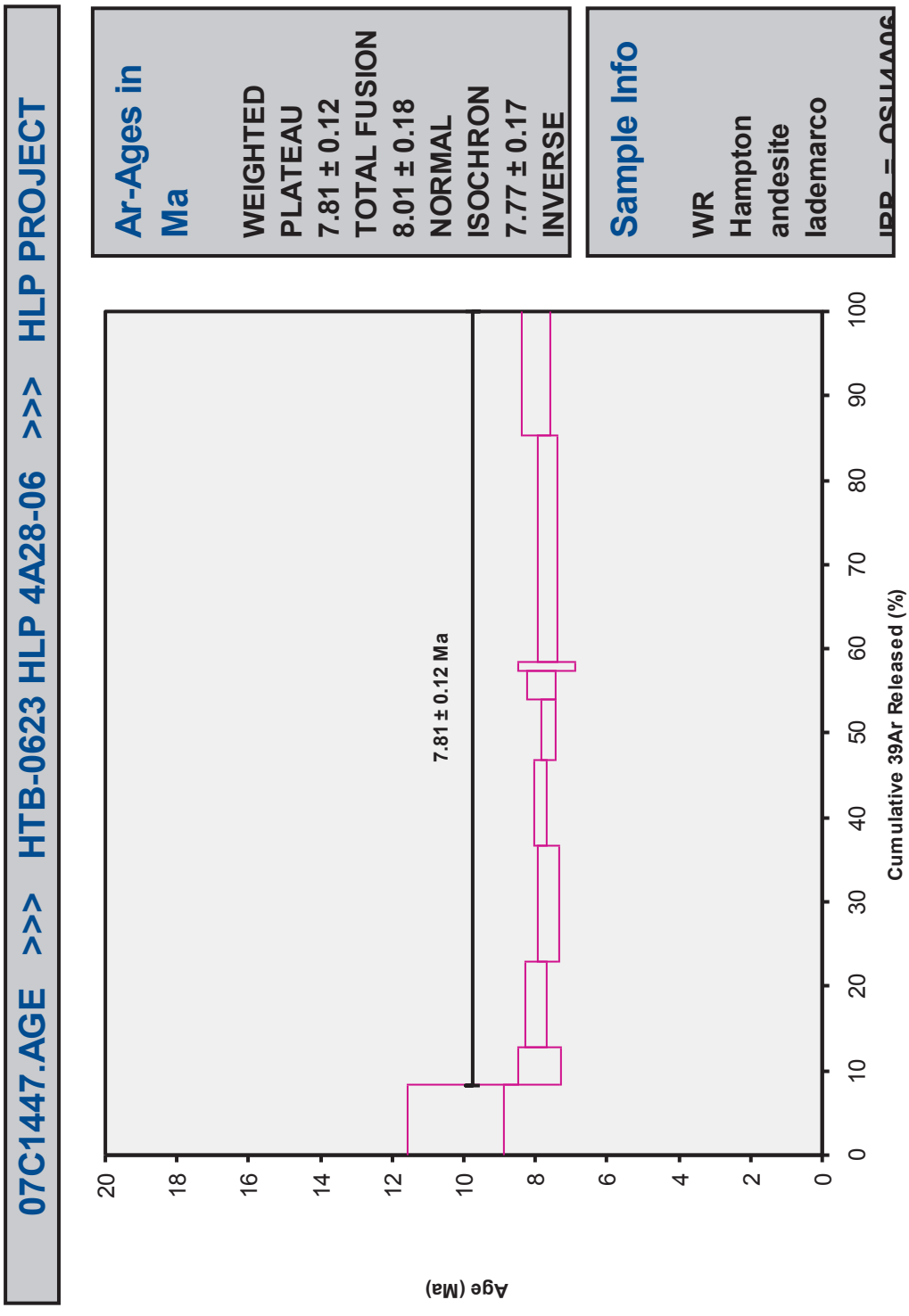
07C1447.AGE >>> HTB-0623 HLP 4A28-06 >>> HLP PROJECT
Ar-Ages in Ma
WEIGHTED PLATEAU
7.81 ± 0.12
TOTAL FUSION
8.01 ± 0.18
NORMAL ISOCHRON
7.77 ± 0.17
INVERSE
Sample Info
WR
Hampton
andesite
lademarco
IRR = OSU4A06
7.81 ± 0.12 Ma
Age (Ma)
Cumulative 39Ar Released (%)
0
2
4
6
8
10
12
14
16
18
20
0
10
20
30
40
50
60
70
80
90
100

Appendix 1 (continued)

Grassy Butte (GB-0701)

Incremental Heating			36Ar(a)	37Ar(ca)	38Ar(cl)	39Ar(k)	40Ar(r)	Age ± 2σ (Ma)	40Ar(r) (%)	39Ar(k) (%)	K/Ca ± 2σ
08C1229	500 °C		0.014996	0.015199	0.001020	0.027130	0.246373	29.09 ± 5.11	5.27	1.75	0.768 ± 0.067
08C1230	600 °C		0.001041	0.018147	0.000973	0.030885	0.059918	6.25 ± 0.44	16.30	1.99	0.732 ± 0.062
08C1231	700 °C	4	0.002573	0.071250	0.002273	0.072548	0.101336	4.51 ± 0.70	11.76	4.69	0.438 ± 0.034
08C1232	775 °C	4	0.003789	0.142356	0.002798	0.091974	0.140875	4.94 ± 0.78	11.18	5.94	0.278 ± 0.020
08C1233	850 °C	4	0.002137	0.233543	0.003930	0.133800	0.189548	4.57 ± 0.39	23.08	8.64	0.246 ± 0.018
08C1234	925 °C	4	0.007043	0.273016	0.004691	0.154215	0.210489	4.40 ± 0.49	9.18	9.96	0.243 ± 0.018
08C1235	1000 °C	4	0.024023	0.273610	0.005111	0.156755	0.249304	5.13 ± 1.71	3.39	10.12	0.246 ± 0.018
08C1236	1075 °C	4	0.019119	0.397376	0.007589	0.235284	0.302596	4.15 ± 1.55	5.08	15.20	0.255 ± 0.019
08C1237	1150 °C	4	0.006114	1.003003	0.014210	0.432905	0.564033	4.20 ± 0.29	23.79	27.96	0.186 ± 0.014
08C1238	1225 °C	4	0.000428	0.661514	0.006200	0.191886	0.243362	4.09 ± 0.12	65.76	12.39	0.125 ± 0.009
08C1239	1400 °C		0.000082	0.064632	0.000400	0.021037	0.043034	6.59 ± 0.48	63.92	1.36	0.140 ± 0.011
		S	0.081345	3.153645	0.049194	1.548419	2.350869				

Information on Analysis	Results	40(r)/39(k) ± 2σ	Age ± 2σ (Ma)	MSWD	39Ar(k) (%,n)	K/Ca ± 2σ
GB-0701 wr HLP 3D7-07 whole rock HLP mi	Weighted Plateau	1.2963 ± 0.0435 ± 3.36%	4.18 ± 0.14 ± 3.37% External Error ± 0.16 Analytical Error ± 0.14	1.83 2.36 1.3523	94.89 8 Statistical T Ratio Error Magnification	0.200 ± 0.053
Project = HLP Irradiation = OSU3D07 J = 0.0017900 ± 0.0000027 FCT-3 = 28.030 ± 0.003 Ma	Total Fusion Age	1.5182 ± 0.1018 ± 6.70%	4.90 ± 0.33 ± 6.70% External Error ± 0.34 Analytical Error ± 0.33		11	0.211 ± 0.007

Normal Isochron			39(k)/36(a) ± 2σ	40(a+r)/36(a) ± 2σ	r.i.
08C1229	500 °C		1.8 ± 0.0	311.9 ± 3.1	0.8540
08C1230	600 °C		29.7 ± 0.4	353.1 ± 4.9	0.9388
08C1231	700 °C	4	28.2 ± 0.6	334.9 ± 7.0	0.9774
08C1232	775 °C	4	24.3 ± 0.5	332.7 ± 6.6	0.9871
08C1233	850 °C	4	62.6 ± 1.6	384.2 ± 9.8	0.9695
08C1234	925 °C	4	21.9 ± 0.3	325.4 ± 3.7	0.9082
08C1235	1000 °C	4	6.5 ± 0.1	305.9 ± 3.6	0.9563
08C1236	1075 °C	4	12.3 ± 0.2	311.3 ± 6.2	0.9871
08C1237	1150 °C	4	70.8 ± 1.5	387.7 ± 8.2	0.9860
08C1238	1225 °C	4	448.1 ± 25.6	863.8 ± 49.2	0.9953
08C1239	1400 °C		256.2 ± 33.1	819.5 ± 106.0	0.9989

Results	40(a)/36(a) ± 2σ	40(r)/39(k) ± 2σ	Age ± 2σ (Ma)	MSWD
Isochron	298.3095 ± 2.1296 ± 0.71%	1.2703 ± 0.0374 ± 2.94%	4.10 ± 0.12 ± 2.95% External Error ± 0.14 Analytical Error ± 0.12	0.91

Statistics				
	Statistical F Ratio	2.10	Convergence	0.0000000109
	Error Magnification	1.0000	Number of Iterations	59
	n	8	Calculated Line	Weighted York-2

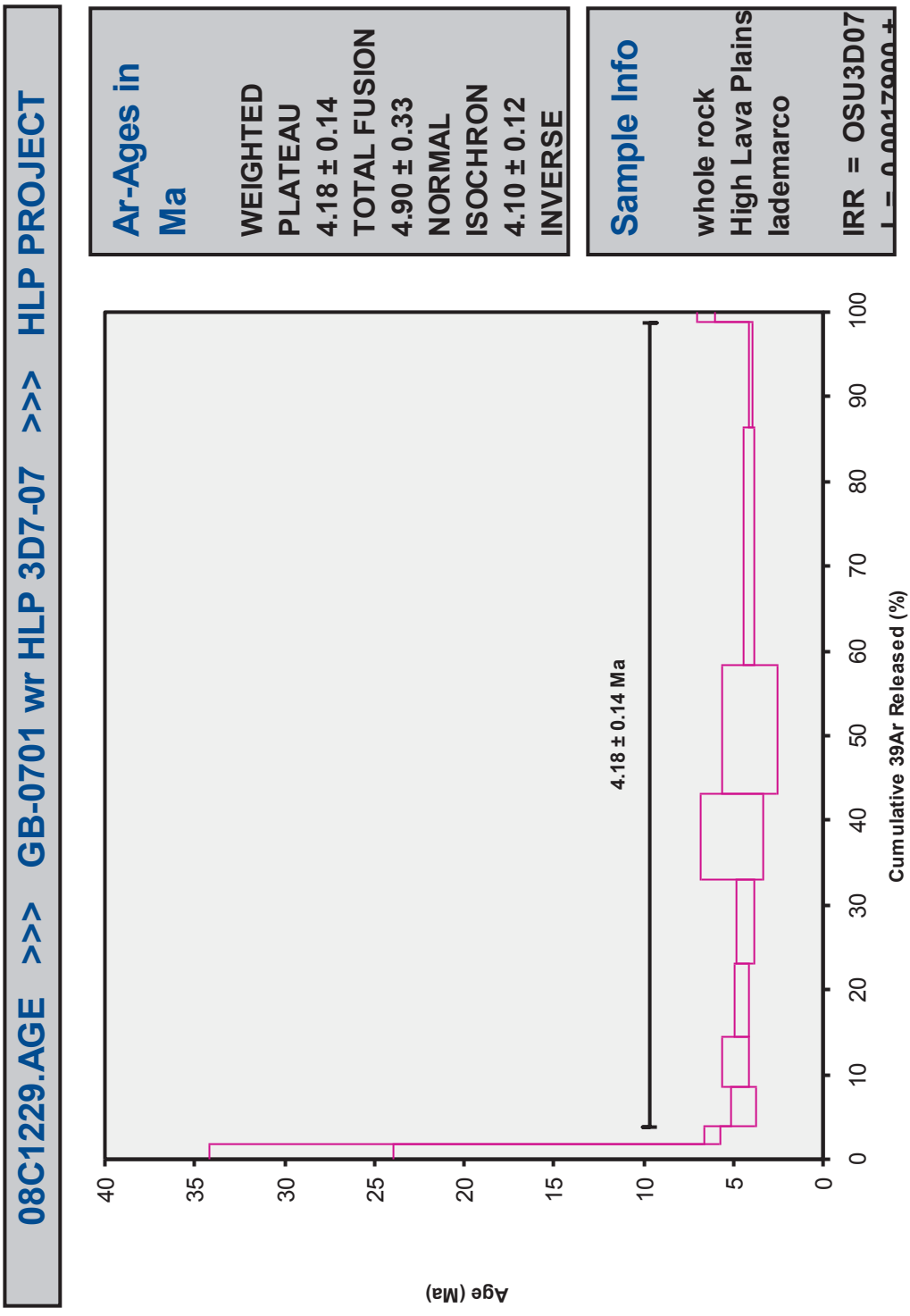
08C1229.AGE >>> GB-0701 wr HLP 3D7-07 >>> HLP PROJECT
Ar-Ages in Ma
WEIGHTED PLATEAU
4.18 ± 0.14
TOTAL FUSION
4.90 ± 0.33
NORMAL ISOCHRON
4.10 ± 0.12
INVERSE
Sample Info
whole rock
High Lava Plains
lademarco
IRR = OSU3D07
4.18 ± 0.14 Ma
Age (Ma)
Cumulative 39Ar Released (%)
0
5
10
15
20
25
30
35
40
0
10
20
30
40
50
60
70
80
90
100

Appendix 1 (continued)

Hampton Tuff (HTB-0701)

Incremental Heating			36Ar(a)	37Ar(ca)	38Ar(cl)	39Ar(k)	40Ar(r)	Age ± 2σ (Ma)	40Ar(r) (%)	39Ar(k) (%)	K/Ca ± 2σ
08C930	500 °C	4	0.000028	0.004045	0.000004	0.001489	0.001588	3.15 ± 5.17	16.23	0.87	0.158 ± 0.017
08C931	600 °C	4	0.000035	0.026137	0.000009	0.009176	0.010453	3.36 ± 0.81	50.20	5.39	0.151 ± 0.010
08C932	700 °C	4	0.000035	0.051997	0.000012	0.017098	0.021330	3.68 ± 0.38	67.26	10.04	0.141 ± 0.009
08C934	800 °C	4	0.000048	0.097437	0.000037	0.030189	0.037451	3.66 ± 0.23	72.43	17.73	0.133 ± 0.009
08C935	875 °C	4	0.000037	0.075875	0.000018	0.023060	0.029513	3.77 ± 0.34	73.03	13.54	0.131 ± 0.009
08C937	1025 °C	4	0.000059	0.101417	0.000024	0.030718	0.040801	3.92 ± 0.23	70.11	18.04	0.130 ± 0.008
08C938	1100 °C	4	0.000064	0.051815	0.000014	0.015478	0.023813	4.54 ± 0.56	55.86	9.09	0.128 ± 0.008
08C939	1175 °C	4	0.000117	0.053581	0.000012	0.016304	0.020813	3.76 ± 0.48	37.54	9.57	0.131 ± 0.008
08C941	1250 °C		0.000168	0.034884	0.000003	0.010426	0.017519	4.95 ± 0.76	26.09	6.12	0.129 ± 0.009
08C942	1325 °C		0.000283	0.028827	0.000017	0.008559	0.017497	6.03 ± 1.06	17.29	5.03	0.128 ± 0.009
08C944	1400 °C		0.000162	0.025774	0.000010	0.007788	0.013312	5.04 ± 0.95	21.73	4.57	0.130 ± 0.009
		S	0.001036	0.551790	0.000160	0.170284	0.234091				

Information on Analysis		Results	40(r)/39(k) ± 2σ		Age ± 2σ (Ma)		MSWD	39Ar(k) (%,n)	K/Ca ± 2σ
HTB-0701 pl HLP 3E15-07 plag hampton butte mi		Weighted Plateau	1.2892	± 0.0544 ± 4.22%	3.80	± 0.16 ± 4.25%	1.59	84.28 8	0.135 ± 0.006
					External Error	± 0.17	2.36	Statistical T Ratio	
					Analytical Error	± 0.16	1.2622	Error Magnification	
Project = HLP Irradiation = OSU3E07 J = 0.0016365 ± 0.0000044 FCT-3 = 28.030 ± 0.003 Ma		Total Fusion Age	1.3747	± 0.0510 ± 3.71%	4.05	± 0.15 ± 3.74%		11	0.133 ± 0.003
					External Error	± 0.16			
					Analytical Error	± 0.15			

Normal Isochron			39(k)/36(a) ± 2σ	40(a+r)/36(a) ± 2σ	r.i.
08C930	500 °C	4	53.7 ± 16.5	352.7 ± 111.2	0.9741
08C931	600 °C	4	261.7 ± 61.2	593.6 ± 140.3	0.9895
08C932	700 °C	4	487.5 ± 98.5	903.7 ± 183.6	0.9940
08C934	800 °C	4	627.2 ± 100.7	1073.6 ± 172.9	0.9962
08C935	875 °C	4	626.5 ± 149.9	1097.3 ± 263.1	0.9971
08C937	1025 °C	4	522.8 ± 67.9	989.9 ± 129.0	0.9946
08C938	1100 °C	4	243.2 ± 36.9	669.7 ± 102.1	0.9938
08C939	1175 °C	4	139.2 ± 10.3	473.2 ± 35.5	0.9823
08C941	1250 °C		62.1 ± 3.2	399.8 ± 21.3	0.9784
08C942	1325 °C		30.2 ± 1.1	357.3 ± 13.1	0.9725
08C944	1400 °C		48.0 ± 2.5	377.5 ± 19.7	0.9938

Results		40(a)/36(a) ± 2σ		40(r)/39(k) ± 2σ		Age ± 2σ (Ma)		MSWD
Isochron		304.4654	± 34.8882 ± 11.46%	1.2554	± 0.0975 ± 7.77%	3.70	± 0.29 ± 7.78%	1.48
						External Error	± 0.29	
						Analytical Error	± 0.29	

Statistics					
	Statistical F Ratio	2.10	Convergence	0.0000000107
	Error Magnification	1.2159	Number of Iterations	67
	n	8	Calculated Line	Weighted York-2

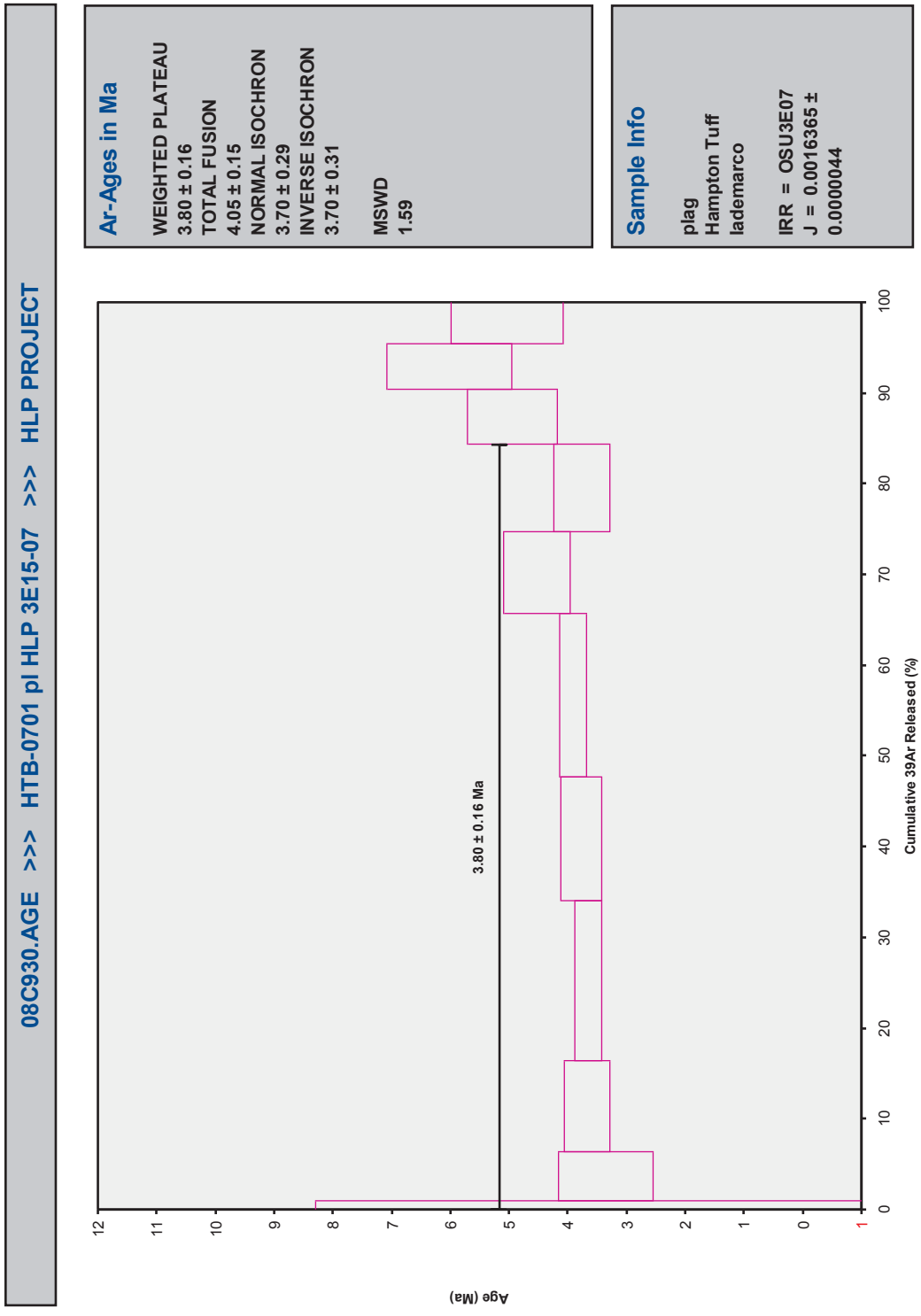
08C930.AGE >>> HTB-0701 pl HLP 3E15-07 >>> HLP PROJECT
Ar-Ages in Ma
WEIGHTED PLATEAU
3.80 ± 0.16
TOTAL FUSION
4.05 ± 0.15
NORMAL ISOCHRON
3.70 ± 0.29
INVERSE ISOCHRON
3.70 ± 0.31
MSWD
1.59
Sample Info
plag
Hampton Tuff
lademarco
IRR = OSU3E07
J = 0.0016365 ±
0.0000044
3.80 ± 0.16 Ma
Age (Ma)
Cumulative 39Ar Released (%)

Appendix 2

After Washington State GeoAnalytical Lab (2009)

WSU XRF precision, limit of determination (2-sigma)

Mar-06	Replicate r2	Replicate LOD
Unnormalized Major Elements (Weight %):		
SiO2	0.99929	0.58
TiO2	0.99992	0.017
Al2O3	0.99949	0.16
FeO*	0.99948	0.20
MnO	0.99983	0.002
MgO	0.99994	0.076
CaO	0.99976	0.064
Na2O	0.99981	0.045
K2O	0.99992	0.031
P2O5	0.99990	0.005
Estimated LOI	0.966	1.00
SO3	0.989	0.07
Cl	0.992	0.002
Normalized Major Elements (Weight %):		
SiO2	0.99992	0.19
TiO2	0.99996	0.012
Al2O3	0.99987	0.082
FeO*	0.99956	0.18
MnO	0.99988	0.002
MgO	0.99994	0.073
CaO	0.99998	0.043
Na2O	0.99989	0.036
K2O	0.99998	0.015
P2O5	0.99996	0.003
Trace Elements (ppm):		
Ni	0.9992	3.5
Cr	0.9998	3.0
Sc	0.997	1.6
V	0.9996	5.0
Ba	0.9997	11.7
Rb	0.9998	1.7
Sr	0.99992	4.6
Zr	0.99994	3.9
Y	0.9987	1.2
Nb	0.99987	1.2
Ga	0.955	2.7
Cu	0.994	7.4
Zn	0.9991	3.3
Pb	0.9966	2.6
La	0.9941	5.7
Ce	0.996	7.9
Th	0.997	1.6
Nd	0.992	4.3
U	0.983	2.7
Bi	0.758	2.0
Cs	0.365	5.1

Appendix 3
Detailed results of modeling

Hampton Butte (HTB-0501)

Sample #	Hampton Butte (HTB-0501)									
	Calc.	0.120	0.370	0.050	0.010		0.290		0.160	Mineral %
	Parent	Titan. mag	Plag	Hbld	Apatite	K-spar	Olivine	Opx	Cpx	Crystals
SiO2	49.333	0.000	53.890	36.340		67.270	40.200	57.100	50.400	41.48
TiO2	1.970	20.080		0.940				0.170	0.870	2.60
Al2O3	13.280	1.840	29.200	14.060		18.350		0.700	3.920	12.36
FeO	12.180	77.670	0.930	28.000		0.920	13.070	5.900	6.410	15.88
MnO	0.349	0.630	0.930	0.750	0.070			0.170	0.130	0.48
MgO	11.610	2.180		3.140	0.100		45.940	34.520	15.450	16.21
CaO	7.195	0.050	11.140	11.820	55.840	0.150	0.230	0.620	21.860	8.84
Na2O	2.660		4.850	1.140		6.450		0.070	0.290	1.90
K2O	0.887		0.290	2.660		7.050		0.030		0.24
P2O5	0.340				42.050					0.42
	99.804	102.450	101.230	98.850	98.060	100.190	99.440	99.280	99.330	100.40
Rb	5									
Sr	691									
Ba	346									

Regression

% xlzn	0.10	0.20	0.30	0.40	0.50	0.60	0.70	0.80	0.90	XRF
SiO2	50.21	51.30	52.70	54.57	57.19	61.12	67.66	80.75	120.03	67.66
TiO2	1.90	1.81	1.70	1.55	1.34	1.03	0.51	-0.53	-3.66	0.51
Al2O3	13.38	13.51	13.68	13.90	14.21	14.67	15.44	16.98	21.61	15.44
FeO	11.77	11.25	10.59	9.71	8.48	6.63	3.55	-2.62	-21.12	3.54
MnO	0.33	0.32	0.29	0.26	0.22	0.15	0.05	-0.17	-0.82	0.05
MgO	11.10	10.46	9.64	8.54	7.01	4.70	0.87	-6.81	-29.83	0.87
CaO	7.01	6.78	6.49	6.10	5.55	4.73	3.35	0.61	-7.62	3.35
Na2O	2.74	2.85	2.99	3.17	3.42	3.80	4.44	5.71	9.52	4.44
K2O	0.96	1.05	1.16	1.32	1.53	1.86	2.40	3.47	6.71	2.40
P2O5	0.33	0.32	0.31	0.29	0.26	0.22	0.15	0.02	-0.38	0.15
	99.74	99.65	99.55	99.40	99.21	98.91	98.41	97.41	94.42	98.41
				Modeled	Rb	17		XRF results	Rb	54
					Sr	318			Sr	382
					Ba	581			Ba	664

Match

	Daughter (ICP-MS)	Daughter (calc)	Residual	R^2
SiO2	67.66	67.66	0.000	0.000
TiO2	0.51	0.51	-0.002	0.000
Al2O3	15.44	15.44	-0.005	0.000
FeO	3.54	3.55	0.003	0.000
MnO	0.05	0.05	-0.005	0.000
MgO	0.87	0.87	-0.004	0.000
CaO	3.35	3.35	0.008	0.000
Na2O	4.44	4.44	-0.002	0.000
K2O	2.40	2.40	-0.002	0.000
P2O5	0.15	0.15	0.006	0.000
	98.41	98.41		
% melt remaining		30.00	√∑R^2= 0.014	

Mineral/melt partition coefficients used (from Rollinson, 1993):

	Rubidium	Strontium	Barium
Titan. Magnetite	0.0	0.0	0.0
Plagioclase	0.071	4.4	1.515
Hornblende	0.014	0.022	0.044
Apatite	0.0	0.0	0.0
Olivine	0.0098	0.014	0.0099
Clinopyroxene	0.031	0.0	0.026

Mineral compositions are from Deer, Howie, and Zussman (1992).

Appendix 3 (continued)

Hampton Butte (HTB-0501)

Rayleigh Fractionation Model - Crystallization

CL/CO=F ^(Di-1)			Rb	CL/CO=F ^(Di-1)			Sr	CL/CO=F ^(Di-1)			Ba
F	Di of a			F	Di of b			F	Di of b		
	0.035				1.643				0.570		
	CL/Co				CL/Co				CL/Co		
0.05	18.021	96.68		0.05	0.146	100.49		0.05	3.628	1256.01	
0.10	9.231	49.52		0.10	0.228	156.91		0.10	2.693	932.19	
0.20	4.728	25.36		0.20	0.355	245.01		0.20	1.998	691.85	
0.30	3.197	17.15		0.30	0.461	317.99		0.30	1.678	581.12	
0.40	2.422	12.99		0.40	0.555	382.59		0.40	1.483	513.48	
0.50	1.952	10.47		0.50	0.640	441.61		0.50	1.347	466.48	
0.60	1.637	8.78		0.60	0.720	496.54		0.60	1.246	431.30	
0.70	1.411	7.57		0.70	0.795	548.27		0.70	1.166	403.62	
0.80	1.240	6.65		0.80	0.866	597.42		0.80	1.101	381.09	
0.90	1.107	5.94		0.90	0.935	644.42		0.90	1.046	362.27	
1.00	1.000	5.36		1.00	1.000	689.58		1.00	1.000	346.21	

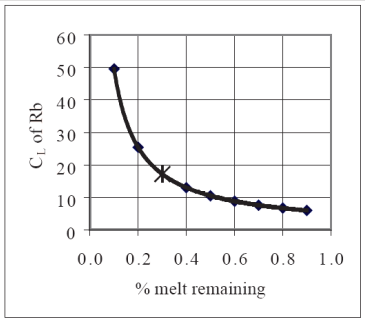

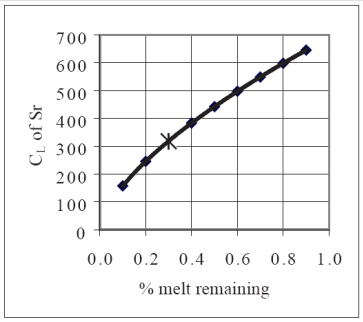

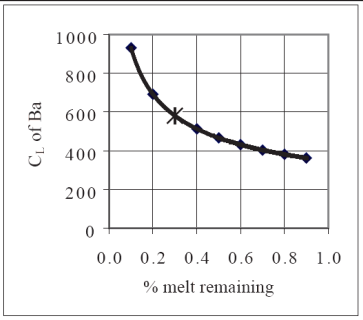

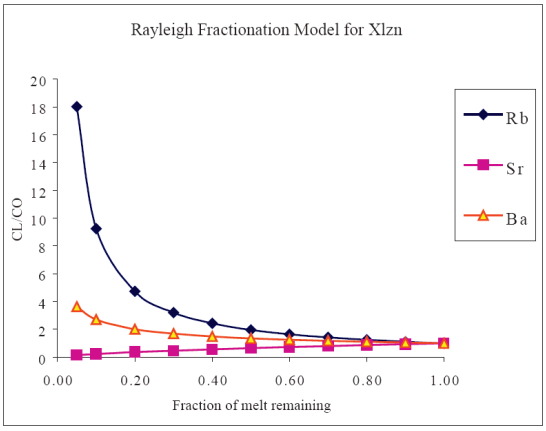

Appendix 3 (continued)

Cougar Butte (HTB-0613)

Sample #	Cougar Butte (HTB-0613)									
	Parent	0.12	0.37	0.05	0.01	0.01	0.29		0.16	Mineral %
	Calc	Titan mag	Plag	Hbld	Apatite	Biotite	Olivine	Opx	Cpx	Crystals
SiO2	48.78		53.89	36.34		34.73	40.20	57.10	50.40	41.56
TiO2	1.87	20.08	0.00	0.94		2.83		0.17	0.87	2.52
Al2O3	13.70	1.84	29.20	14.06		16.67		0.70	3.92	12.37
FeO	11.75	77.67	0.93	28.00		25.20	13.07	5.90	6.41	15.74
MnO	0.35	0.63	0.93	0.75	0.07	1.21	0.00	0.17	0.13	0.48
MgO	11.79	2.18		3.14	0.10	5.95	45.94	34.52	15.45	16.26
CaO	7.47	0.05	11.14	11.82	55.84		0.23	0.62	21.86	8.79
Na2O	2.71		4.85	1.14		0.41		0.07	0.29	1.88
K2O	0.65		0.29	2.66		9.35		0.03		0.33
P2O5	0.34			0.00	42.05					0.42
	99.40	102.45	101.23	98.85	98.06	96.35	99.44	99.28	99.33	100.35
Rb	5									
Sr	691									
Ba	321									

Regression

% xlzn	0.10	0.20	0.30	0.40	0.50	0.60	0.70	0.80	0.90	XRF
SiO2	49.58	50.59	51.88	53.60	56.00	59.62	65.64	77.68	113.79	65.64
TiO2	1.80	1.71	1.59	1.43	1.22	0.89	0.34	-0.74	-4.01	0.36
Al2O3	13.85	14.03	14.27	14.59	15.03	15.70	16.81	19.03	25.70	16.84
FeO	11.31	10.75	10.04	9.09	7.76	5.77	2.44	-4.21	-24.15	2.45
MnO	0.33	0.31	0.29	0.25	0.21	0.14	0.03	-0.20	-0.89	0.04
MgO	11.29	10.67	9.87	8.81	7.32	5.08	1.35	-6.10	-28.47	1.37
CaO	7.32	7.14	6.91	6.59	6.15	5.50	4.40	2.21	-4.37	4.40
Na2O	2.80	2.92	3.07	3.26	3.54	3.96	4.65	6.04	10.20	4.66
K2O	0.68	0.72	0.78	0.85	0.96	1.11	1.37	1.90	3.46	1.36
P2O5	0.33	0.32	0.31	0.29	0.26	0.22	0.15	0.02	-0.38	0.15
	99.30	99.16	98.99	98.77	98.45	97.98	97.19	95.61	90.88	97.28
								XRF results	Rb	15
									Sr	1011
									Ba	786

	Match			
	Daughter (ICP-MS)	Daughter (calc)	Residual	R^2
SiO2	65.64	65.64	-0.007	0.000
TiO2	0.36	0.34	-0.016	0.000
Al2O3	16.84	16.81	-0.030	0.001
FeO	2.45	2.44	-0.007	0.000
MnO	0.04	0.03	-0.011	0.000
MgO	1.37	1.35	-0.018	0.000
CaO	4.40	4.40	-0.001	0.000
Na2O	4.66	4.65	-0.007	0.000
K2O	1.36	1.37	0.010	0.000
P2O5	0.15	0.15	0.000	0.000
	97.28	97.19		
% melt remaining		30.00	√∑R^2= 0.043	

Mineral/melt partition coefficients used (from Rollinson, 1993):

	Rubidium	Strontium	Barium
Titan. Magnetite	0.0	0.0	0.0
Plagioclase	0.041	1.830	0.503
Hornblende	0.014	0.022	0.044
Apatite	0.0	0.0	0.0
Biotite	3.260	0.120	6.360
Olivine	0.0098	0.014	0.0099
Clinopyroxene	0.031	0.0	0.026

Mineral compositions are from Deer, Howie, and Zussman (1992).

Appendix 3 (continued)

Cougar Butte (HTB-0613)

Rayleigh Fractionation Model - Crystallization

CL/CO=F ^(Di-1)			CL/CO=F ^(Di-1)			CL/CO=F ^(Di-1)		
F	Di of a	Rb	F	Di of b	Sr	F	Di of b	Ba
	0.056			0.684			0.256	
	CL/Co			CL/Co			CL/Co	
0.05	16.908	81.94	0.05	2.576	1780.64	0.05	9.275	2978.44
0.10	8.789	42.59	0.10	2.070	1430.47	0.10	5.540	1778.97
0.20	4.569	22.14	0.20	1.663	1149.16	0.20	3.309	1062.55
0.30	3.116	15.10	0.30	1.463	1011.00	0.30	2.448	786.00
0.40	2.375	11.51	0.40	1.336	923.17	0.40	1.976	634.64
0.50	1.924	9.32	0.50	1.245	860.33	0.50	1.674	537.62
0.60	1.620	7.85	0.60	1.175	812.18	0.60	1.462	469.46
0.70	1.400	6.79	0.70	1.119	773.58	0.70	1.304	418.63
0.80	1.234	5.98	0.80	1.073	741.62	0.80	1.180	379.06
0.90	1.105	5.35	0.90	1.034	714.54	0.90	1.081	347.28
1.00	1.000	4.85	1.00	1.000	691.14	1.00	1.000	321.11

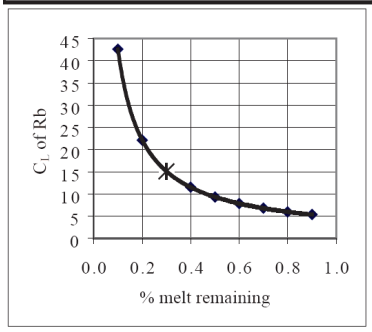

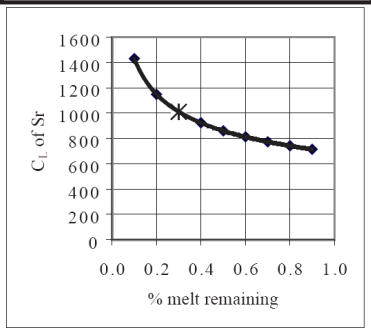

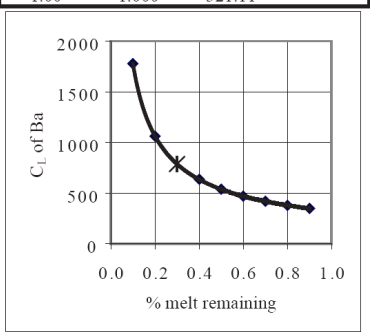

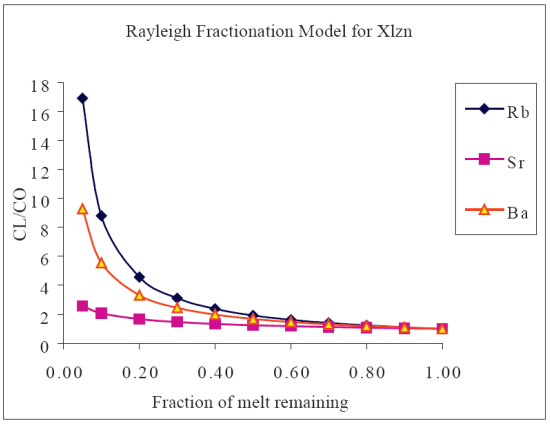

Appendix 3 (continued)

Parent of Cougar Butte (HTB-613) to the parent of Hampton Butte (HTB-0501)

Sample # Model CB Parent to HTB Parent

	CB Parent	0.05	0.56	0.09	0.03		0.27		0.00	Mineral %
	Calc	Titan. Mag	Plag	Hbld	Apatite	K-spar	Olivine	Opx	Cpx	Crystals
SiO2	48.78	0.00	53.89	36.34		67.27	40.20	57.10	50.40	43.85
TiO2	1.87	20.08		0.94				0.17	0.87	0.98
Al2O3	13.70	1.84	29.20	14.06		18.35		0.70	3.92	17.48
FeO	11.75	77.67	0.93	28.00		0.92	13.07	5.90	6.41	9.92
MnO	0.35	0.63	0.93	0.75	0.07			0.17	0.13	0.61
MgO	11.79	2.18		3.14	0.10		45.94	34.52	15.45	12.77
CaO	7.47	0.05	11.14	11.82	55.84	0.15	0.23	0.62	21.86	8.93
Na2O	2.71		4.85	1.14		6.45		0.07	0.29	2.79
K2O	0.65		0.29	2.66		7.05		0.03		0.39
P2O5	0.34				42.05					1.26
	99.40	102.45	101.23	98.85	98.06	100.19	99.44	99.28	99.33	98.99
Rb	5									
Sr	691									
Ba	321									

Regression

% xlzn	0.10	0.20	0.30	0.40	0.50	0.60	0.70	0.80	0.90	Calc. HTB Parent
SiO2	49.33	50.01	50.89	52.07	53.71	56.17	60.28	68.49	93.13	49.33
TiO2	1.97	2.09	2.25	2.46	2.76	3.20	3.94	5.42	9.85	1.97
Al2O3	13.28	12.75	12.08	11.18	9.92	8.02	4.87	-1.44	-20.36	13.28
FeO	11.95	12.21	12.53	12.97	13.58	14.49	16.02	19.07	28.22	12.18
MnO	0.32	0.28	0.23	0.17	0.08	-0.05	-0.27	-0.71	-2.04	0.35
MgO	11.68	11.54	11.37	11.14	10.81	10.32	9.50	7.86	2.95	11.61
CaO	7.31	7.11	6.85	6.50	6.01	5.28	4.07	1.64	-5.64	7.20
Na2O	2.70	2.69	2.68	2.66	2.63	2.59	2.53	2.40	2.00	2.66
K2O	0.67	0.71	0.76	0.82	0.90	1.03	1.25	1.68	2.97	0.89
P2O5	0.24	0.11	-0.05	-0.27	-0.58	-1.04	-1.81	-3.35	-7.95	0.34
	99.45	99.50	99.58	99.68	99.82	100.02	100.37	101.06	103.13	99.80
									Rb	5
									Sr	691
									Ba	346

Match

	CB Parent	HTB Parent	Residual	R^2
SiO2	49.33	49.33	-0.005	0.000
TiO2	1.97	1.97	-0.001	0.000
Al2O3	13.28	13.28	0.000	0.000
FeO	12.18	11.95	-0.227	0.051
MnO	0.35	0.32	-0.033	0.001
MgO	11.61	11.68	0.071	0.005
CaO	7.20	7.31	0.113	0.013
Na2O	2.66	2.70	0.041	0.002
K2O	0.89	0.67	-0.213	0.046
P2O5	0.34	0.24	-0.102	0.010
	99.80	99.45		
% melt remaining		0.90	√∑R^2= 0.358	

Mineral/melt partition coefficients used (from Rollinson, 1993):

	Rubidium	Strontium	Barium
Titan. Magnetite	0.0	0.0	0.0
Plagioclase	0.071	1.830	0.503
Hornblende	0.014	0.022	0.044
Apatite	0.0	0.0	0.0
Olivine	0.0098	0.014	0.0099
Clinopyroxene	0.031	0.0	0.026

Mineral compositions are from Deer, Howie, and Zussman. (1992).

Appendix 3 (continued)

Parent of Cougar Butte (HTB-613) to the parent of Hampton Butte (HTB-0501)

Rayleigh Fractionation Model - Crystallization

CL/CO=F ^(Di-1)			CL/CO=F ^(Di-1)			CL/CO=F ^(Di-1)		
F	Di of a	Rb	F	Di of b	Sr	F	Di of b	Ba
	0.043			1.021			0.286	
	CL/Co			CL/Co			CL/Co	
0.05	17.570	85.14	0.05	0.938	648.07	0.05	8.500	2729.35
0.10	9.052	43.87	0.10	0.952	657.79	0.10	5.180	1663.47
0.20	4.664	22.60	0.20	0.966	667.66	0.20	3.157	1013.84
0.30	3.164	15.33	0.30	0.974	673.50	0.30	2.363	758.89
0.40	2.403	11.64	0.40	0.981	677.67	0.40	1.924	617.91
0.50	1.941	9.41	0.50	0.985	680.93	0.50	1.641	526.86
0.60	1.630	7.90	0.60	0.989	683.60	0.60	1.440	462.52
0.70	1.407	6.82	0.70	0.992	685.87	0.70	1.290	414.29
0.80	1.238	6.00	0.80	0.995	687.84	0.80	1.173	376.60
0.90	1.106	5.36	0.90	0.998	689.58	0.90	1.078	346.21
1.00	1.000	4.85	1.00	1.000	691.14	1.00	1.000	321.11

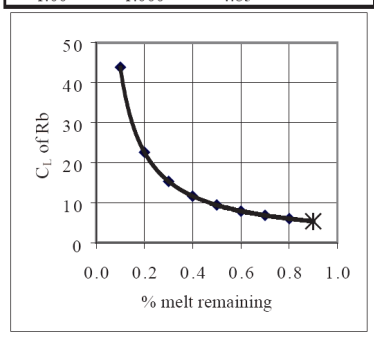

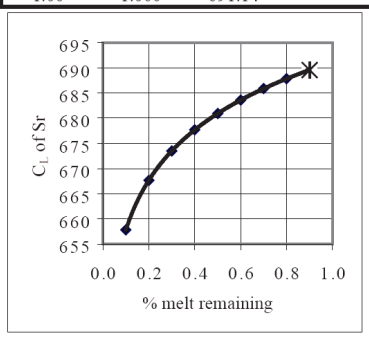

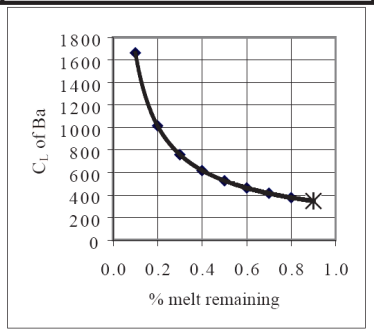

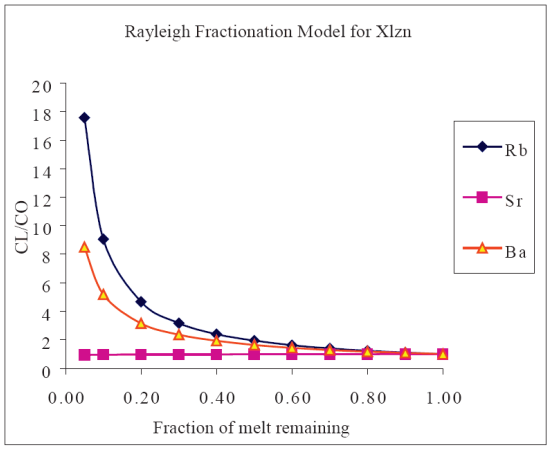

Appendix 3 (continued)

Potato Hills (HLP-0704)

Sample #	Potato Hills (HLP-0704)									
	Parent	0.110	0.450	0.090	0.01000		0.300		0.040	% Minerals
	Calc	titan. mag	Plag	Hornblende	Apatite	K-spar	Olivine	OPX	CPX	Crystals
SiO2	48.006	0.0000	53.89	36.34		67.270	40.200	57.100	50.400	41.60
TiO2	1.875	20.0800	0.00	0.94			0.000	0.170	0.870	2.33
Al2O3	14.350	1.8400	29.20	14.06		18.350	0.000	0.700	3.920	14.76
FeO	12.655	77.6700	0.93	28.00		0.920	13.070	5.900	6.410	15.66
MnO	0.46	0.63	0.93	0.75	0.070		0.000	0.170	0.130	0.56
MgO	11.95	2.18	0.00	3.14	0.100		45.940	34.520	15.450	14.92
CaO	6.150	0.05	11.14	11.82	55.840	0.150	0.230	0.620	21.860	7.58
Na2O	2.660		4.85	1.14		6.450	0.000	0.070	0.290	2.30
K2O	1.182		0.29	2.66		7.05	0.00	0.03	0.00	0.37
P2O5	0.339			0.00	42.050		0.000			0.42
	99.63	102.45	101.23	98.85	98.06	100.19	99.44	99.28	99.33	100.51
Rb	11.13									
Sr	0.35									
Ba	3.46									

Regression

% xlzn	0.10	0.20	0.30	0.40	0.50	0.60	0.70	0.80	0.90	XRF
SiO2	48.72	49.61	50.75	52.28	54.41	57.62	62.96	73.64	105.69	73.64
TiO2	1.82	1.76	1.68	1.57	1.42	1.20	0.82	0.06	-2.20	0.06
Al2O3	14.30	14.25	14.17	14.07	13.94	13.73	13.38	12.69	10.62	12.69
FeO	12.32	11.90	11.37	10.65	9.65	8.15	5.64	0.64	-14.39	0.64
MnO	0.45	0.43	0.42	0.39	0.36	0.31	0.22	0.06	-0.45	0.06
MgO	11.62	11.20	10.67	9.96	8.97	7.48	5.01	0.05	-14.83	0.05
CaO	5.99	5.79	5.54	5.19	4.72	4.00	2.80	0.41	-6.76	0.41
Na2O	2.70	2.75	2.82	2.90	3.02	3.20	3.51	4.11	5.93	3.80
K2O	1.27	1.39	1.53	1.72	1.99	2.40	3.08	4.43	8.49	4.43
P2O5	0.33	0.32	0.30	0.28	0.26	0.22	0.15	0.01	-0.39	0.01
	99.53	99.40	99.25	99.04	98.74	98.30	97.57	96.10	91.70	95.80
									Rb	52.41
									Sr	0.46
									Ba	11.85

Match

	Daughter (ICP-MS)	Daughter (calc)	Residual	R^2
SiO2	73.64	73.64	-0.001	0.000
TiO2	0.06	0.06	0.000	0.000
Al2O3	12.69	12.69	0.006	0.000
FeO	0.64	0.64	0.001	0.000
MnO	0.06	0.06	-0.005	0.000
MgO	0.05	0.05	-0.003	0.000
CaO	0.41	0.41	-0.001	0.000
Na2O	3.80	4.11	0.312	0.098
K2O	4.43	4.43	-0.002	0.000
P2O5	0.01	0.01	-0.002	0.000
	95.80	96.10		
% melt remaining		0.20	√∑R^2=	0.312

Mineral/melt partition coefficients used (from Rollinson, 1993):

	Rubidium	Strontium	Barium
Titan. Magnetite	0.0	0.0	0.0
Plagioclase	0.071	1.830	0.503
Hornblende	0.014	0.022	0.044
Apatite	0.0	0.0	0.0
Olivine	0.0098	0.014	0.0099
Clinopyroxene	0.031	0.0	0.026

Mineral compositions are from Deer, Howie, and Zussman. (1992).

Appendix 3 (continued)

Potato Hills (HLP-0704)

Rayleigh Fractionation Model - Crystallization

CL/CO=F ^(Di-1)			CL/CO=F ^(Di-1)			CL/CO=F ^(Di-1)		
F	Di of a	Rb	F	Di of b	Sr	F	Di of c	Ba
	0.037			0.832			0.234	
	CL/Co			CL/Co			CL/Co	
0.05	17.881	199.05	0.05	1.653	0.58	0.05	9.910	34.3
0.10	9.175	102.14	0.10	1.471	0.52	0.10	5.829	20.1
0.20	4.708	52.41	0.20	1.310	0.46	0.20	3.429	11.9
0.30	3.187	35.47	0.30	1.224	0.43	0.30	2.514	8.7
0.40	2.416	26.89	0.40	1.166	0.41	0.40	2.017	7.0
0.50	1.949	21.69	0.50	1.123	0.39	0.50	1.700	5.9
0.60	1.635	18.20	0.60	1.089	0.38	0.60	1.479	5.1
0.70	1.410	15.69	0.70	1.062	0.37	0.70	1.314	4.5
0.80	1.240	13.80	0.80	1.038	0.36	0.80	1.186	4.1
0.90	1.107	12.32	0.90	1.018	0.36	0.90	1.084	3.7
1.00	1.000	11.13	1.00	1.000	0.35	1.00	1.000	3.5

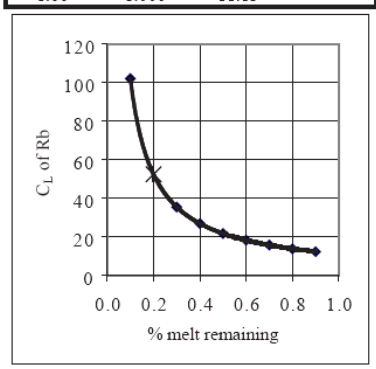

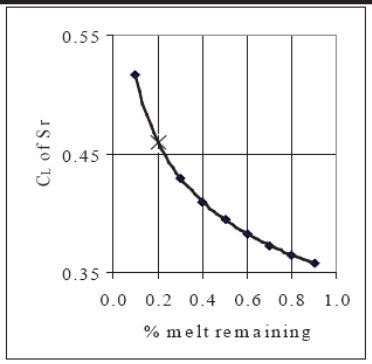

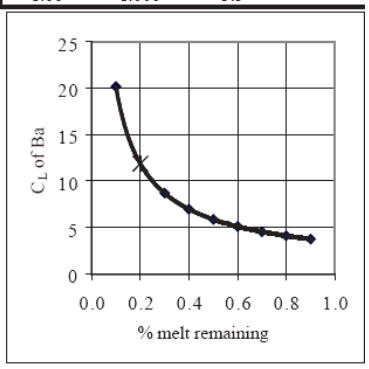

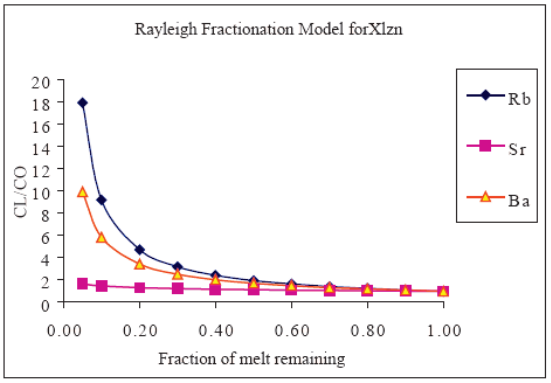

Appendix 3 (continued)

Hampton andesite (HTB-0623)

Sample #	HTB-0623 Hampton andesite									
	Parent	0.095	0.600	0.000	0.00700	0.000	0.168	0.000	0.130	% Mineral
	Calc	Titan. mag	Plag	Hbld	Apatite	K-spar	Olivine	Opx	Cpx	Crystals
SiO2	48.270		53.89	36.34		67.270	40.200	57.100	50.400	45.64
TiO2	1.784	20.0800		0.94				0.170	0.870	2.02
Al2O3	17.974	1.8400	29.20	14.06		18.350		0.700	3.920	18.20
FeO	10.014	77.6700	0.93	28.00		0.920	13.070	5.900	6.410	10.97
MnO	0.53	0.63	0.93	0.75	0.070			0.170	0.130	0.64
MgO	8.66	2.18		3.14	0.100		45.940	34.520	15.450	9.93
CaO	9.280	0.05	11.14	11.82	55.840	0.150	0.230	0.620	21.860	9.96
Na2O	3.070		4.85	1.14		6.450		0.070	0.290	2.95
K2O	0.548		0.29	2.66		7.05		0.03		0.17
P2O5	0.305				42.050					0.29
	100.43	102.45	101.23	98.85	98.06	100.19	99.44	99.28	99.33	100.78
Rb	5.92									
Sr	579.76									
Ba	286.46									

Regression

% xlzn	0.10	0.20	0.30	0.40	0.50	0.60	0.70	0.80	0.90	XRF
SiO2	48.56	48.93	49.40	50.02	50.90	52.22	54.41	58.79	71.94	58.80
TiO2	1.76	1.72	1.68	1.63	1.55	1.43	1.23	0.84	-0.35	0.84
Al2O3	17.95	17.92	17.88	17.82	17.74	17.63	17.44	17.05	15.90	17.05
FeO	9.91	9.78	9.61	9.38	9.06	8.59	7.79	6.21	1.45	6.21
MnO	0.52	0.51	0.49	0.46	0.43	0.38	0.29	0.12	-0.40	0.12
MgO	8.52	8.34	8.11	7.81	7.38	6.74	5.68	3.55	-2.84	3.55
CaO	9.20	9.11	8.99	8.83	8.60	8.26	7.69	6.56	3.15	6.56
Na2O	3.08	3.10	3.12	3.15	3.19	3.25	3.36	3.56	4.17	3.56
K2O	0.59	0.64	0.71	0.80	0.92	1.11	1.42	2.04	3.91	2.04
P2O5	0.31	0.31	0.31	0.31	0.32	0.32	0.33	0.35	0.40	0.35
	100.40	100.35	100.29	100.21	100.09	99.92	99.63	99.06	97.35	99.08
									Rb	27.40
									Sr	487.00
									Ba	874.00

Match

	Daughter (ICP-MS)	Daughter (calc)	Residual	R^2
SiO2	58.80	58.79	-0.008	0.000
TiO2	0.84	0.84	-0.002	0.000
Al2O3	17.05	17.05	0.002	0.000
FeO	6.21	6.21	0.001	0.000
MnO	0.12	0.12	-0.005	0.000
MgO	3.55	3.55	0.002	0.000
CaO	6.56	6.56	0.000	0.000
Na2O	3.56	3.56	-0.003	0.000
K2O	2.04	2.04	0.006	0.000
P2O5	0.35	0.35	-0.005	0.000
	99.08	99.06		
% melt remaining		0.20	√∑R^2= 0.013	

Mineral/melt partition coefficients used (from Rollinson, 1993):

	Rubidium	Strontium	Barium
Titan. Magnetite	0.0	0.0	0.0
Plagioclase	0.071	1.830	0.503
Hornblende	0.014	0.022	0.044
Apatite	0.0	0.0	0.0
Olivine	0.0098	0.014	0.0099
Clinopyroxene	0.031	0.0	0.026

Mineral compositions are from Deer, Howie, and Zussman. (1992).

Appendix 3 (continued)

Hampton andesite (HTB-0623)

Rayleigh Fractionation Model - Crystallization

CL/CO=F ^(Di-1)				CL/CO=F ^(Di-1)				CL/CO=F ^(Di-1)			
F	Di of a		Rb	F	Di of b		Sr	F	Di of c		Ba
	0.048				1.108				0.307		
	CL/Co				CL/Co				CL/Co		
0.05	17.307	102.51		0.05	0.723	419.09		0.05	7.975	2284.5	
0.10	8.948	53.00		0.10	0.779	451.77		0.10	4.933	1413.0	
0.20	4.626	27.40		0.20	0.840	487.00		0.20	3.051	874.0	
0.30	3.145	18.63		0.30	0.878	508.87		0.30	2.304	659.9	
0.40	2.392	14.17		0.40	0.906	524.98		0.40	1.887	540.6	
0.50	1.934	11.46		0.50	0.928	537.82		0.50	1.617	463.1	
0.60	1.626	9.63		0.60	0.946	548.55		0.60	1.425	408.2	
0.70	1.404	8.32		0.70	0.962	557.79		0.70	1.280	366.8	
0.80	1.237	7.32		0.80	0.976	565.92		0.80	1.167	334.4	
0.90	1.105	6.55		0.90	0.989	573.18		0.90	1.076	308.2	
1.00	1.000	5.92		1.00	1.000	579.76		1.00	1.000	286.5	

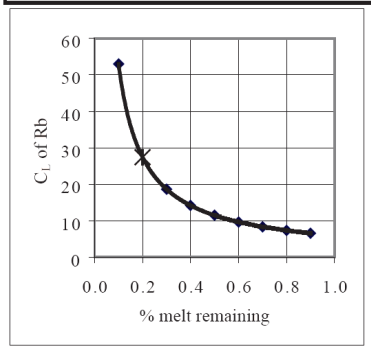

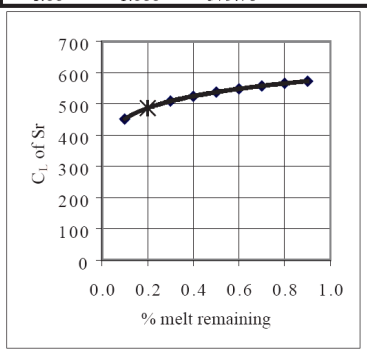

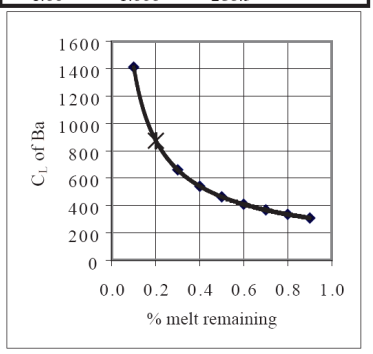

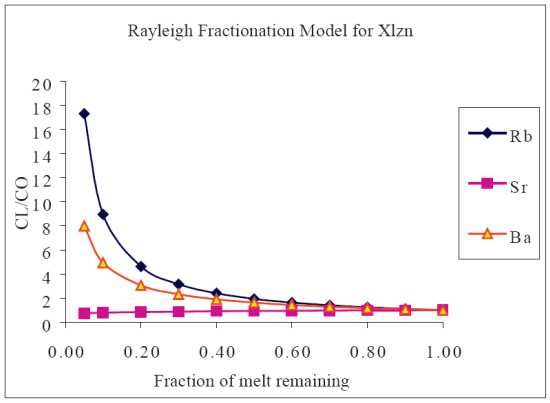

Appendix 3 (continued)

Grassy Butte (GB-0701)

Sample #	Grassy Butte (GB-0701)									
	Parent	0.095	0.500		0.00500		0.140		0.260	% Mineral
	Calc	Ilmenite	Plag	Hbld	Apatite	K-spar	Olivine	Opx	Cpx	Crystals
SiO2	50.07	0.0000	53.89	36.34		67.270	40.200	57.100	50.400	45.68
TiO2	2.07	20.0800	0.00	0.94			0.000	0.170	0.870	2.13
Al2O3	15.70	1.8400	29.20	14.06		18.350	0.000	0.700	3.920	15.79
FeO	10.69	77.6700	0.93	28.00		0.920	13.070	5.900	6.410	11.34
MnO	0.41	0.63	0.93	0.75	0.070		0.000	0.170	0.130	0.56
MgO	7.51	2.18	0.00	3.14	0.100		45.940	34.520	15.450	10.66
CaO	9.46	0.05	11.14	11.82	55.840	0.150	0.230	0.620	21.860	11.57
Na2O	3.14		4.85	1.14		6.450	0.000	0.070	0.290	2.50
K2O	0.61		0.29	2.66		7.05	0.00	0.03	0.00	0.15
P2O5	0.26			0.00	42.050		0.000			0.21
	99.91	102.45	101.23	98.85	98.06	100.19	99.44	99.28	99.33	100.59
Rb	13.34									
Sr	417.46									
Ba	261.85									

Regression

% xlzn	0.10	0.20	0.30	0.40	0.50	0.60	0.70	0.80	0.90	XRF
SiO2	50.56	51.17	51.95	53.00	54.46	56.65	60.31	67.63	89.59	56.65
TiO2	2.06	2.05	2.04	2.03	2.01	1.97	1.92	1.81	1.50	1.97
Al2O3	15.69	15.68	15.66	15.64	15.61	15.56	15.48	15.32	14.85	15.56
FeO	10.62	10.53	10.41	10.26	10.04	9.71	9.17	8.09	4.84	9.71
MnO	0.40	0.38	0.35	0.31	0.27	0.19	0.07	-0.18	-0.91	0.19
MgO	7.15	6.72	6.15	5.40	4.35	2.78	0.15	-5.10	-20.86	2.78
CaO	9.23	8.93	8.56	8.05	7.35	6.30	4.54	1.02	-9.53	6.30
Na2O	3.21	3.30	3.41	3.56	3.77	4.09	4.62	5.68	8.87	4.09
K2O	0.66	0.73	0.81	0.92	1.08	1.31	1.70	2.47	4.80	1.31
P2O5	0.26	0.27	0.27	0.28	0.30	0.32	0.36	0.43	0.66	0.32
	99.83	99.74	99.62	99.45	99.23	98.89	98.32	97.19	93.80	98.88
									Rb	32.00
									Sr	444.00
									Ba	516.00

Match

	Daughter (ICP-MS)	Daughter (calc)	Residual	R^2
SiO2	56.65	56.65	0.000	0.000
TiO2	1.97	1.97	0.001	0.000
Al2O3	15.56	15.56	-0.001	0.000
FeO	9.71	9.71	0.008	0.000
MnO	0.19	0.19	0.004	0.000
MgO	2.78	2.78	0.001	0.000
CaO	6.30	6.30	-0.003	0.000
Na2O	4.09	4.09	0.000	0.000
K2O	1.31	1.31	0.001	0.000
P2O5	0.32	0.32	-0.002	0.000
	98.88	98.89		
% melt remaining		0.40	√∑R^2= 0.010	

Mineral/melt partition coefficients used (from Rollinson, 1993):

	Rubidium	Strontium	Barium
Ilmenite	0.0	0.0	0.0
Plagioclase	0.071	1.830	0.503
Hornblende	0.014	0.022	0.044
Apatite	0.0	0.0	0.0
Olivine	0.0098	0.014	0.0099
Clinopyroxene	0.031	0.0	0.026

Mineral compositions are from Deer, Howie, and Zussman. (1992).

Appendix 3 (continued)

Grassy Butte (GB-0701)

Rayleigh Fractionation Model - Crystallization

CL/CO=F ^(Di-1)				CL/CO=F ^(Di-1)				CL/CO=F ^(Di-1)			
F	Di of a		Rb	F	Di of b		Sr	F	Di of c		Ba
	0.045				0.933				0.260		
	CL/Co				CL/Co				CL/Co		
0.05	17.481	233.16		0.05	1.223	510.65		0.05	9.186	2405.5	
0.10	9.017	120.27		0.10	1.168	487.39		0.10	5.499	1440.0	
0.20	4.651	62.04		0.20	1.114	465.19		0.20	3.292	862.0	
0.30	3.158	42.12		0.30	1.084	452.67		0.30	2.438	638.5	
0.40	2.399	32.00		0.40	1.064	444.00		0.40	1.971	516.0	
0.50	1.939	25.86		0.50	1.048	437.39		0.50	1.671	437.4	
0.60	1.629	21.73		0.60	1.035	432.06		0.60	1.460	382.2	
0.70	1.406	18.75		0.70	1.024	427.60		0.70	1.302	341.0	
0.80	1.238	16.51		0.80	1.015	423.78		0.80	1.180	308.9	
0.90	1.106	14.75		0.90	1.007	420.43		0.90	1.081	283.1	
1.00	1.000	13.34		1.00	1.000	417.46		1.00	1.000	261.9	

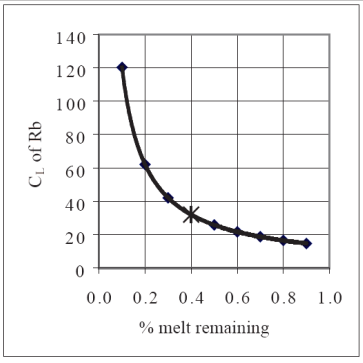

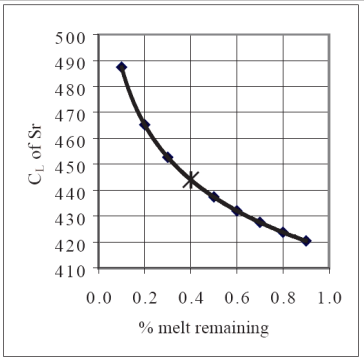

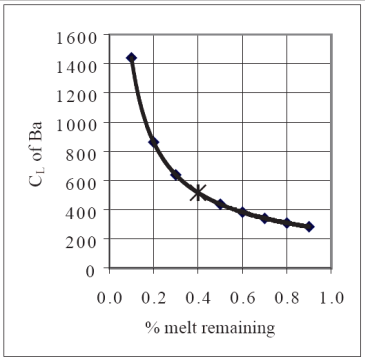

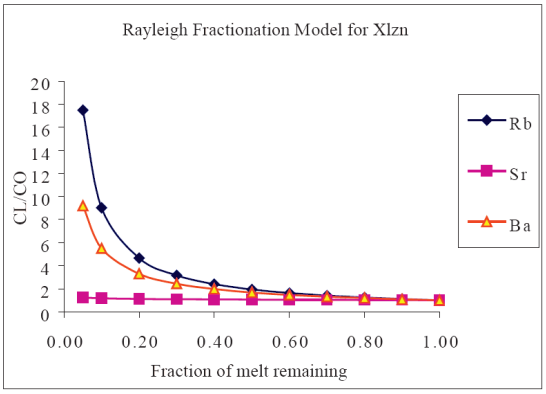

Appendix 3 (continued)

Hampton Tuff (HTB-0701)

Sample #	Hampton Tuff (HTB-0701)									
	Parent	0.12	0.37		0.01		0.20			0.30 % Minerals
Element	Calc	Titan. mag	Plag	Hbld	Apatite	K-spar	Olivine	Opx	Cpx	Crystals
SiO2	49.08		53.89	36.34		67.27	40.20	57.10	50.40	43.26
TiO2	2.19	20.08		0.94				0.17	0.87	2.67
Al2O3	12.42	1.84	29.20	14.06		18.35		0.70	3.92	12.29
FeO	11.99	77.67	0.93	28.00		0.92	13.07	5.90	6.41	14.20
MnO	0.39	0.63	0.93	0.75	0.07		0.00	0.17	0.13	0.46
MgO	11.31	2.18		3.14	0.10		45.94	34.52	15.45	14.09
CaO	9.12	0.05	11.14	11.82	55.84	0.15	0.23	0.62	21.86	11.16
Na2O	2.48		4.85	1.14		6.45		0.07	0.29	1.90
K2O	0.72		0.29	2.66		7.05		0.03		0.11
P2O5	0.24				42.05					0.29
	99.92	102.45	101.23	98.85	98.06	100.19	99.44	99.28	99.33	100.43
Rb	14.86									
Sr	57.09									
Ba	327.31									

Regression

% xlzn	0.10	0.20	0.30	0.40	0.50	0.60	0.70	0.80	0.90	XRF
SiO2	49.73	50.53	51.57	52.96	54.90	57.81	62.66	72.36	101.45	72.36
TiO2	2.14	2.07	1.98	1.87	1.71	1.47	1.07	0.27	-2.14	0.27
Al2O3	12.43	12.45	12.47	12.50	12.54	12.60	12.71	12.92	13.55	12.92
FeO	11.74	11.43	11.04	10.51	9.77	8.66	6.82	3.12	-7.96	3.12
MnO	0.38	0.37	0.35	0.33	0.31	0.27	0.21	0.08	-0.31	0.08
MgO	11.00	10.62	10.12	9.46	8.53	7.15	4.83	0.21	-13.67	0.20
CaO	8.89	8.61	8.24	7.76	7.08	6.06	4.36	0.96	-9.23	0.96
Na2O	2.54	2.62	2.72	2.86	3.06	3.35	3.83	4.80	7.70	4.80
K2O	0.79	0.87	0.98	1.13	1.33	1.64	2.15	3.17	6.23	3.17
P2O5	0.24	0.23	0.22	0.21	0.19	0.16	0.12	0.03	-0.24	0.03
	99.87	99.80	99.71	99.59	99.42	99.17	98.75	97.91	95.38	97.90
									Rb	69.90
									Sr	92.00
									Ba	1191.00

Match

	Daughter (ICP-MS)	Daughter (calc)	Residual	R^2
SiO2	72.36	72.36	-0.001	0.000
TiO2	0.27	0.27	-0.001	0.000
Al2O3	12.92	12.92	0.006	0.000
FeO	3.12	3.12	0.002	0.000
MnO	0.08	0.08	0.000	0.000
MgO	0.20	0.21	0.007	0.000
CaO	0.96	0.96	0.002	0.000
Na2O	4.80	4.80	0.000	0.000
K2O	3.17	3.17	-0.005	0.000
P2O5	0.03	0.03	-0.006	0.000
	97.90	97.91		
% melt remaining		0.20	√∑R^2= 0.012	

Mineral/melt partition coefficients used (from Rollinson, 1993):

	Rubidium	Strontium	Barium
Titan. Magnetite	0.0	0.0	0.0
Plagioclase	0.071	1.830	0.503
Hornblende	0.014	0.022	0.044
Apatite	0.0	0.0	0.0
Olivine	0.0098	0.014	0.0099
Clinopyroxene	0.031	0.0	0.026

Mineral compositions are from Deer, Howie, and Zussman. (1992).

Appendix 3 (continued)

Hampton Tuff (HTB-0701)

Rayleigh Fractionation Model - Crystallization

CL/CO=F ^(Di-1)			Rb	CL/CO=F ^(Di-1)			Sr	CL/CO=F ^(Di-1)			Ba
F	Di of a			F	Di of b			F	Di of c		
	0.038				0.704				0.197		
	CL/Co				CL/Co				CL/Co		
0.05	17.862	265.35		0.05	2.430	138.76		0.05	11.070	3623.2	
0.10	9.168	136.19		0.10	1.979	112.99		0.10	6.347	2077.3	
0.20	4.705	69.90		0.20	1.611	92.00		0.20	3.639	1191.0	
0.30	3.185	47.32		0.30	1.429	81.58		0.30	2.628	860.2	
0.40	2.415	35.88		0.40	1.312	74.91		0.40	2.086	682.8	
0.50	1.948	28.94		0.50	1.228	70.12		0.50	1.744	570.9	
0.60	1.635	24.29		0.60	1.163	66.43		0.60	1.507	493.2	
0.70	1.409	20.94		0.70	1.112	63.46		0.70	1.331	435.8	
0.80	1.240	18.41		0.80	1.068	61.00		0.80	1.196	391.5	
0.90	1.107	16.44		0.90	1.032	58.91		0.90	1.088	356.2	
1.00	1.000	14.86		1.00	1.000	57.09		1.00	1.000	327.3	

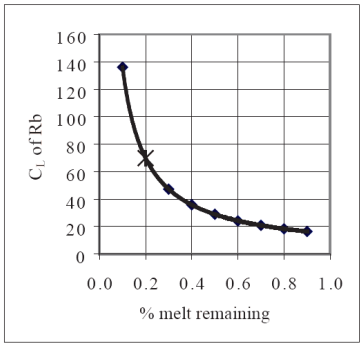

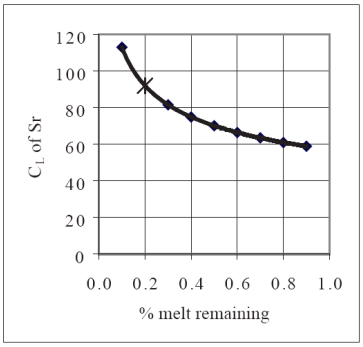

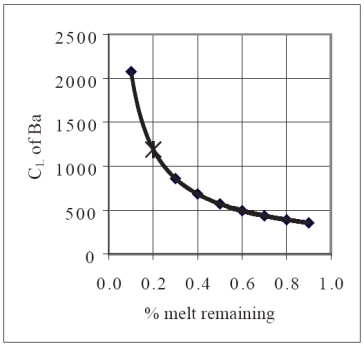

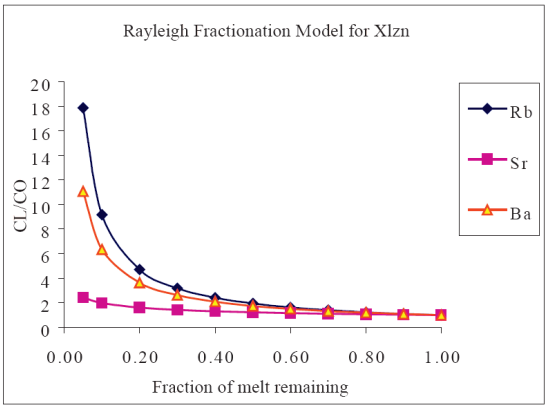

Appendix 4: Rocks of the northern margin compared to samples from the High Lava Plains

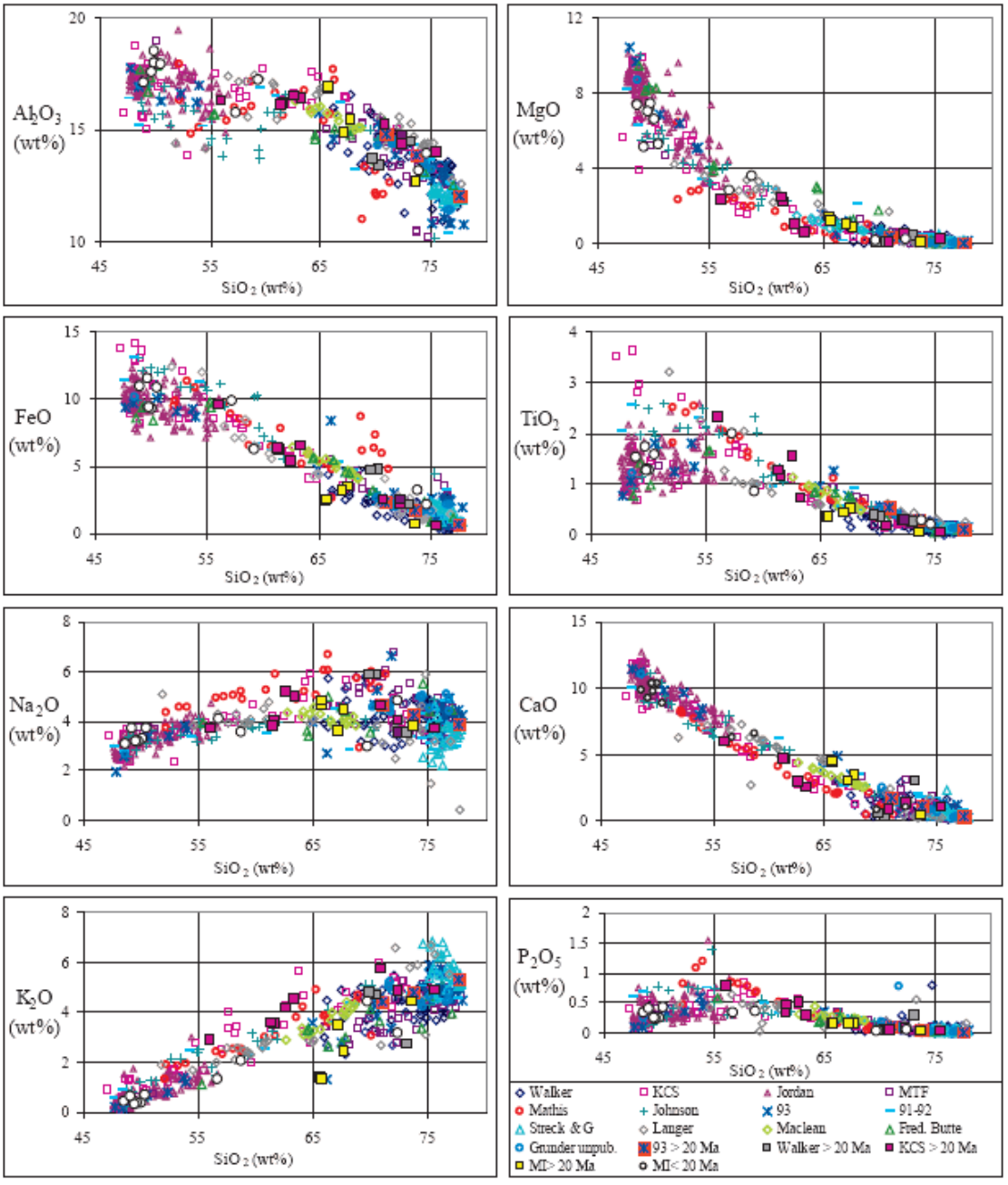

Appendix 4 (continued)

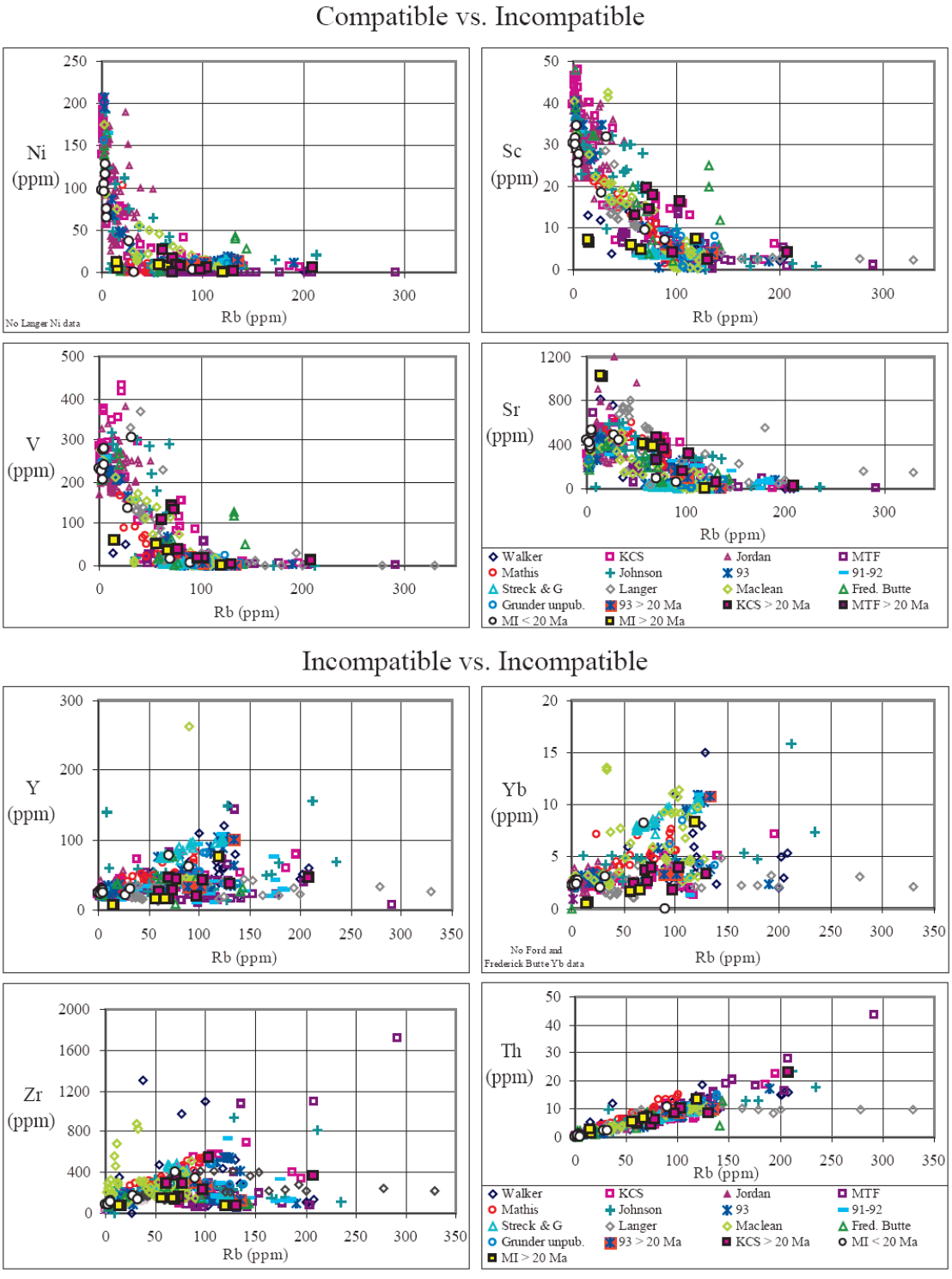

Appendix 4 (continued)

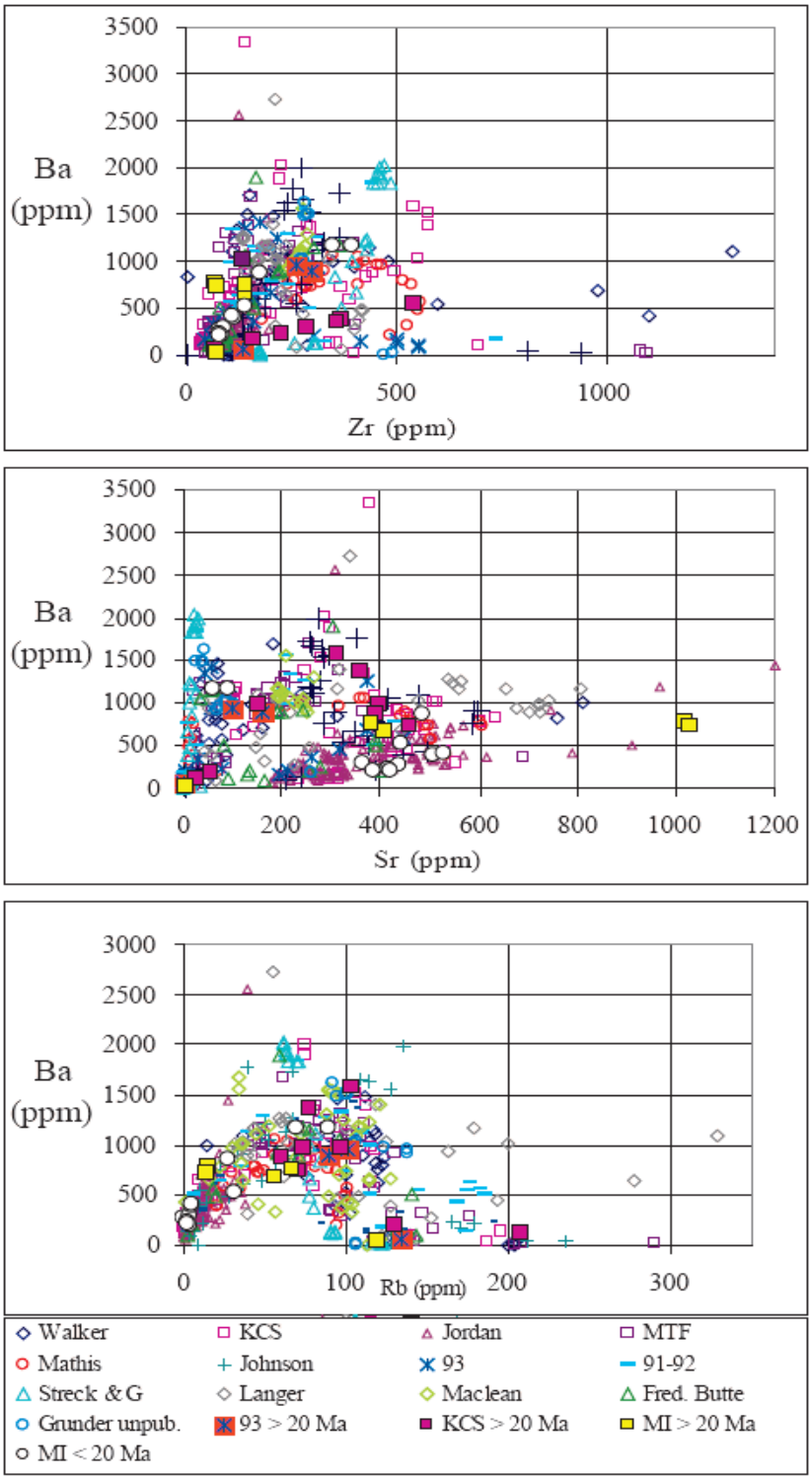

Appendix 4 (continued)

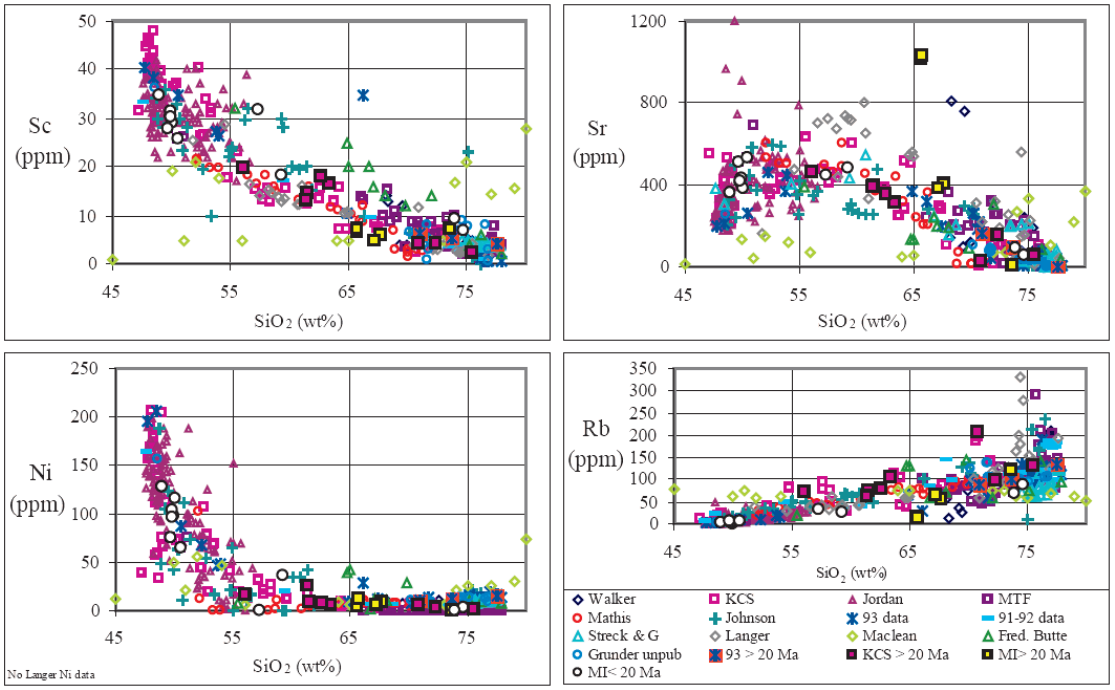

Data from: Walker, 1981, Johnson, 1998, Johnson and Grunder, 2000, Jordan and Grunder,2004, Hart and Carlson, 1987, Hart, 1984, Jordan, et al., 2002, Berri, 1982, Johnson,1984, Langer, 1991, Mathis, 1993, MacLean, 1994, Johnson, 1995, Jordan, 2001, Scarberry, 2007, Ford, unpub., Streck & Grunder , unpub., Iademarco, unpub. Data compiled by Mark Ford, OSU.